Determination of The Drag Coefficient of an Autonomous Solar Lighting Column Using Wind Tunnel Simulation and Computational Analysis

Vitor Hugo da Silva Dias

Dissertation presented to

Higher School of Technology and Management

Polytechnic Institute of Bragança

to obtain the master's degree at

Industrial Engineering

Report made under supervision of

Professor Carlos Alberto Rodrigues Andrade

Co-supervision of

Professor João Carlos Almendra Roque

Professor Sérgio Manuel de Sousa Rosa

Professor Francisco Augusto Aparecido Gomes

This dissertation does not include the critics and and suggestions made by the Jury

october 2019

Acknowledgments

First of all I would like to thank both the Federal Technological University of Paraná and the Bragança Polytechnic Institute for signing the double degree agreement that allowed me to do this work.

Secondly, I would like to thank my advisers for all their help and also for their patience in dealing with the problems that arose during the course of this work and were often caused by myself.

Thirdly I would like to thank everyone who has been supporting me, especially emotionally in the moments that I needed most, especially my boyfriend who helped me strongly to make this work the best possible and my friends who lived with me during this and who did not. They let up.

Last but most importantly, I would like to thank my family who have always sacrificed themselves to allow me to have the best possible opportunities especially my mother who has always been an inspiring image to me for her perseverance and determination. Without her I would be nothing.

Abstract

Photovoltaic solar panels have many applications and among them are the autonomous solar lighting columns, which has been growing in popularity in urban and rural enviroments. These columns are installed in open regions and have their structure exposed to the mechanical actions imposed by the wind, so they need to be correctly designed to support them. There are aerodynamic variables that must be determined for the design of these columns, especially the drag coefficient, a property linked to the geometry of a body, which represents its interaction with a flowing fluid. Due to the complexity of determining these variables, experimental methods are constantly used to obtain these values. Classically, wind tunnel simulations are used for this purpose, but they can be expensive and difficult to perform, so that fluid computational analysis has been widely applied to replace physical analysis. In this work, the drag coefficient of an autonomous solar illumination column is determined by wind tunnel simulations and computational analysis using various body positions in relation to the direction of flow. The drag coefficient determined using wind tunnel simulations varies between 0.65 and 0.80 while for computational methods it varies between 0.43 and 0.73. With the obtained results it is possible to perform a verification of the fidelity of the data obtained by computational means when compared to those obtained through the wind tunnel simulations obtaining an average error of 9.2% and 27.2% for the computational methods used.

Keywords: Wind-tunnel simulations; CFD analyses; Drag-coefficient; Drag-force; Fluid-dynamics

RESUMO

Painéis solares fotovoltaicos possuem muitas aplicações e entre elas estão as colunas de iluminação solar autônomas, que vem crescendo em popularidade principalmente nos ambientes urbanos e industriais. Estas colunas são instaladas em regiões abertas e têm sua estrutura exposta às ações mecânicas impostas pelo vento, desta forma, precisam ser corretamente projetadas para suporta-las. Existem variáveis aerodinâmicas que devem ser determinadas para o projeto dessas colunas em especial o coeficiente de arrasto, propriedade ligada à geometria de um corpo, que representa a interação deste com um fluido em escoamento. Devido à complexidade de determinação dessas variáveis, métodos experimentais são constantemente utilizados para obter estes valores. Classicamente, as simulações em túnel de vento são utilizadas para este propósito, porém, estas podem ser caras e de difícil realização, de modo que as análises computacionais fluidodinâmicas vêm sendo muito aplicadas para substituir as análises físicas. Neste trabalho, o coeficiente de arrasto de uma coluna de iluminação solar autônoma é determinado por meio de simulações em túnel de vento e por meio de análises computacionais utilizando diversos posicionamentos do corpo em relação à direção do escoamento. O coeficiente de arrasto determinado utilizando as simulações em tunel de vento varia entre 0,65 e 0,80 enquanto para os métodos computacionais varia entre 0,43 e 0,73. Com os resultados obtidos é possível realizar uma verificação da fidelidade dos dados obtidos por meios computacionais quando comparados aos obtidos através das simulações em túnel de vento obtendo-se um erro médio de 9,2% e 27,2% para os métodos computacionais utilizados.

Palavras-chave: Simulações em túnel de vento; Análises CFD; Coeficiente de arrasto; Força de arrasto; Fluido-dinâmica

Index

List of tables

List of figures

1. Introduction

In the scenario of searches for alternatives with lower environmental impacts, the methods of electric energy production are the target of studies that open space for the use of clean energy sources that have little or no emission and generation of pollutants, reducing environmental impacts [1].

The Sun is the largest source of energy available and the means to explore this potential are the target of several lines of research. Among the solutions developed is photovoltaic technology, present in a wide variety of possible applications such as homes or buildings in order to fulfill the energy needs of these places and the use for construction of power plants [2].

Photovoltaic panels are widely used when generating decentralized energy, a method that represents one of the greatest revolutions of energy systems [1, 2].

For small-scale applications of photovoltaic technology, autonomous solar lighting columns are increasingly present, mainly in urban areas, being found in avenues, parks, gardens or even on roads and industries. [1]

These columns use solar photovoltaic panels to capture solar radiation, in order to convert into electricity and conserve the energy generated in storage cells to provide the necessary illumination during nighttime.

Autonomous solar lighting columns can be found on the market under different brands and each of them has several models that can present different characteristics like the hight of the column body, the power generation capacity of the photovoltaic solar panel and the storage capacity of the energy cells.

Its design, usually very simple, needs to be carefully thought in mechanical terms since these objects are installed in open and unprotected places and are therefore exposed to the mechanical action of winds that can generate strong loads capable of impairing the structural integrity of these objects.

Among the forces experienced by structures exposed to the environment is the drag force coming from the winds.

The present work aims to determine some fluid-dynamics properties, focusing on the drag coefficient and the drag force of an autonomous solar lighting column produced by the Valled company using experimental methods in a wind tunnel and Computational Fluid Dynamics (CFD) analysis.

1.1.   Justification

In fluid mechanics, purely theoretical methods of analysis present a high complexity to be solved due to the nature of the phenomena involved. This difficulty causes a limitation in the amount of information that can be obtained by these methods.

This complexity motivated the development of new methods of analysis and turn the experimental methods, both physical and computational, in the most valuable tool to obtain fluid dynamic properties. Between these properties is the drag coefficient, whose correct determination is important to permit a correctly designed component that can be applied in the best possible way in service with a low risk of failure.

To assist in the determination of this parameter, wind tunnel tests using scale models of the studied component were used for a long time as the only possible alternative to be used, but with technological advances computational methods are becoming more common specialy in cases that presents a high Reynolds number, like the one used in this work whose values are between 10E4 to 4,3E6.

This factor may make wind tunnel experiments impossible, or make them very complex and expensive making computational analysis even more attractive.

1.2.   Objectives

The main objective of this work is to evaluate the drag coefficient of an autonomous solar lighting column produced by Valled company and comparing the results obtained through CFD simulations with those obtained through experimentation in wind tunnel to verify the reliability of the computational methods.

To fulfill the general objective, the following specific objectives were defined:

a) Modeling a three-dimensional component using technical drawings that were provided with real dimensions. To permit the model impression and its usage in the wind tunnel, the component was also modeled using a scale factor with the necessary adaptations. This process is realized using a Computational Aided Design (CAD) software;

b) Conversion of the CAD file using the real dimensions of the component to a compatible format and importation to CFD software used;

c) Simulation of the component with real dimensions aiming the determination of the force acting on the body and calculation of the drag coefficient for five different positions. Two different softwares will be used to perform these analyses;

d) Prototype printing with scale factor using a 3D printer provided by the Manufacture Laboratory of the Polytechnic Institute of Bragança;

e) Execution of the wind tunnel experiments using the same five positions used in the CFD Analysis. Four tests of each position should be performed using the equipment present in the Fluid Mechanics and Hydraulic Laboratory of the Polytechnic Institute of Bragança;

f) Review of the obtained results;

g) Comparison of the obtained results for wind tunnel simulations and CFD analysis.

1.3.   Presentation of the used softwares

In the execution of this work, different softwares were used in different moments.

1.3.1. SOLIDWORKS™

SOLIDWORKS™ software was used in this work to perform the three-dimensional modeling of the studied component. Two different components were modeled, one using a scale factor for usage in the wind tunnel simulations and one using the real dimensions for usage in computational analyses.

The software was also used to perform a CFD analysis using the *Flow Simulation* tool

1.3.2. ANSYS™

ANSYS™™ software was used in this work to perform a CFD analysis.

1.4.   Company presentation

This work is realized using an autonomous solar lighting column produced by the Valled company, located in the industrial zone of Bragança – Portugal.

The Valled company, showed in Figure 1.1 has a product list of more than 3000 products produced. The company also has 8 exclusive products and one of them is the autonomous solar lighting column that is the object of study of this work [3].

The company is a specialist in the fabrication and selling of renewable energy solutions and the principal areas of work are LED illumination, electro pumps and energy-saving solutions [3].

Figure 1.1 – Aerial view of the Valled company [3].

1.5. Structure of the studied component

The object of the study of this work is the model of an autonomous solar lighting column named Gazela produced by Valled company shown in Figure 1.2. This model consists of four principal modules that are [4]:

- "Contentor" responsible for the storage of the control components e batteries that permits an autonomy of 3 to 5 days;
- "Fuste" is the element responsible for the elevation of the lamps e can be found in models with 6 to 10 meters high;
- The support for the lamps that can present a pump of 60W e 40W;
- The elevator for the photovoltaic module that consists of a multi-crystalline pannel with 72 photovoltaic cells with variable potency.
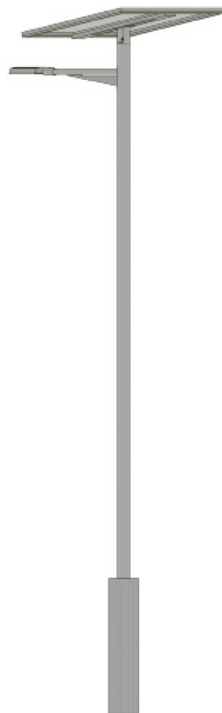
Figure 1.2 – Schematic representation fo the column model studied [4].

The company produces different models of lighting columns to fulfill the application needs. To the model studied, the technical properties are shown in Table 1.1 and the variations available are shown in Table 1.2.

Table 1.1 – Technical properties of the autonomous solar lighting column model studied [4].

Power	30, 40, 50, 60 e 80W
Input voltage	24V DC
Working temperature	-20°C a +60°C
Protection index	IP 65
Light loss	Less than 1% for every 3000 hours (h) in constant operation
Material	Galvanized iron
Lifespan	35000 to 50000 h

Table 1.2 – Variations available to the autonomous solar lighting column model studied [4].

Ref.	High	Power	Light flux (lm)	Color temperature (k)
VL1080 GA WW	10 m	80 W	6400	3000
VL1080 GA CW	10 m	80 W	8000	6000
VL860 GA WW	8 m	60 W	4800	3000
VL860 GA CW	8 m	60 W	6000	6000
VL640 GA WW	6 m	40 W	3200	3000
VL640 GA CW	6 m	40 W	4000	6000

1.6. Work structure

To present the theoretical contents necessary and to demonstrate the experimental method correctly, this work is divided into the following sections.

In chapter 2 are listed previous works that use similar concepts, seak for fluid dynamic properties or use the same methods.

In chapter 3 are presented the basic concepts that allow the correct understanding of the phenomenon that occurs during the proposed analyses. In this chapter is also presented a historical content that permits the understanding of the importance of experimental methods.

In chapter 4 are presented the experimental procedures used in the analyses.

In chapter 5 are shown the obtained results and commentaries about then

In chapter 6 are presented the conclusions that can be made after the experiments performed.

2. State of the art

In the studies realized in 2001 by G.J. Z. Núñes [5] from the Federal University of Rio Grande do Sul to the experimental and theoretical determination of the transversal response to the wind action over a telecommunication tower of reinforced concrete. In this study considering a soft and uniform flow, were obtained values for the drag coefficient between 0,4 to 1,1 for turbulent flow; 0,4 to 0,9 for p equal to 0,11 and 0,3 to 0,8 for p equal to 0,23.

In 2003, L.F. Limas [6] from the Federal University of Rio Grande do Sul studied a series of profiles of bridges cross-sections using a wind tunnel under soft and turbulent flows for different angles of incidence. These models had their aerodynamic properties determined, including the drag coefficient that presented values between 0,22 to 0,41 to laminar flow and 0,22 to 0,37 to a turbulent flow.

A. Machado [7] form the Federal University of Rio Grande do Sul made a study in 2003 to determinate the characterization of aerodynamics properties of metallic towers using different angles of incidence under soft and turbulent flows. To these parameters, the values discovered for the drag coefficient were between 2,58 to 3,47 for a soft flow and 2,53 to 3,12 for a turbulent flow.

In 2005 a study was realized by L. I. Rippel [8] from the Federal University of Rio Grande do Sul to determinate the drag coefficient for a series of models of towers in different angles of incidence. In this study was considered two different pressure levels, one at 588,6 N/m^2 and other at 1922,8 N/m^2. The values obtained to the drag coefficient are comprehended in a range between 1,62 to 4,02.

In the study realized by N. F. P. L. Santos [9] from the University of Coimbra in 2012, the rolling coefficient and the drag coefficient of a high-efficiency car were obtained using experimental methods obtaining a value of 0,202 for the drag coefficient considering a Reynolds number of 10^6.

3.   Theoretical content

The studied component is exposed to a bidimensional external airflow where two dimensions of the body exposed are used during the analysis process [10].

Like other fluid flows, an airflow presents a large number of phenomena related to fluid mechanics as well as properties that depend on the fluid characteristics and shape, size and orientation fo the body immersed in this flow [10, 11].

In this chapter are presented some basic concepts necessary for the correct realization of the proposed analyses and to interpret the results obtained. In this chapter is also presented a historical content.

3.1.   Introduction to fluid mechanics

Fluid Mechanics is the study of fluid, whether it is in movement or stationary, describing its properties and interactions with other materials. This branch of mechanics can be applied in different areas such as pump and pipes design and air conditioning of houses buildings [12, 13].

A fluid can be found in a liquid or gaseous state and have as principal characteristic the continuous deformation when a shear or tangential stress is applied that occurs independently of the stress modulus. It is usual to say that a fluid can flow when exposed to any type of interaction with the environment in it is inserted [12, 13].

In fluid mechanics, the movement of the fluid particles is described using current lines that allow us to see what happens to a fluid when it encounters a solid body immersed in the flow, and makes possible the identification of some interest points [12].

The first point is called the stagnation point in which every particle of the fluid is at rest. Surrounding the body, the current lines tend to open representing that, near to the body surface the velocities are low and consequently, the pressures have a high value [12].

When a fluid in movement interacts with a stationary solid body, the no-slip condition makes the velocity of the fluid on the surface of the body equals to zero. This phenomenon is responsible for the development of a velocity profile and the formation of a boundary layer as it is shown in Figure 3.1 [13].
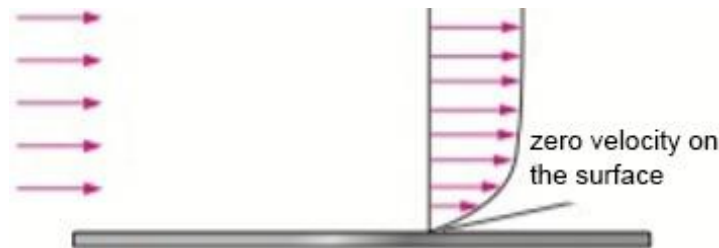
Figure 3.1 – Boundary layer and velocity profile in a fluid flow over a solid surface [13].

As the flow develops, the velocity tends to increase causing a pressure decrease. Due to the formation of the boundary layer and the adverse pressure gradient existing over the solid body, in a certain point, known as the separation point, the fluid particles begin to detach from the body surface causing the formation of a region known as wake turbulence [12]. In Figure 3.2, point A represents the stagnation point, point B is a low-pressure point and point D represents the separation point.

Inside the wake turbulence region, the flow is turbulent and the pressure as a low value but in contrast, the region that surrounds the wake turbulence region presents a higher pressure level. This adverse gradient is responsible for the formation of the drag phenomenon [12].
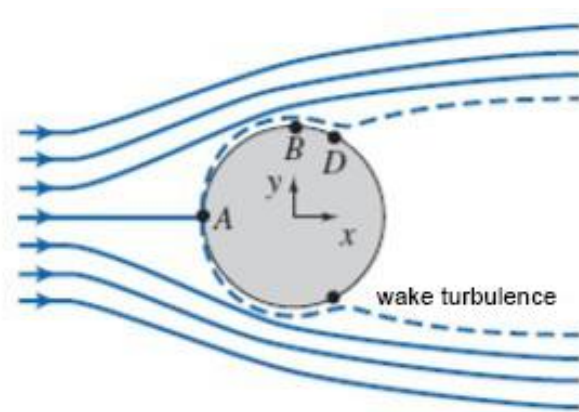
Figure 3.2 – Behavior of the current lines over a solid body immersed in the flow [12].

9

3.2. Drag force

When a solid body is immersed in a flow of any fluid, it is exposed to the action of a series of forces. Among these forces is the drag force that represents a force acting parallel to the direction of the fluid flow but in the opposite direction [6, 12].

The drag force is a composition of pressure and shear forces and consists of flow lose that must be overcome to allows the movement of the body that is immersed in a flow. This phenomenon is undesirable and must be minimized to guarantee higher safety in structures exposed to fluid flows and increase its useful life [6, 13].

Fluid dynamics forces present a complex origin that makes their determination complex for direct analytical determination and it is no different for the drag force. To assist the determination of the drag force acting on a body, its drag coefficient (C_D) can be used through the Eq. 1 [12].

$$C_D = \frac{D}{\frac{1}{2}\rho U^2 A} \qquad \textit{Eq. 1}$$

where

C_D is the drag coefficient;

D is the drag force measure in N;

  is the specific weight of the fluid according to the application temperature;

U is the flow velocity measured in m/s;

A is the frontal area measured in m^2.

It is possible to see in the Eq. 1 that C_D depends on the geometry of the body once its frontal area is part of this equation and can classify a body as aerodynamic or blunt according to the flow direction. C_D is also dependent on the flow velocity, and consequently of the Reynolds number (R_e) to low velocities flows where its values tend to increase once the boundary layer becomes turbulent. This phenomenon occurs because

the major contribution of the drag force is derived from shear forces and these ones are higher in turbulent flows [10, 11].

C_D values can be found in tables for a series of simple geometries but for complex geometries, it needs to be determined by other methods.

To determinate C_D using Eq. 1, it is also needed to know the specific weight of the fluid according to its temperature. This property can be found in tables for a series of materials. For the air, considering an atmospheric pressure of 1 atm, its specific weight is shown in Table 3.1 and the behavior of this propertie with temperature change is shown in Figure 3.3.
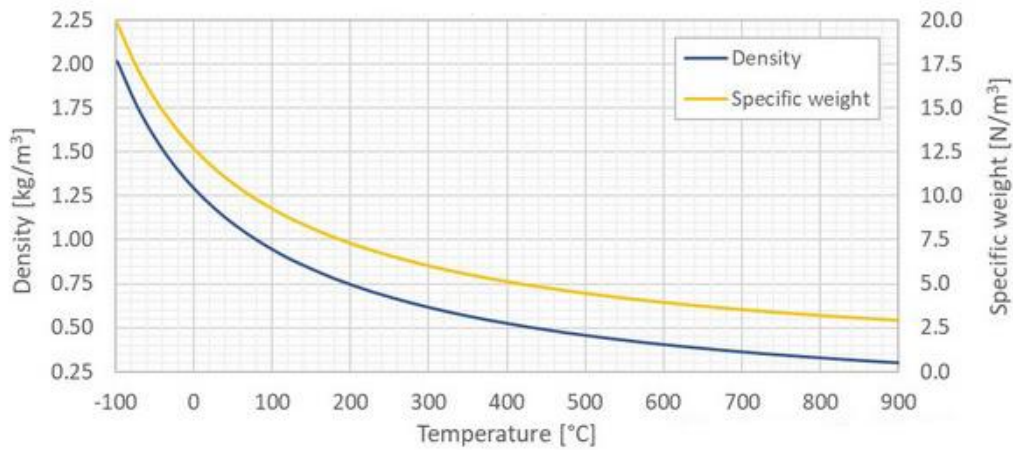
Figure 3.3 - Air density and specific weight at atmospheric pressure [14].

Table 3.1 – Specific weight o fair for 1 atm. [14]

Temperature (C)	Density (kg/m^3)
30	1,164
25	1,184
20	1,204
10	1,246
5	1,268
0	1,292
-5	1,316

Once the drag phenomenon is related to the wake turbulence, it is possible to control it by making alterations in the geometry of the body to achieve an aerodynamic form, so that a lower pressure gradient is obtained at the back of the body.

The drip shape shown in Figure 3.4 is an example if an aerodynamic shape that is used as a reference to design many components, especially on the aeronautic and automobilists industries once the drag force must be minimized for this applications [11].
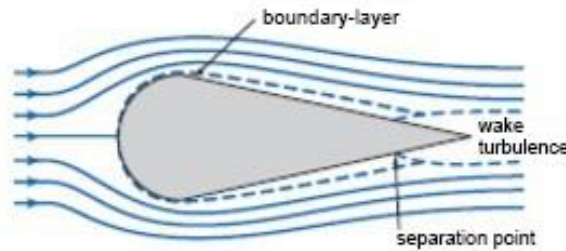
Figure 3.4 – Current lines over a drip shaped body [11].

3.3. Mechanical action of the wind

The wind acts on a body directly in the form of pressures and can vary with time. For turbulent flows, a simplified representation can be made using equivalent forces in a cartesian plane [15].

The wind velocity can be divided into two components known as average velocity and float velocity. The average velocity (v_m) is more important and can be calculated using Eq. 2 [15].

$$v_m = c_r(z) * c_0(z) * v_b \qquad \textit{Eq. 2}$$

where

v_m is the average velocity of the wind measured in m/s in certain high (z) above the ground;

c_o is the orography coefficient, usually defined as 1,0;

$c_r(z)$ is the roughness coefficient and can be defined as:

$$c_r = 0.19 * \left(\frac{z_0}{0.05}\right)^{0.07} * ln\left(\frac{z}{z_0}\right) \text{ para } z_{min} \quad z \quad 200 \text{ m}$$

$$c_r = c_r(z_{min}) \text{ para } z \quad z_{min}$$

The values for z_o and z_{min}, that represents respectivly the roughness length and the minimum height, must be determined according to the ground type. Its possible values are defined in Table 3.2 and exemplified in Figure 3.5.

Table 3.2 – Values for z_o e z_{min} according to the ground type [15].

	Ground type	Z_0 (m)	Z_{min} (m)
0	Sea or coast zone exposed to winds coming from the sea	0.003	1
I	Lakes or plane zones with almost no vegetation and free of obstacles	0.01	1
II	Zone with ground vegetation and isolated obstacles (trees or builds) with a distance of, at least, 20 times its highness between them	0.05	2
III	Zones with regular vegetation or buildings coverage with isolated obstacles with a maximum of 20 times its highness between them (villages, permanent forests)	0.3	5
IV	Zone with at least 15% of the surface is covered by builds with at least 15 m high.	1	10

The roughness coefficient can also be determined using the curves shown in Figure 3.6 that relates the ground type with the high decrease the ground.

The reference value of the wind velocity (v_b) can be determined using Eq. 3 [17]:

$$v_b = c_{dir} * c_{season} * v_{b,0} \qquad \textit{Eq. 3}$$

where

v_b is the reference value of the wind velocity;

$v_{b,0}$ is the basic value of the wind velocity;

c_{dir} is the direction coefficient usually adopted as 1,0;

c_{season} is the seasonal coefficient usually adopted as 1,0.
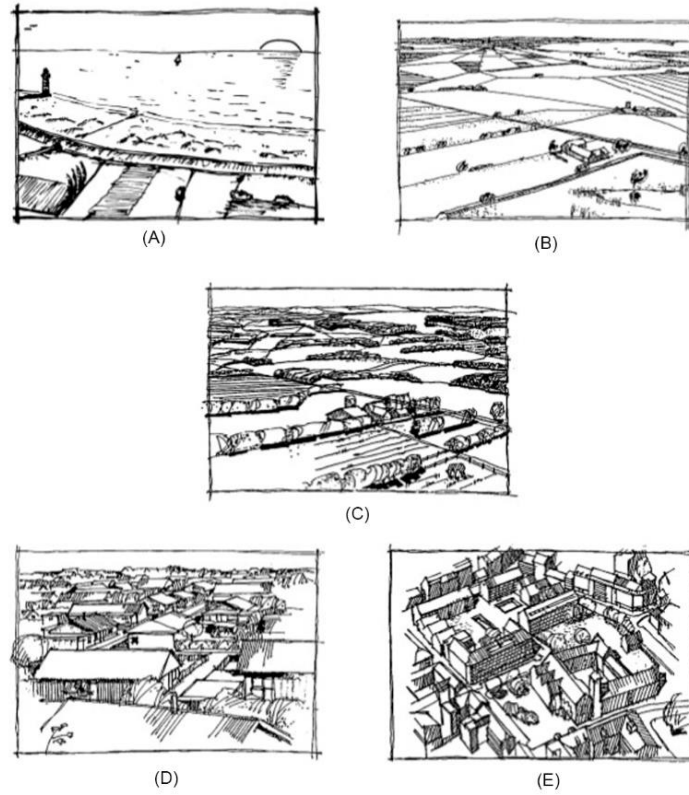
Figure 3.5 – Representation of the groud types where (A) is type 0, (B) is type I, (C) is type II, (D) is type III e (E) is type IV [15].
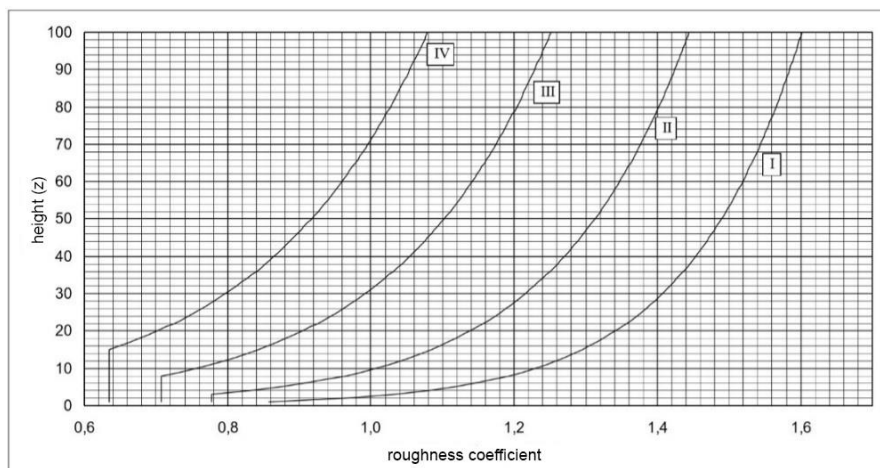
Figure 3.6 – Roughness coefficient curves according to the ground type and high in relation to the ground [15].

The basic value of the wind velocity can be determined according to the ground type as shown in Table 3.3.

Table 3.3 – Basic value of the wind velocity according to the ground type [15].

ZONE	$V_{b,0}$ (m/s)
(A)General ground	27
(B)Açores archipelago and Madeira; continental regions located on the coast with at least 5km length or high of at least 600 m	30

3.4. Introduction to the wind tunnel

Wind tunnels are an old technology that has passed for many changes due to the scientific and technological advances in aerodynamics, especially after the XVIII century to validate new postulations and optimize old ones [16].

3.4.1. Historical background

In the XIX century, humanity felt attracted by the flight of birds and started to pay more attention to this, acquiring inspiration to create flying machines. Many tries were made to conquer the sky and mostly initial prototypes were inspired by Leonardo da Vinci´s planners [17, 18].

Once humanity tried to fly, the first researchers noticed that the current theories about drag and sustentation forces were wrong and these phenomenons are more difficult to describe than they though. This difficulty is attributed to the complex nature of aerodynamic phenomenons that depends on a series of factors such as the flow characteristics and properties and geometry of the body that is immersed in the flow [6, 18].

Due to this complexity, it is hard to describe fluid dynamics phenomenons using only analytical approaches, making the use of simulations an indispensable tool [6].

To perform these simulations, the development of equipment capable of simulate a fluid flow was necessary [6].

The whirling arm was the first equipment developed and its first prototype was created by the English mathematician Benjamin Robins. This equipment consisted of an arm with 1-meter length triggered by the drop of a weight and achieving low velocities of a few meters per second [18]. Figure 3.7 shows the equipment developed by Robins.
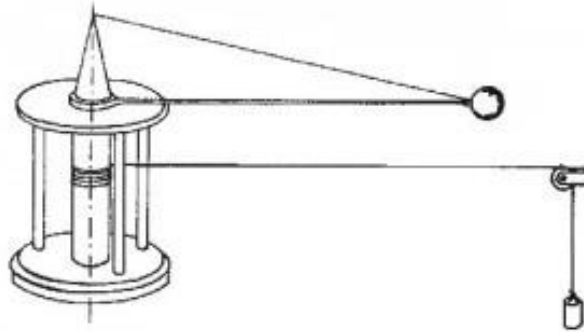
Figure 3.7 – Whirling arm developed by Benjamin Robins [19].

Although this equipment showed great importance to determinate the aerodynamic properties that were known until the end of the XIX century, the rotative movement of the air imposed by the operation principle of this equipment had a negative influence on the experiments making the results not so reliable. This influence motived the creation of a new equipment that has a different operation principle with less influence on the experiment [18].

The substitute of the whirling arm is the wind tunnel, a simple equipment that uses a fan or other appropriate trigger system, propel an airflow through a passage. The first prototype was created by Frank H. Wenham in 1871 [18].

Over time, a series of models for this equipment was developed, but all of them present five basic elements named: fan, output diffuser, constriction section, reassurance chamber or diffuser and test section [20].

Since the body to be studied may not fit into the test section in its original dimension, a scale model is often used to perform the experiments using a wind tunnel [18].

The use of this scale factor created uncertainty regarding the reliability of the results obtained in wind tunnel experiments, and only with the studies made by Osborne

Reynolds was proved that the behavior of a body immersed in a flow is equal both to the real and scaled model [18].

This affirmation is true once a parameter determined by Reynolds is maintained constant to both models. This parameter is called the Reynolds number and can be calculated using the relation shown in Eq. 4 [11, 18].

$$R_e = \frac{\rho * V * L}{\mu}$$

Eq. 4

where

R_e is the Reynolds number;

is the specific weight of the fluid according to the application temperature;

V is the flow velocity measured in m/s;

L is characteristic length;

μ is the fluid viscosity, according to the application temperature.

For the air, considering an atmospheric pressure of 1 atm, its specific weight were showed in Table 3.1 and its viscosity is shown in Table 3.4. The behavior of the air viscosity with temperature change is shown in Figue 3.8.
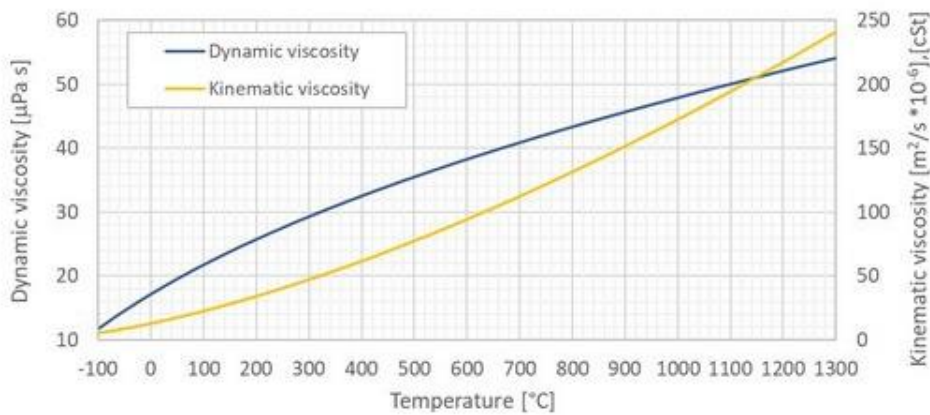
Figue 3.8 - Air dynamic and kinematic viscosity at atmospheric pressure [21].

Table 3.4 - Dynamic viscoity of air for 1 atm. [21]

Temperature (C)	Dynamic viscosity (μPa/s)
30	18,60
25	18,37
20	18,13
10	17,64
5	17,40
0	17,15
-5	16,90

In addition to meeting the needs that may not be met by other methods of analysis, wind tunnels allow obtaining various information on the behavior of the component subjected to a flow action. Its creation represented a major technological advance at the time and today is of great importance for the study of fluid dynamics and for the correct development of a new product not only for the aeronautic industry but also for other engineering areas [21, 22].

3.4.2. Operation principle

Wind tunnel simulations have as operation principle the correspondence between the real model and the scaled model used. This correspondence is known as the similarity principle and some conditions must be attended [17].

The first condition is the geometric similarity where the physical characteristics such as surface rugosity, details and positions must be assured. To attend this condition, only one scale factor can be used in the model [10, 17].

The second condition is the kinetic or kinematics similarity where the same flow characteristics must be assured maintaining a constant relation between the velocities [10, 17].

The geometric similarity is necessary to obtain the kinetic similarity obeying to only one scale factor that can be less, greater or equal to one [17]. Figure 3.9 shows the concept of these conditions.

The third condition is the dynamic similarity where proportional forces must be guaranteed between both flows maintaining a constant relation using, for example, the Reynolds number [6, 13].
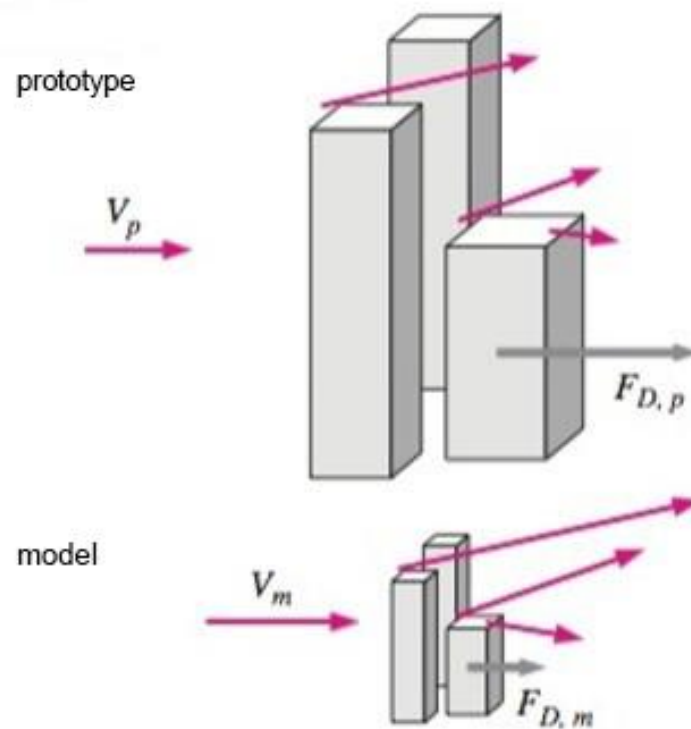
Figure 3.9 – Concept of geometric and kinetic similarity [13].

The complete similarity is obtained when all three conditions are attended but once the kinetic similarity is necessary but not sufficient to guarantee the dynamic similarity, in some cases, it is possible to attend the first two conditions without attending the last condition. To guarantee the dynamic similarity it is possible to detect situations that go beyond the technical capacities of the equipment that will be used to perform the simulations making it impossible to proceed with them [12].

Using as an example, the drag coefficient presents a constant value after a certain value of R_e that shows that it is possible to obtain reliable results even if the complete similarity can`t be assured. This condition is called incomplete similarity and it is largely used to perform wind tunnel simulations [13]. Figure 3.10 shows this behavior.

Using this condition, velocities values close to the maximum obtained in the used equipment to obtain the properties that can be extrapolated as reliable values for the real model [13].
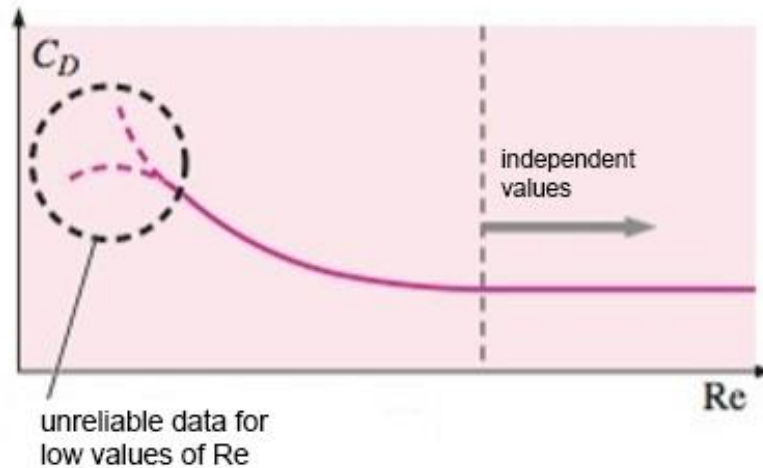
Figure 3.10 – Behavior of the drag coefficient according to the Reynolds number [13].

3.4.3. Typology of wind tunnels

The large variety of models for wind tunnels that can be found were created two principal ways to classify them. This classification can be made according to the flow velocity that can be obtained and to the geometry of the equipment [17].

3.4.3.1.   Classification according to the flow velocity

According to the flow velocity, wind tunnels can be classified using the Mach number (M_a) of the flow. This value represents the relation between the maximum velocity provided by the fan and the sound velocity at the sea level in the standard temperature that is approximately 340 m/s [23, 24]. Table 3.5 contains the classifications according to the velocity for wind tunnels.

Wind tunnels are normally projected to a specific purpose and the compressibility factors related to the flow velocity make some changes to the position of the test section necessary [25].

Table 3.5 – Classification of wind tunnels according to the flow velocity [23, 24].

Classification	Mach number (M_a)	Aplications
Low velocity (subsonic)	Maximum of 0.4	Airfoil study; antennas; calibration of meteorological instruments; atmospheric scenario simulation
High velocity (subsonic)	0.4 to 0.6	Study of airfoils and commercial aircraft
Transonic	0.6 to 1.5	Air compressibility effects; combat aircraft
Supersonic	1.5 to 5.0	Non-Newtonian gas behavior; air compressibility effects
Hypersonic	Higher than 5.0	Simulation of reentry of objects in the atmosphere; meteorite debris impact simulation against satellites

To subsonic flows, it is desired that the velocity in the test section is higher as possible. Once the fluid density remains practically constant, a constraint of the transverse section causes an increase of the velocity and a decrease of the pressure, therefore, the test section has to be placed after the constriction section and before the diffuser [25].

In Figure 3.11 the models discussed above are showed where M represents the Mach number, V is the velocity of the flow and p is the pressure. The region named as plenum represents the external ambient to an open return wind tunnel or the decantation chamber in a closed return wind tunnel. These concepts will be discussed in a future section.
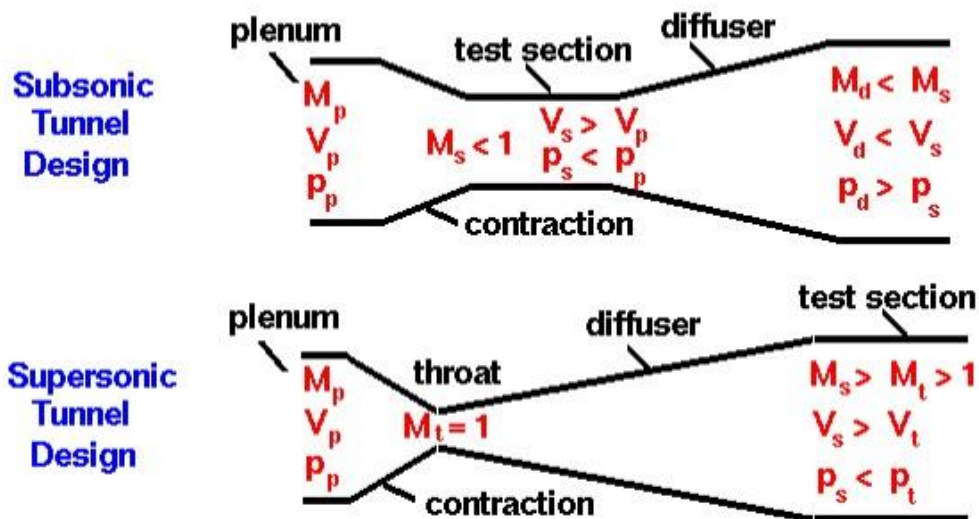
Figure 3.11 – Variations in wind tunnel projects according to the type of flow [25].

The flow velocity also exerts an influence on the choice of fluid to be used. To subsonic flows is normally used atmospheric air as fluid and for supersonic or hypersonic flows gases with a low density such as helium or nitrogen are normally used [17].

3.4.3.2.   Classification according to the geometry

According to the geometry of the equipment, a wind tunnel classification vary according to the flow velocity. To a low-velocity subsonic flow, wind tunnels can be classified as open return or closed return [26].

In an open return wind tunnel, the fluid flow that passes through the test section is thrown in the ambient in which the equipment is Installed as it is shown in Figure 3.12 [26].

This type of equipment has some advantages such as a lower construction cost and better visualization when working with thrusters or using smoke for flow visualization but in contrast, it has disadvantages such as poor flow quality in the test section, higher noise level, and higher operating costs [26].

An open return wind tunnel can be subdivided into other two categories according to the position of the fan. Those whose fan is located at the entrance of the flow are called blowing type and those whose fan is located at the exit of the flow are called suction type [17].
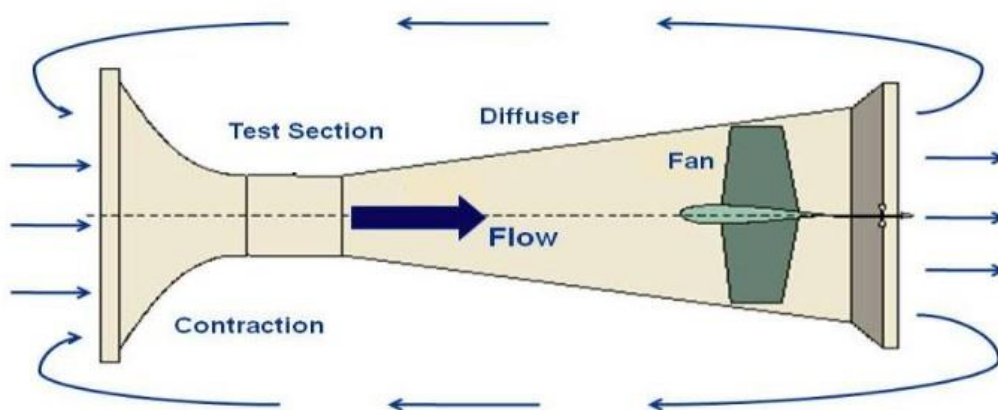
Figure 3.12 – Open return wind tunnel [26].

In a closed return wind tunnel, the fluid flow that passes through the test section circulates continuously as shown in Figure 3.13 [27].

This type of equipment has some advantages such as higher flow quality of the test section, lower operating costs, and lower noise levels but on the other hand, it has disadvantages such as higher construction cost, poor visualization when working with thrusters or smoke flow visualization due to possible accumulation of these products in the test section and a rise in temperature during operation making it necessary to use a cooling system [27].
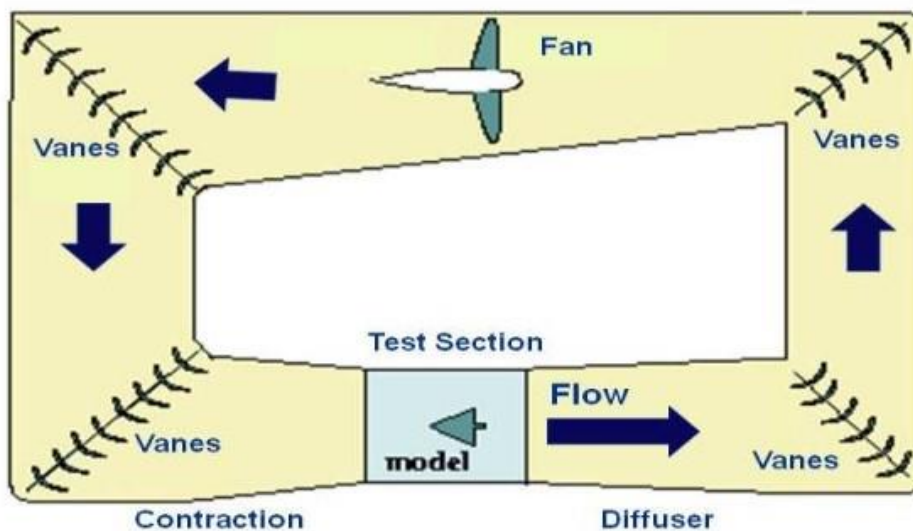
Figure 3.13 – Closed return wind tunnel [27].

3.4.4. Flow control

Wind tunnels have elements that perform functions necessary to guarantee some necessary characteristics, linearizing the flow velocities and eliminating small vortices that may exist before the flow passes through the test section [17].

In general, the following components must be found: After the fan is an inlet diffuser where a transition occurs smoothly due to the deceleration of flow provided by the gradual increase of cross-section in this region. After the inlet diffuser, a grid is positioned to unify the flow velocity distribution and attenuate the boundary layer. Honeycombs are located after this grid and consist of a set of small tubular profiles that have the function of reducing the trasnversal and vertical components of turbulence. Before proceeding to

23

the constriction section the flow is again subjected to passing through a second grid [28, 29].

3.5.   Introduction to computational fluid dynamics simulation

Computational Fluid Dynamics (CFD), has become increasingly popular to reduce the project cycle and the number of tests needed, allowing the determinations of global properties such as the lift and the drag force faster and also permits the determination of the flow field characteristics [13].

A CFD analysis has some essential steps like the mesh generation and boundary conditions determination. This type of analysis accurately deals with laminar flows and often acts in conjunction with experimental analysis to validate the solutions found [13].

Simply put, a CFD analysis works from the iterative solution of Eq. 5 and Eq. 6 respectively called the continuity equation and the Navier-Stokes equation, initially selecting a domain and creating a mesh that will contain small elements in which the equations will be solved [5].

Once the mesh is correctly defined, it is possible to specify the boundary conditions according to the studied problem, defining the fluid type and its properties and finally selecting the solution algorithms present in the software used to perform the simulations [5].

$$\vec{\nabla} * \vec{V} = 0 \qquad\qquad \textit{Eq. 5}$$

where

$\vec{V}$ is the flow velocity.

$$\left(\vec{V} * \vec{\nabla}\right)\vec{V} = -\frac{1}{\rho}\vec{\nabla}P' + \upsilon\nabla^2\vec{V} \qquad\qquad \textit{Eq. 6}$$

where

$\vec{V}$ is the flow velocity;

  is the specific weight of the fluid according to the application temperature;

is the kinematic viscosity of the fluid defined as $= \mu/$;

P' is the modified pressure due to the absence of free surface effects.

3.5.1. Mesh generation

One of the most important steps in a CFD simulation is the preparation of the mesh that will be used, taking as long as it takes to ensure that the mesh will present the best possible characteristics [13].

Even though it is more difficult to obtain for complex geometries, ideally try to obtain a structured mesh in wich its elements can be numbered according to an i, j, k coordinate system. This type of mesh generates fewer elements and also allows for finer resolution in areas of higher interest, i.e. it has greater reliability of results [13].

Another point to consider within mesh design is its quality. It is always necessary to ensure the lowest possible inclination of the elements and to avoid sudden variations in their size ensuring that the convergence of CFD codes is not hindered. Therefore, an unstructured mesh, i.e. whose elements do not obey the coordinate system i, j and k, but has a higher quality than a structured mesh is more recommended for application [13].

To ensure mesh quality, you can opt for a hybrid system that has a structured mesh in regions that require higher resolution, as well as an unstructured mesh in regions that require lower resolution [13].

3.5.2. Boundary conditions

In order to obtain a solution through CFD analysis, it is necessary to model the flow correctly using the correct boundary conditions. The first and simplest of these boundaries is called a "wall" in which a fluid cannot pass through and both the normal and tangential components of fluid velocity are equal to zero. It is also possible to model a wall in which the fluid can slip along. This type of wall is called a non-viscous wall and can be used for free surface cases or when the model boundary represents an open environment [13].

It is also necessary the specification of the flow inlet and outlet conditions and it can be done in various ways. For flow inlet, it can be defined as a velocity or pressure input

where the flow inlet velocity or the total pressure along the inlet must be defined respectively. In the case of the pressure output, the pressure along the surface outside the computational domain, whose value is normally assumed to be the atmospheric pressure value shall be provided. Due to the coupling of velocity and pressure equations to avoid mathematical overspeeding, pressure values should not be provided in the velocity input boundary conditions and the same is true for situations where pressure inputs or outputs are used where velocities values should not be provided [13].

Another usual condition for domain output is to define it as an outflow boundary condition. This type of condition is used for the case where the flow is fully developed, i.e. the velocity profile does not change with the flow evolution, in which case no flow property must be specified so that they are forced to have a null gradient in the normal direction to the exit [13].

4. Methodology

In order to obtain the desired results, three tools were used in this work: a suction type open-circuit wind tunnel provided by the Bragança Polytechnic Institute and the SOLIDWORKS™ and ANSYS™ softwares for the computational analysis.

Each tool described above has different operating characteristics and procedures as described below. Shown below are the technical characteristics of the equipment used for wind tunnel simulation, fitting it to the previously described classifications. Furthermore, the steps necessary to perform the modeling and printing of the models used to perform the wind tunnel simulations and also the CFD analyses are described.

4.1. Wind tunnel simulations

To perform the wind tunnel simulation for this work, the following procedures were made.

4.1.1. Characterization of the used equipment

In the present work, the wind tunnel available from the Laboratory of Fluid Mechanics and Hydraulics (LMFH) of the Polytechnic Institute of Bragança (IPB) was used.

The equipment used is a subsonic open-circuit suction type wind tunnel with a test section of 30 x 30 x 40 (height x width x length), measured in centimeters.

The fan is driven by a 60Hz power motor delivering a speed curve shown in Figure 4.1 that were determinated by previous experiments and described by Eq. 7 that represents the conversion of frequency values into velocity values for the wind flow.

This equipment can reach a maximum speed of 28 m/s under standard conditions, i.e. the pressure of 1 atm. and a temperature of 25 C. The motor frequency control is done through a frequency inverter shown in Figure 4.4.

$$V = 0{,}4694 * f + 0{,}28$$

where

V is the inlet flow velocity;

f is the frequency applied.
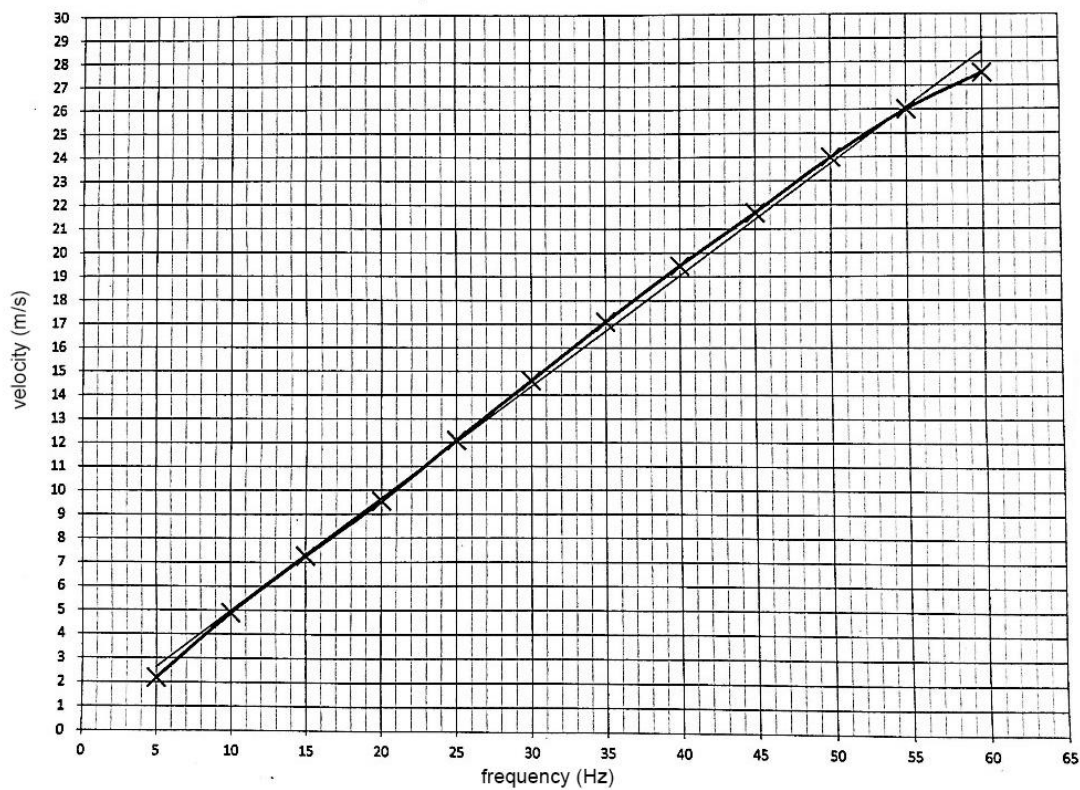
Figure 4.1 – Curve of flow velocity according to the frequency applied.

Figure 4.2 shows the equipment used and Figure 4.3 shows the testing section of this equipment. In Table 4.1 are listed the technical characteristics of the motor that drives the tunnel fan.

Figure 4.2 – Subsonic open-circuit suction type wind tunnel of LHMF from IPB.

Figure 4.3 – Test section of the used equipment.

Table 4.1 – Technical characteristics of the motor.

Frequency	60Hz
Potency	1.5 kW
Voltage	220-240 / 380-415 (V)
Amperage	5.5-5.9 / 3.2-3.4 (A)
R/min	2850 rpm

Figure 4.4 – Frequency inverter.

The model is fixed in the equipment using a bracket located at the bottom of the test section. In this support is also located a mechanism that allows the rotation of the modelto change its position according to the flow direction, and also a system for measuring the force acting on the model under test as shown in Figure 4.5.
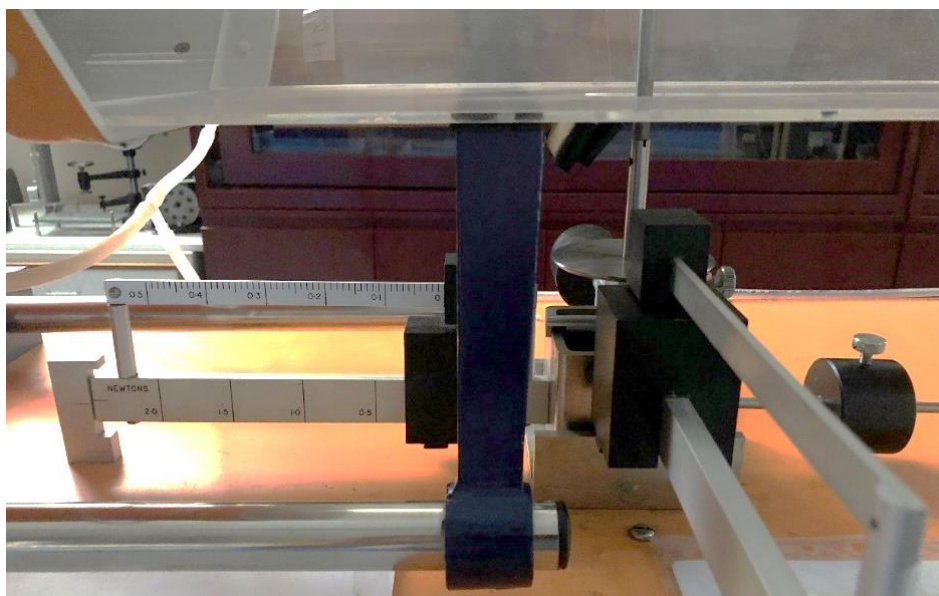
Figure 4.5 – Fixation and force measurement systems.

4.1.2. Modeling and 3D printing

To perform the wind tunnel experiments, the studied component was modeled using SOLIDWORKS™ and then, printed using a 3D printer. The equipment used for printing the model is the CEL™ RobxDual model.

Seeking to satisfy the limitations imposed by the equipment used for printing the model, some modifications were made in each module of the studied component in a way that the result was not influenced.

Therefore, the following modifications were made:

- The "contentor" and "fuste" were modeled solidly since the thin walls of the real model would not allow the printing of these components at the desired scale;
- The "fuste" was modeled in two separate parts due to its thin geometry;
- The lamp support was removed from the model because it did not exert significant influence when compared to the other components of the model;
- The elevator lift for photovoltaic modules that previously had a more complex base geometry was modeled as a simple cylinder and the fixture details that were present on it were removed;
- Photovoltaic modules and their support has been integrated into the elevator model;
- A support has been added to the model to allow it to be attached to the wind tunnel;
- Fittings have been added at the intersections of each part to allow for final assembly and to ensure their proper fixation.

Following these modifications, a scale factor of 1/34 was applied so that the size of the final model would be compatible with the size of the wind tunnel test section. Figure 4.6 shows the final components after modifications and scale factor application.
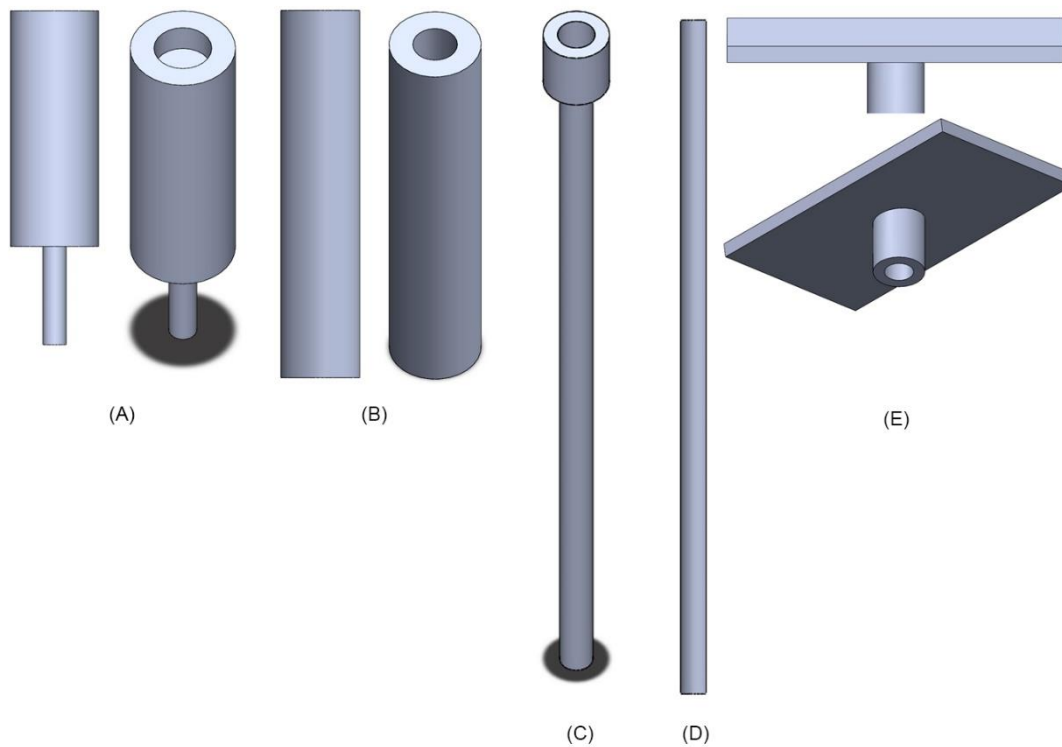
Figure 4.6 – Final components obtained where (A) is the support for fixation in the wind tunnel, (B) is the "contentor", (C) is the lower part of the "fuste", (D) is the higher part of the "fuste" and (E) is the solar panel with integrated lift.

To obtain the final model for the simulations, the parts must be mounted using the designed fittings. Following the nomenclature shown in Figure 4.6 the assembly sequence for obtaining the body shown in Figure 4.7 will be:

- Piece (B) is connected to the piece (A);
- Piece (C) is connected to the piece (B);
- Piece (D) is connected to the piece (C);
- Piece (E) is connected to the piece (D).
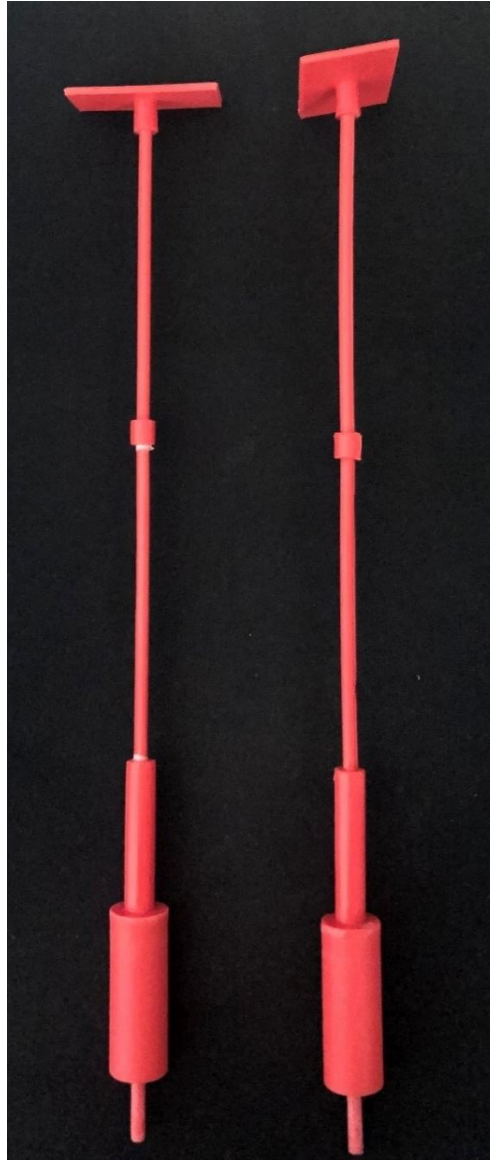
Figure 4.7 – Final model obtained after assembly.

4.1.3. Experimental procedures

To produce reliable results in wind tunnel experiments a basic sequence of steps that are described in this section must be followed.

Initially, the printed model was attached to the wind tunnel testing section using the bracket that was modeled as shown in section 4.1.2

To perform the experiments, the model was submitted to tests using five different positions for CD evaluation. After the fixation of the model, the opening that exists at the

bottom of the test section must be sealed using a plate available in the laboratory for this purpose as shown in Figure 4.8. The force measurement system must be calibrated to present a zero value when the wind tunnel is turned off as shown in Figure 4.9. This calibration is made using a set of weights present in the system itself.
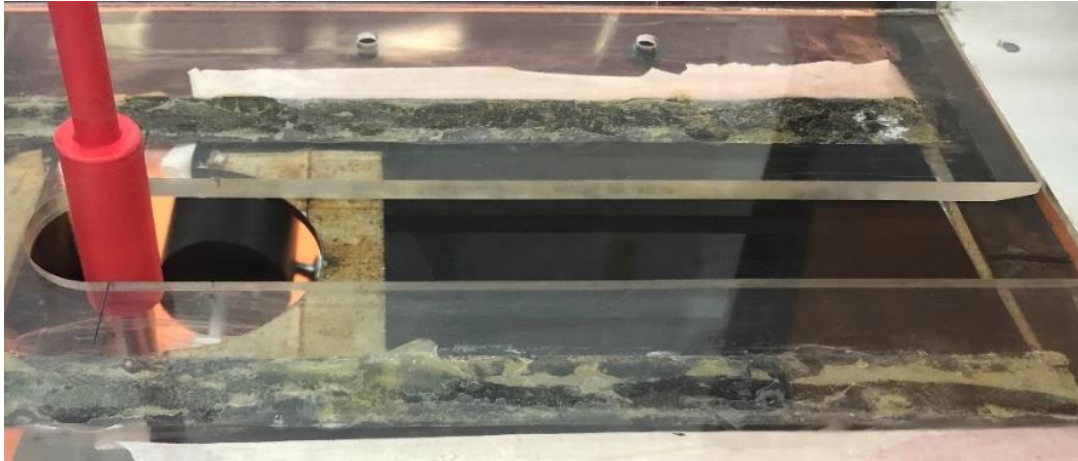
Figure 4.8 – Fixation of the sealing plate.
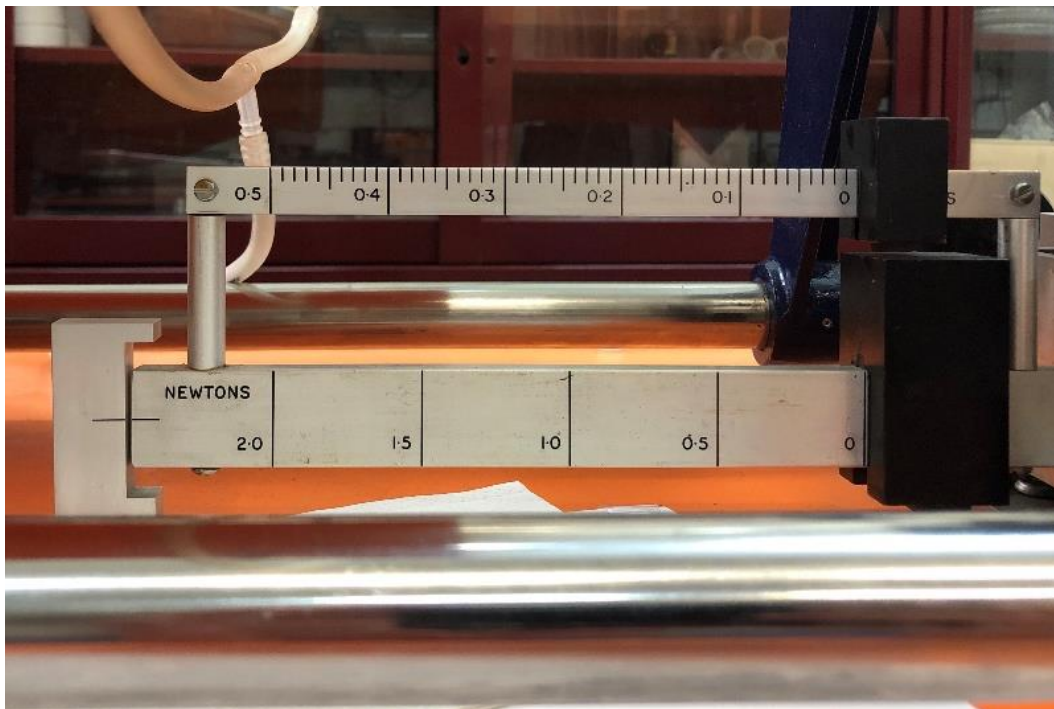
Figure 4.9 – Force measurement system calibrated.

The first position was made in a way that the largest dimension of the component that represents the photovoltaic module was aligned perpendicular to the flow direction. The

other positions considered were obtained using the fixation system to obtain the needed angles. In Figure 4.10 is shown a representation of the considered positions and in Figure 4.11 their application on the wind tunnel.
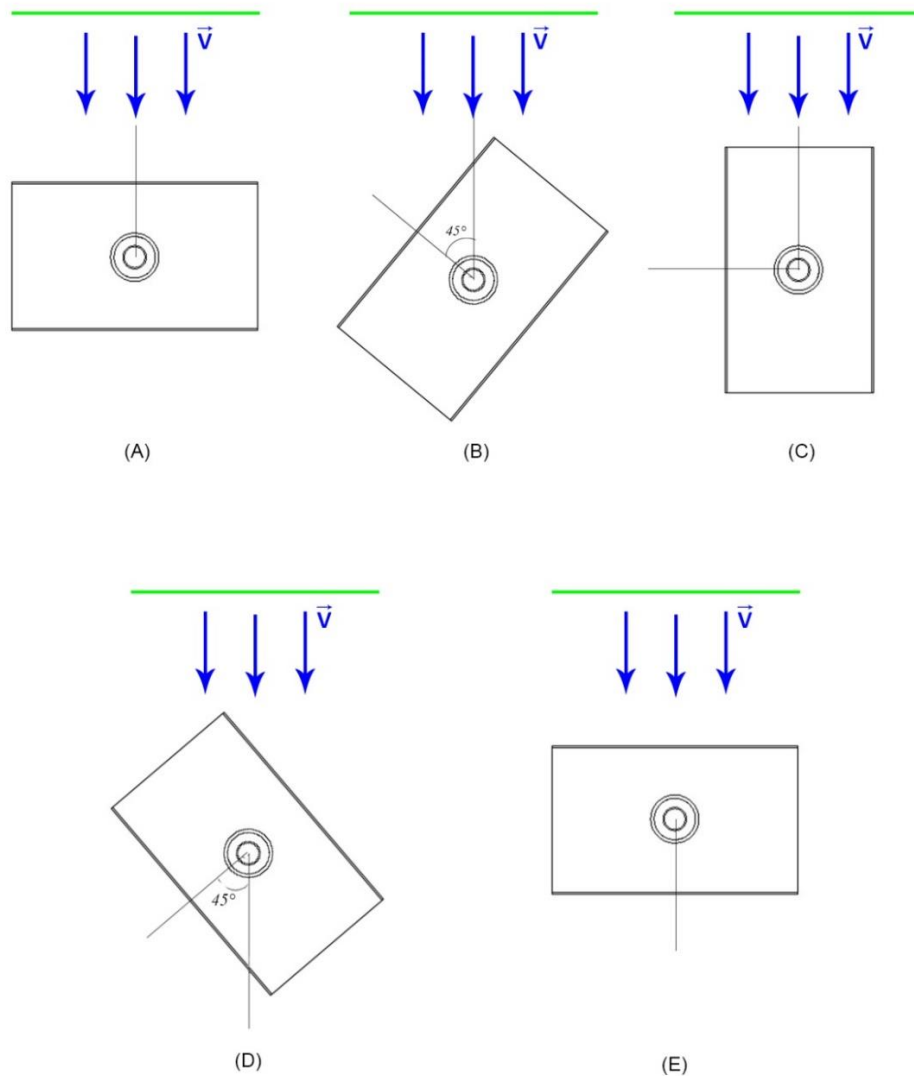
Figure 4.10 – Representation of the position used where (A) is the first position, (B) is the second position, (C) is the third position, (D) is the fourth position and (E) is the fifth position

To avoid the interaction with the boundary layer both in the bottom and top of the section test, a distance of 5 cm were adopted.

Figure 4.11 - Position used where (A) is the first position, (B) is the second position, (C) is the third position, (D) is the fourth position and (E) is the fifth position

The flow velocity to be used in the simulation can be determined using Eq. 2 in conjunction with Eq. 3. Using the data provided in section 3.3 the average wind speed values for terrain categories A and B for each type are presented in Table 4.2.

Table 4.2 – Average wind speed to each ground category.

	A					B				
	0	I	II	III	IV	O	I	II	III	IV
Vm (m/s)	34	32	27	20	15	38	35	30	23	13

Note that the critical case is for terrain type 0 in category B and therefore this will be the value to be considered for analysis.

However, the value obtained above cannot be directly applied at the flow input since the model used has a scale factor in relation to the real model. It is possible to compensate for this factor in velocity using the concept of similarity.

To do this, comparing the Reynolds number of the scaled model with the real model, we obtain

$$\frac{\rho_m * v'_m * L_m}{\mu_m} = \frac{\rho_p * v_m * L_p}{\mu_p}$$

$$v'_m = v_m * \left(\frac{\mu_m}{\mu_p}\right) * \left(\frac{\rho_p}{\rho_m}\right) * \left(\frac{L_p}{L_m}\right)$$

Since the flowing fluid is the atmospheric air in both the model under analysis and in the real model, the properties of this material remain constant, reducing the above equation to

$$v'_m = v_m * \left(\frac{34}{1}\right)$$

By the similarity method, the input speed to be used in the wind tunnel will be

$$v'_m = 1254,6 \, m/s$$

It is observed that to respect the principle of similarity, the velocity to be used in the analysis becomes very high, surpassing the equipment capacity. To allow the experiments to be carried out, the concept of incomplete similarity will be used and, to prove the CD behavior previously described, input speeds corresponding to frequencies from 5 Hz to 60 Hz with a range of 1 Hz between them will be used. The correlation between frequency and speed will be made from Eq. 7.

The speeds to be used are determined, four tests were performed for the mentioned speed set using each position chosen to obtain the acting force on the model in each one.

To obtain the value of C_D is necessary to solve Eq. 1 and for this, it is still necessary to know the frontal area exposed to the flow. This value varies for each position and can be determined using a sketch in SOLIDWORKS™ software as shown in Figure 4.12 to obtain the values shown in Table 4.3.

Table 4.3 – Frontal area exposed to the flow for each position in wind tunnel simulations.

POSITION	EXPOSED AREA (m^2)
I	0,00167970
II	0,00164247
III	0,00144661
IV	0,00164247
V	0,00167970

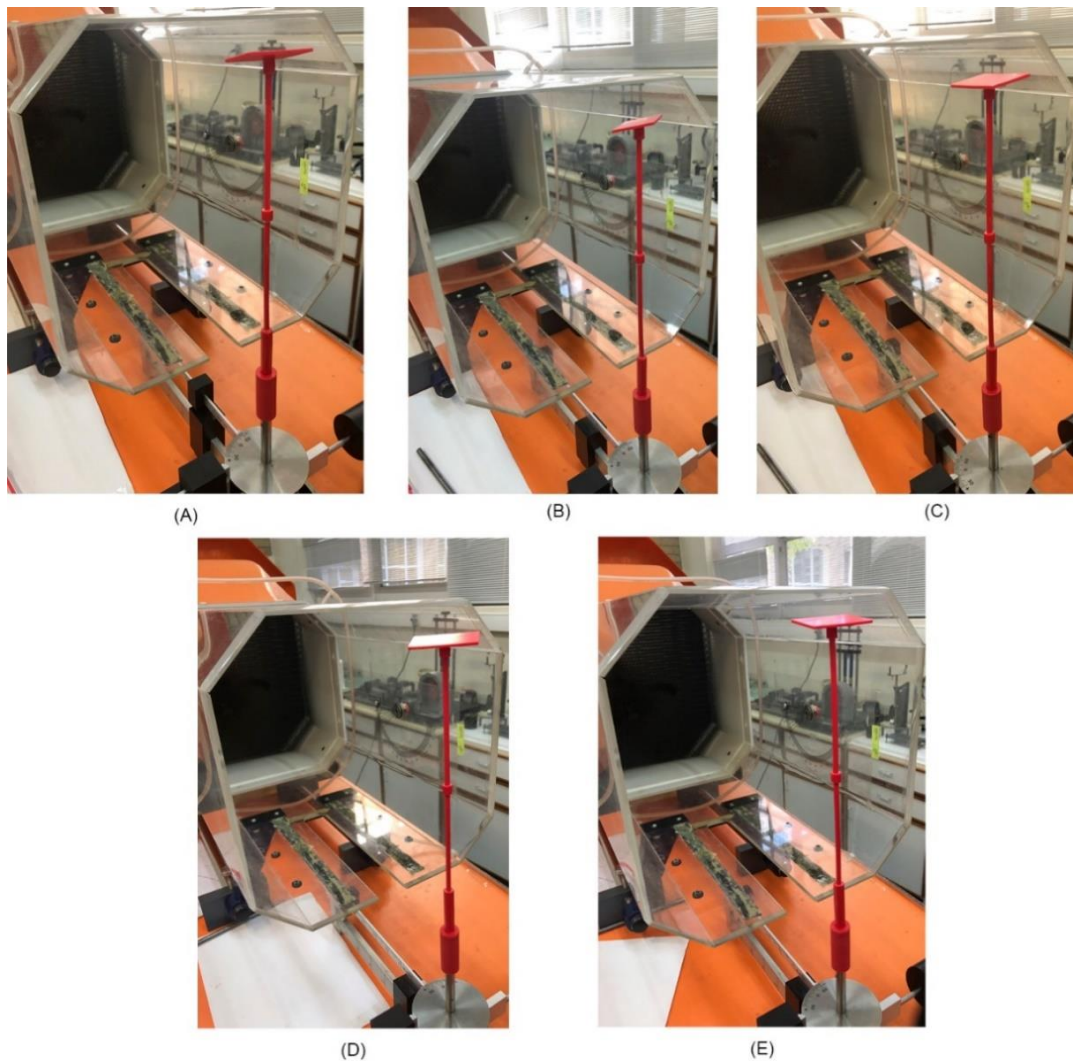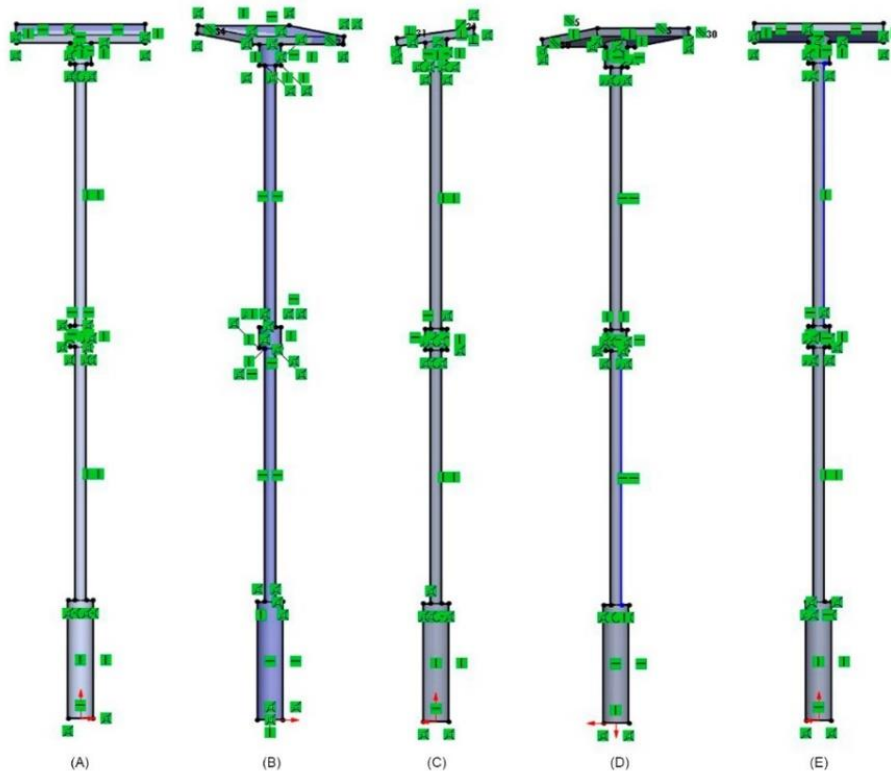**Figure 4.12** – Sketches used to determinate the exposed area where (A) is the first position, (B) is the second position, (C) is the third position, (D) is the fourth position and (E) is the fifth position.

Knowing the frontal area exposed to the flow Eq. 1 was solved using the forces obtained in each of the four experiments for all velocities for each position of the model. This resolution considered a room temperature of 25 C, the value of which represents the approximate temperature at which the experiments were performed.

To analyse the behavior of the fluid dynamic properties, it is also need to determinate the Reynolds number for each positiong given by Eq. 4. The characteristic length for each positiong can be determinated as shown in Figure 4.13 with the obtained values shown in Table 4.4.

Table 4.4 - Characteristic length for each position considered in wind tunnel simulations.

POSITION	CHARACTERISTIC LENGHT (m)
I	0,03
II	0,05
III	0,05
IV	0,05
V	0,03
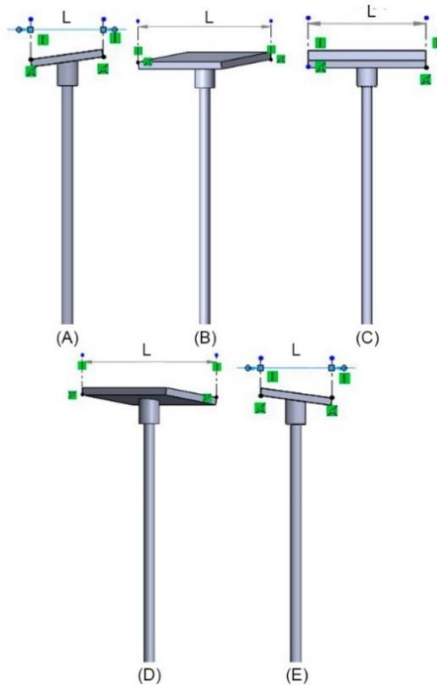
Figure 4.13 - Characterist length measurement for wind tunnel simulations where (A) is the first position, (B) is the second position, (C) is the third position, (D) is the fourth position and (E) is the fifth position.

4.2. Computational analyses

The structuring of a CFD analysis goes through several procedures to obtain more accurate and reliable results. This section describes the procedures used in this paper and the terms in the italic format are derived from ANSYS™ and SOLIDWORKS™ software and may differ for other platforms.

4.2.1. Component modeling

For computational analysis, the model that will be used will be modeled using the real dimensions of the studied product. Using SOLIDWORKS™ basing on a set of technical drawings of the product, it was modeled obtaining the result shown in Figure 4.14.

Figure 4.14 – Final model used in CFD analyses.

4.2.2. ANSYS™ analysis

The computational analysis procedure using ANSYS™ software requires a sequence of steps that must be performed in the order shown below to enable reliable results to be obtained.

4.2.2.1.   Simulation domain construction

The first step that must be done is the creation of the domain that involves the model using the software SOLIDWORKS™. To the first, third and fifth position considered the frontal plane was used to create the necessary sketch and for the second and fourth position, a reference plane oriented at 45° in relation to the frontal plane was used to the same purpose. To create the domain the following steps were done:

- From the center of the model, a rectangle was drawn to serve as the basis for the sketch of the simulation domain.;
- Using the feature extrude with a *midplane* orientation and the *merge results* option disabled, a body was created to delimit the simulation domain;
- Using the feature *combine* as *subtract* selecting as *main body* the object created in the previous step and as *bodies to combine* the objects that represent the illumination column.

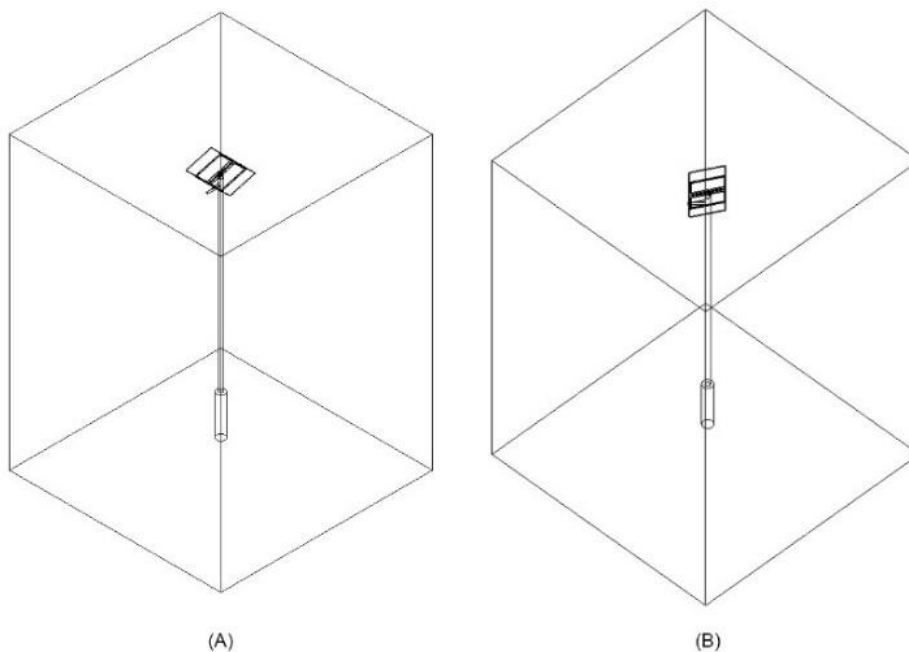The simulation domain created is shown in Figure 4.15.

Figure 4.15 – Simulation domain for (A) first, third and fifth position and (B) second and fourth position.

4.2.2.2.   Model importation

The model obtained needs to be saved in compatible formate to the software that will be used to perform the CFD analysis and in this work, the format *Parasolid (.x_t) was chosen.*

To perform the CFD analysis were used the *fluid flow (CFX)* tool that is part of the ANSYS™ software in *workbench*. The .x_t document is imported to the *geometry* space.

4.2.2.3.   Mesh generation

To perform the computational analysis, ANSYS™ software needs a mesh that can be automatically generated and the insertion of mesh controls can be used to improve the quality of the mesh.

For the geometry of the model to be studied, due to its dimensions, the student license of the software does not allow the creation of a thin mesh controls and, therefore, only the *face meshing* control was inserted in the faces that represent the simulation domain.

Despite the lack of mesh controls, the result presented in this paper is shown as an unstructured mesh with small deformations in the regions of greatest interest and can be considered as a good quality mesh. The quality value of the mesh can be analysed inside the software during its creation.

The global parameters of the obtained mesh are shown in Table 4.5 and, since the geometry is identical for all considered positions, these parameters repeats in every model.

Table 4.5 – Global parameters of the mesh obtained.

Physics preference	CFD
Solver preference	CFX
Element order	Linear
Nodes	93018
Elements	516615
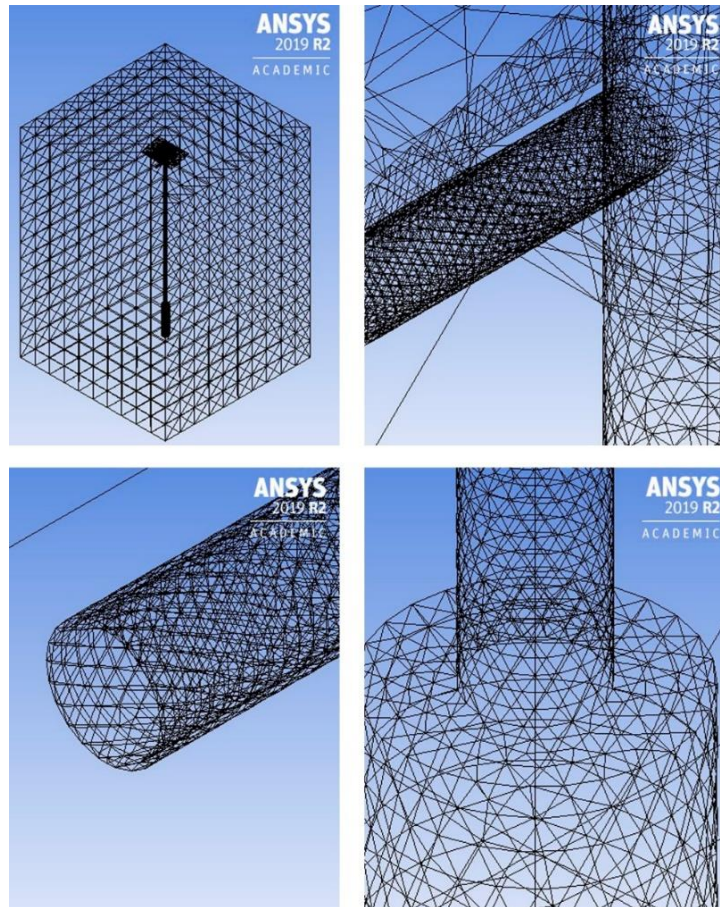
Figure 4.16 – Final mesh obtained.

4.2.2.4. Definition of the boundary condition and initial condition

With the domain region correctly determined, it is possible to define the boundary conditions and initial conditions that are required for CFD analysis. Firstly, using the *design modeler* tool four *named selections*: inlet, outlet, walls, and body whose positions can be viewed in Figure 33 to Figure 36.

Using the *cfx-pre* tool from *setup*, the boundary conditions were created using the *boundary* tool as described below.

To represent the flow entry, the boundary *inlet* was created and applied to the *named selection* equally named. This boundary was defined as a velocity entry.

The velocity that will be used is the same that was previously calculated but this time, as the body doesn't use a scale factor the velocity value of 38 m/s for the critical case can be directly applied.

To verify the behavior of C_D, velocities values between 2 m/s and 38 m/s with a range of 2 m/s between then were used as shown in Table 4.6. Figure 4.17 shows the location of the described boundary for each position.

Table 4.6 – Inlet velocities used in CFD analysis.

Análise	Velocidade (m/s)
I	2
II	4
III	6
IV	8
V	10
VI	12
VII	14
VIII	16
IX	18
X	20
XI	22
XII	24
XIII	26
XIV	28
XV	30
XVI	32
XVII	34
XVIII	36
XIX	38

To the flow exit, the boundary *outlet* was created and applied to the *named selection* equally named. This boundary was defined as a pressure output. The required relative pressure was defined as 0 Pa once the body is located in an open area and exposed to the atmospheric pressure. Figure 4.18 shows the location of the described boundary for each position.

To the walls, the boundary *walls* were created and applied to the *named selection* equally named. This boundary was defined as a *free-slip wall* once the lighting column is located

in an open area. Figure 4.19 shows the location of the described boundary for each position.

The last boundary created is the *body* and was applied to the *named selection* equally named. This boundary was defined as a *non-slip wall* to represent a solid body. Figure 4.20 shows the location of the described boundary for each position.

Table 4.7 – Configurations used for each boundary condition.

Boundary condition	Type	Configuration
inlet	Velocity entry	Normal velocity according to Table 4.6
outlet	Pressure exit	Relative pressure of 0 Pa
walls	Free-slip wall	--
body	Non-slip wall	--

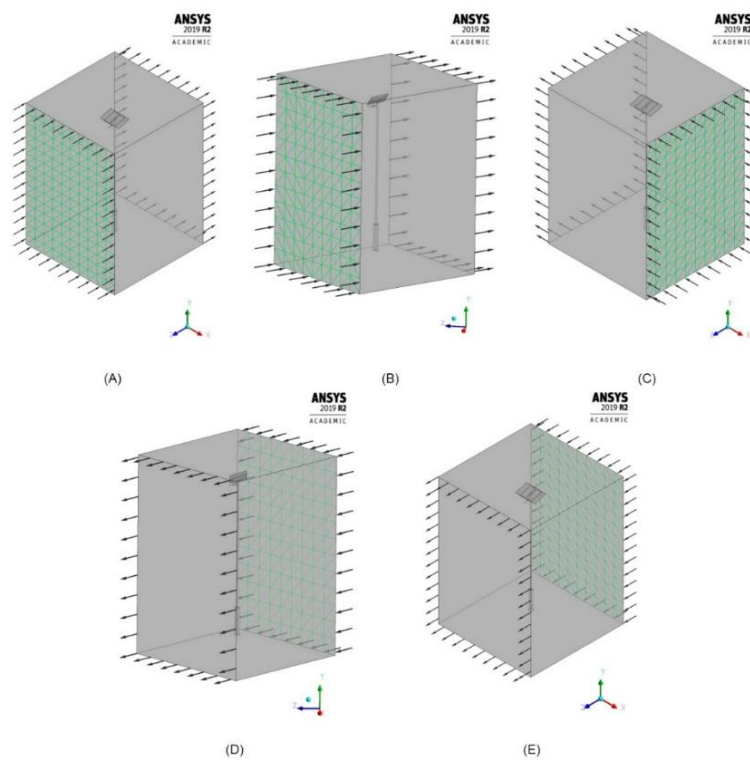**Figure 4.17** – Inlet boundary position for (A) position I, (B) position II e (C) position III (D) position IV and (E) position V.
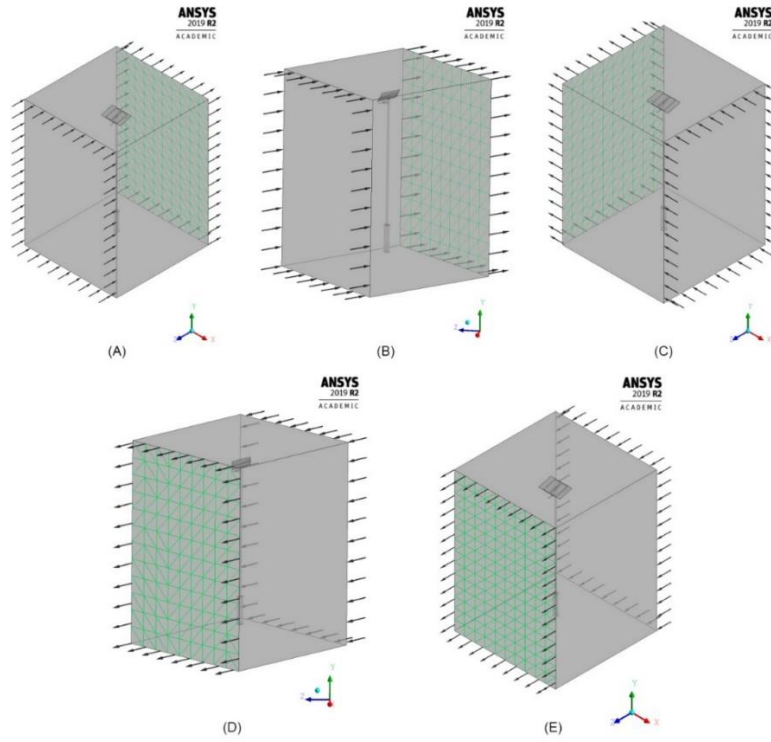
Figure 4.18 - Outlet boundary position for (A) position I, (B) position II e (C) position III (D) position IV and (E) position V.
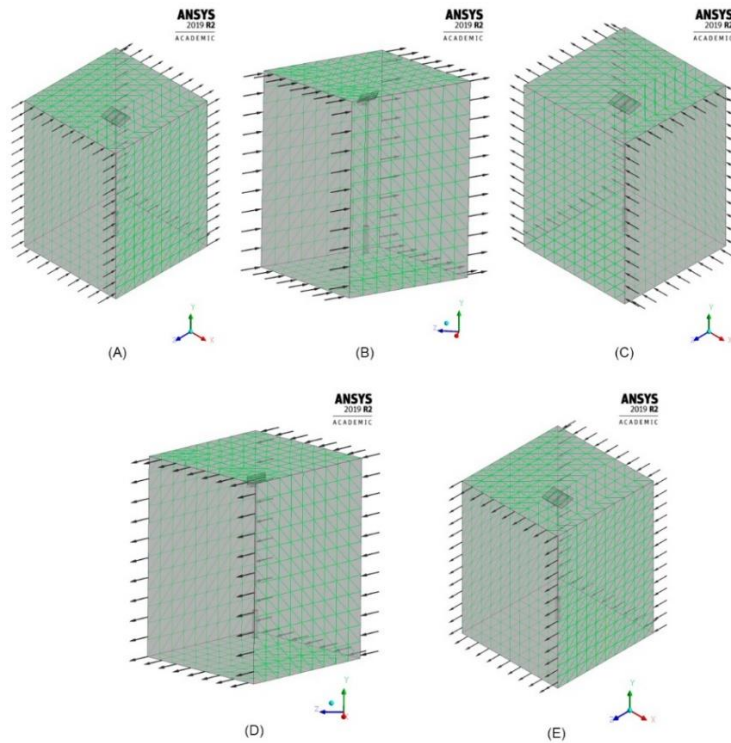

Figure 4.19 - Walls boundary position for (A) position I, (B) position II e (C) position III (D) position IV and (E) position V.

46
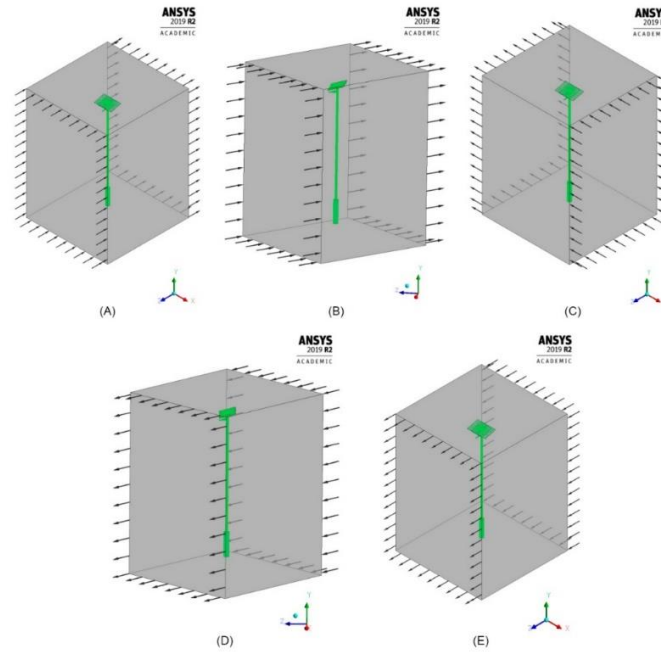
Figure 4.20 - Body boundary position for (A) position I, (B) position II e (C) position III (D) position IV and (E) position V.

In Table 4.7 are resumed the conditions that were used and its configurations.

The domain was defined as fluid and the flowing material was set as air at 25°C. Using the *global initialization* tool, the initial conditions were set using *cartesian coordinates* to set the flow initial velocity. In this process, the orientation of the body according to the *global coordinate system* needs to be analyzed to insert a sign if necessary to represent correctly the flow direction. Table 4.9 resumes the values inserted.

The determination of the frontal area for solve the Eq. *1* can be done in the same way as for wind tunnel simulations. The delimited areas are shown in Figure 4.21 and their values are gathered in Table 4.8.

Table 4.8 – Frontal area exposed to the flow for each position in CFD analyses.

Position	Exposed area (m^2)
I	1,98
II	1,88
III	1,57
IV	1,88
V	1,98

Table 4.9 – Cartesian components of the flow velocity used as the initial condition for each position.

Position	Velocity component		
	U (m/s)	V (m/s)	W (m/s)
I	0	0	Integral velocity value shown in Table 4.6 with a negative sign.
II	The component at 45 of the velocities values shown in Table 4.6 with a negative sign.	0	The component at 45 of the velocities values shown in Table 4.6 with a negative sign.
III	Integral velocity value shown in Table 4.6 with a negative sign.	0	0
IV	The component at 45 of the velocities values shown in Table 4.6.	0	The component at 45 of the velocities values shown in Table 4.6.
V	0	0	Integral velocity value shown in Table 4.6.

At the end of the analyses, it is possible to obtain the values of the forces that are acting on the body using the *function calculator tool* in *cfd-post* and then calculate the values for C_D for each position using the methods previously discussed.
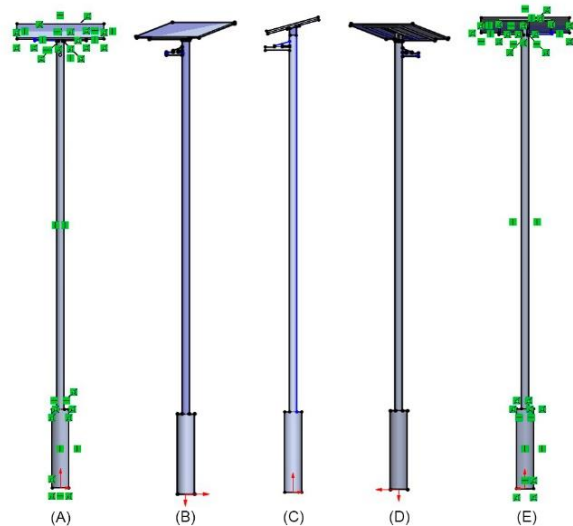
Figure 4.21 - Sketches used to determinate the exposed area where (A) is the first position, (B) is the second position, (C) is the third position, (D) is the fourth position and (E) is the fifth position.

48

As with wind tunnel simulations, the Reynolds number must be calculated. The characteristic length for each positiong can be determined as shown in Figure 4.22 with the obtained values gathered in Table 4.10.

Table 4.10 - Characteristic length for each position considered in CFD analyses.

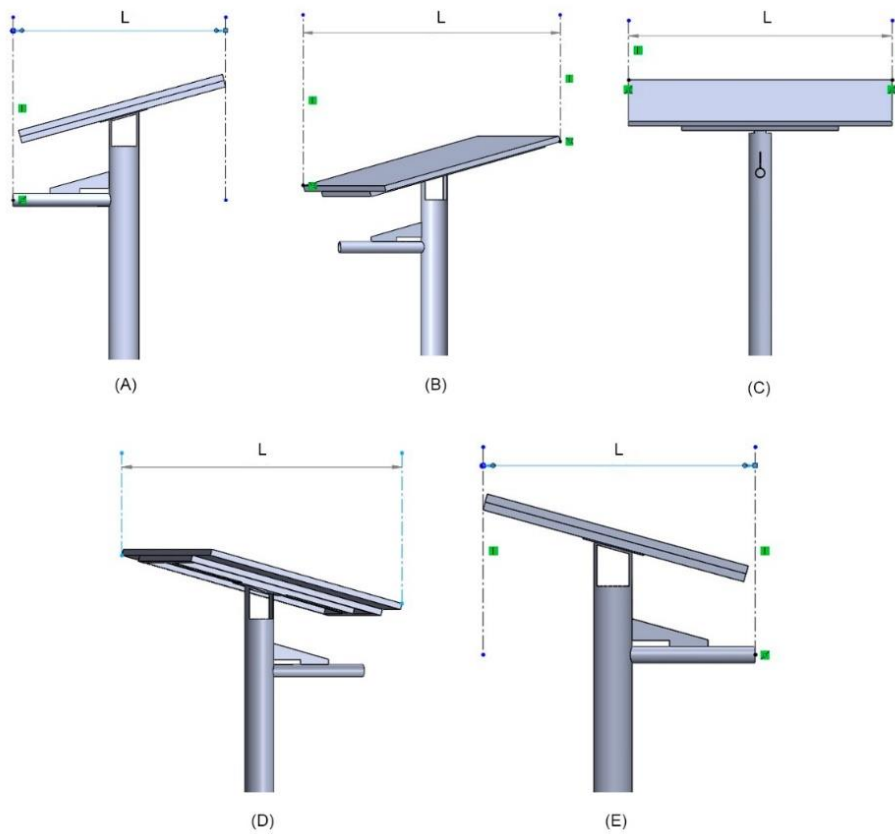| POSITION	CHARACTERISTIC LENGTH (m)
I	1,00
II	1,36
III	1,67
IV	1,36
V	1,00

Figure 4.22 – Characterist length measurement for CFD analyses where (A) is the first position, (B) is the second position, (C) is the third position, (D) is the fourth position and (E) is the fifth position.

4.2.3. SOLIDWORKS™ flow simulation analysis

The CFD analysis procedure using SOLIDWORKS™ software is simpler than that presented in section 4.2.2 for ANSYS™ software. Using the final geometry shown in Figure 4.14 and activating the Flow Simulation add-in it is possible to have access to the necessary tools to perform the analysis and through the *Wizard* tool, an analysis can be created in a simplified way:

- System units must be defined. For the present work the international unit system, SI, (m, kg, s) was used.
- The type of analysis flow should be defined. For the present work, an external flow was defined to represent the application of the studied product. At this stage, the necessary configurations were still selected so that the software excludes internal spaces without flow from the analysis.
- Flow fluid must be defined. For the present work, Air with the properties predefined by the software was selected in a subsonic regime that considers both laminar and turbulent flow.
- Domain walls must be defined. For the present work, they were defined as adiabatic and without roughness to represent an open environment.
- The initial conditions of the simulation must be defined. For the present work, the standard thermodynamic properties of the software were maintained and for the velocity values, the same settings shown in Table 4.9 were used.

Table 4.11 below resumes the parameters used in each step previously described.

Table 4.11 – Configurations of the CFD analyses using SOLIDWORKS™ Flow.

PARAMETER	CHARACTERISTIC
Unity system	SI (m, kg, s)
Analysis type	External; exclude cavities without flow condition; delete inner spaces
Fluid	Air (gas) with software preset properties
Walls	Adiabatic; roughness of 0 μm
Initial conditions	Thermodynamic parameters predefined by the software; speed parameters according to *Table 4.9*

After the analysis is created, the computational domain must be adjusted to encompass the entire model. This adjustment can be done through Cartesian coordinates or through the guides as shown in Figure 4.23.
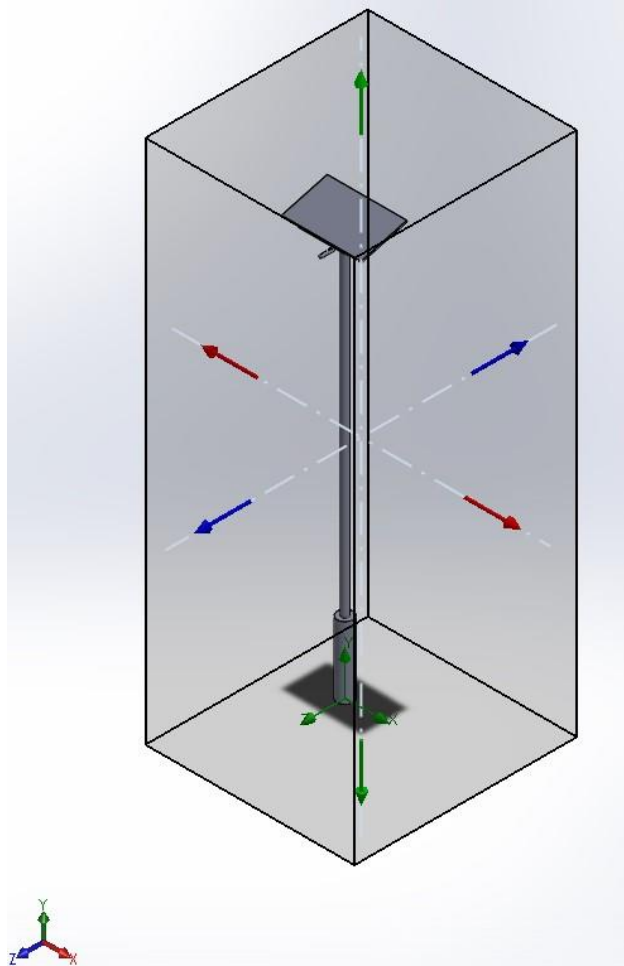
Figure 4.23 – Definition of the computational domain used for SOLIDWORKS™ software.

To obtain the drag force its is possible to use the *Goals* tool to request the calculation of this parameter and then calculate the values for C_D for each position using the methods previously discussed.

The values for the characterist lengTh used to calculte the number of Reynolds are the same as those used in the previous section gathered in Table 4.10.

5.   Results and discussions

The results obtained for both wind tunnel simulations and computational analysis are described in the following sections.

5.1.   Obtained results for wind tunnel simulations

Using the methodology described in section 4.1, it is possible to use the collected data from the experiments to determinate the behavior of the drag force acting on the body in all position considered. For all experiments, the obtained results are shown in Figure 5.1 to Figure 5.5.

Figure 5.1 - Drag force behavior versus the Reynolds number for position I.

Figure 5.2 - Drag force behavior versus the Reynolds number for position II.
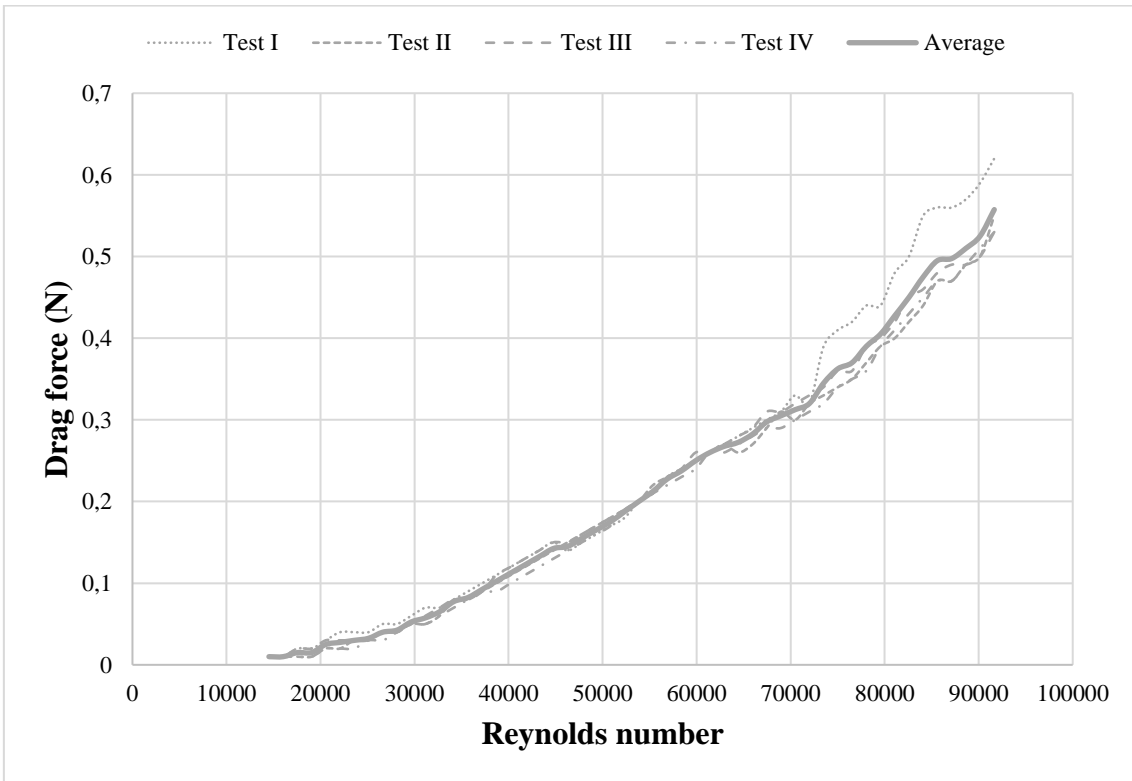
Figure 5.3 - Drag force behavior versus the Reynolds number for position III.
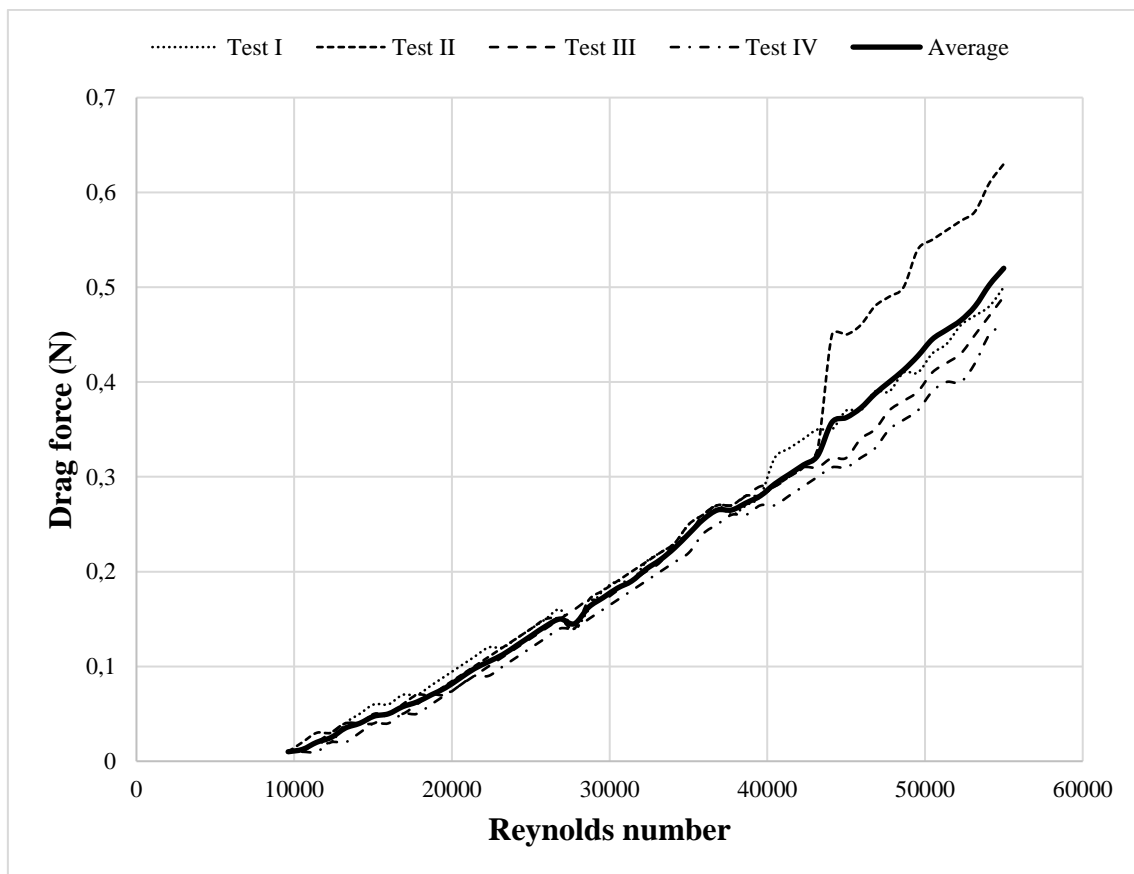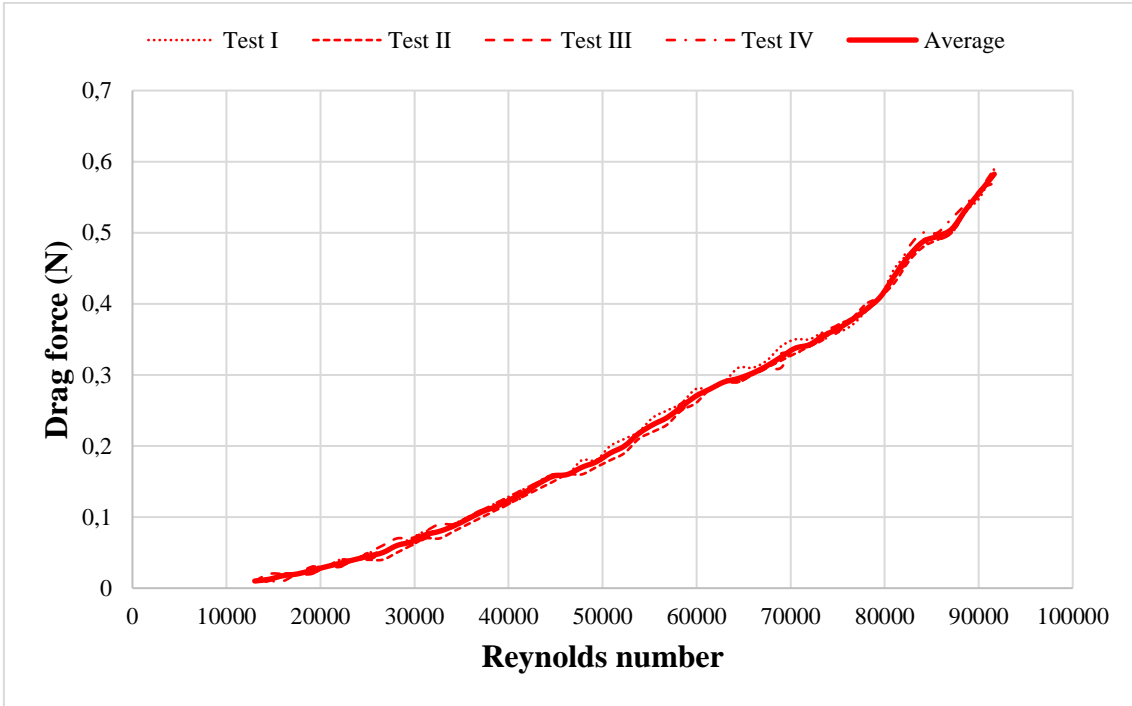
53
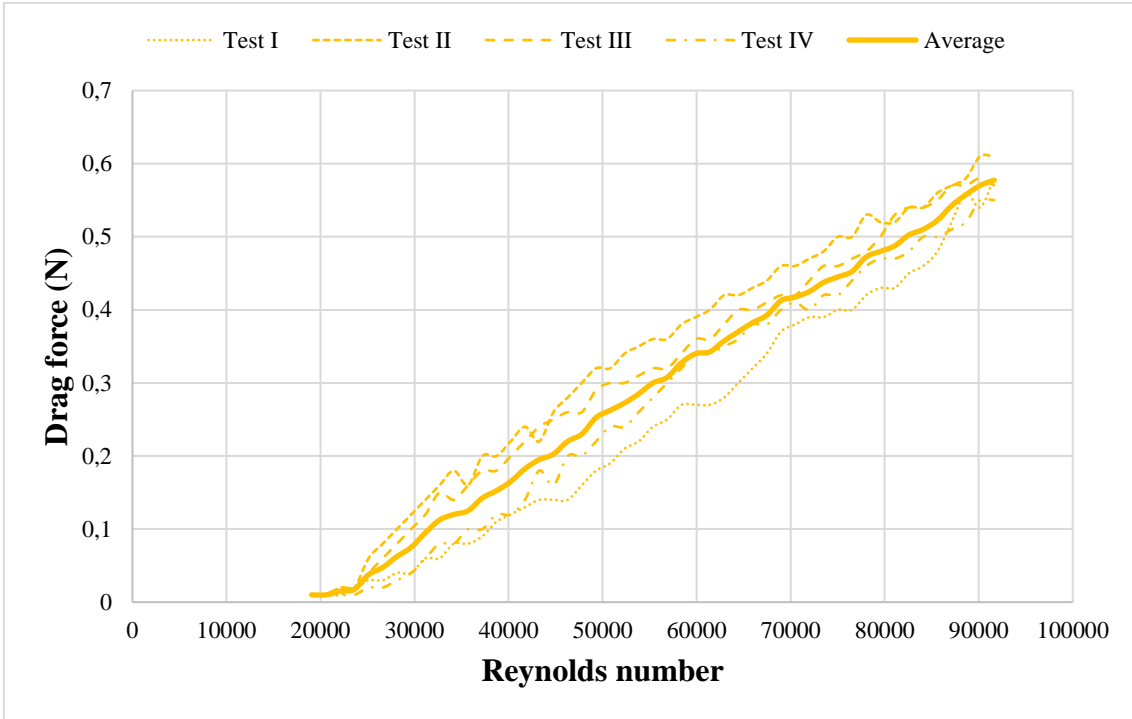
Figure 5.4 - Drag force behavior versus the Reynolds number for position IV.
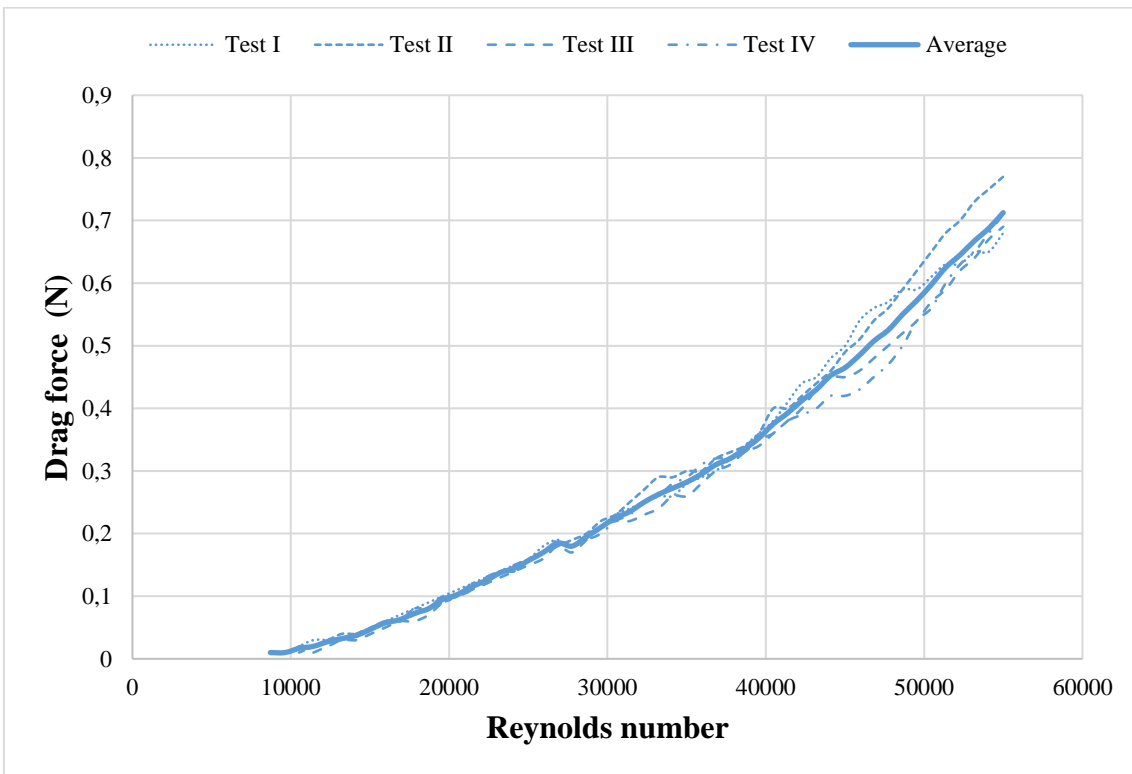
Figure 5.5 - Drag force behavior versus the Reynolds number for position V.

For all the averages values of drag force, the behavior shown in Figure 5.6 can be observed.
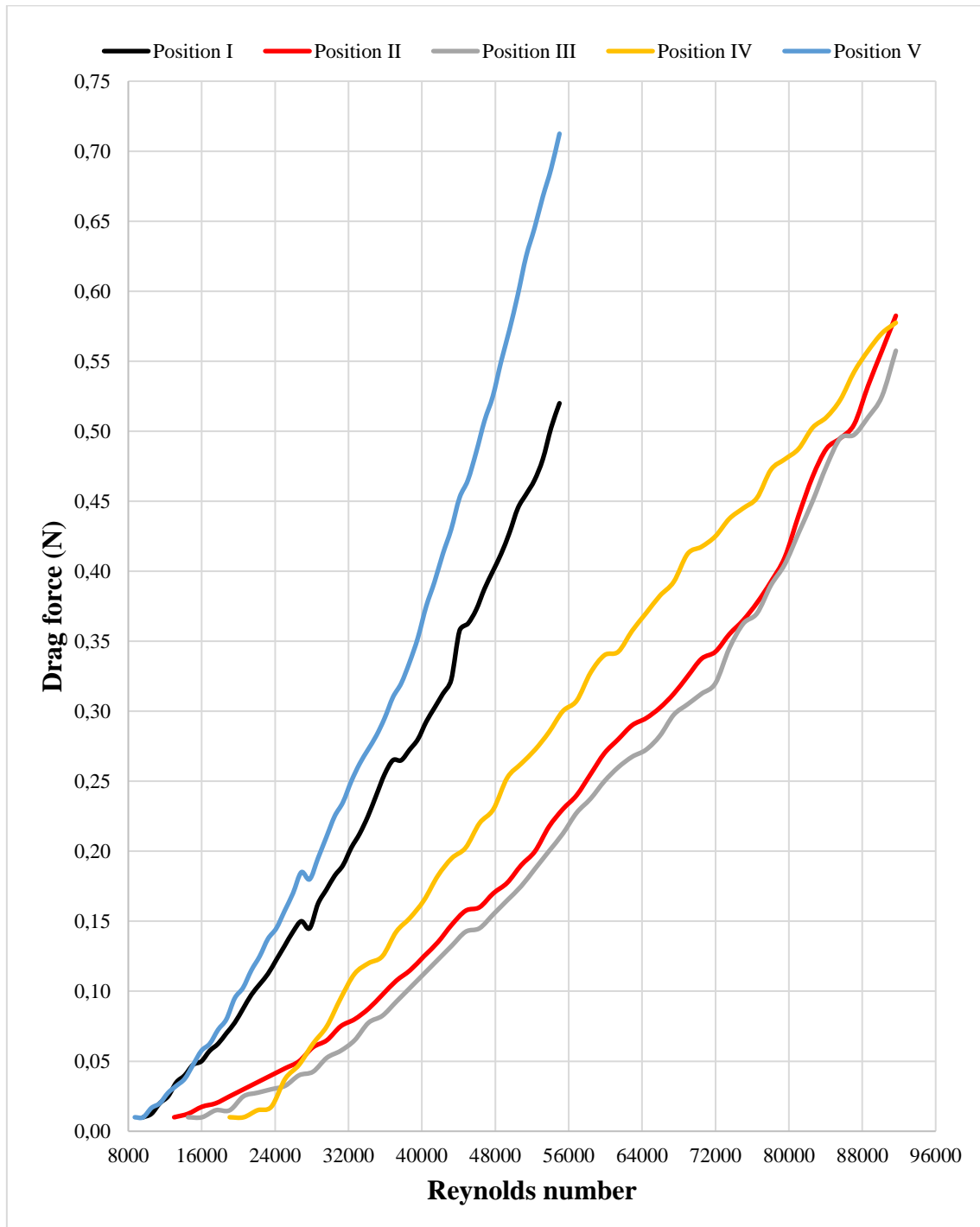
Figure 5.6 - Average value of drag force versus the Reynolds number for all considered positions.

Solving Eq. *1* using the data collected from wind tunnel, it is possible to determinate the behavior of C_D for each considered position. The obtained results are shown in Figure 5.7.
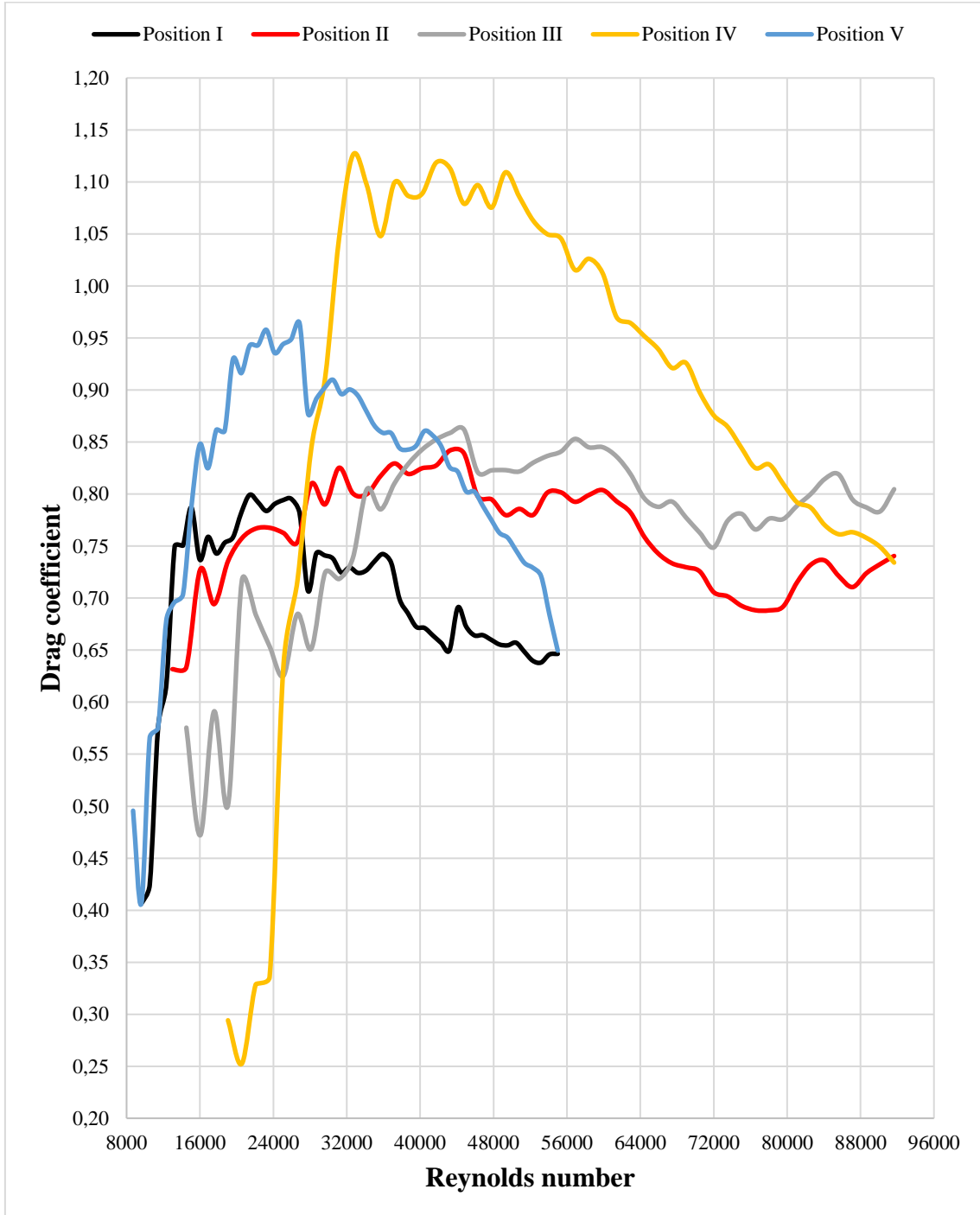
Figure 5.7 - Drag coefficient obtained for each considered position using wind tunnel simulations.

5.1.1. Results discussion for wind tunnel simulations

In Figure 5.6, the average values of the drag force for the five position considered are gather and it is possible to see the crescent behavior that this parameter presents once the Reynolds number increases, i.e. the higher the flow velocity, the greater the drag force present.

The unstable behavior of the obtained values can be explained by the vibrations that occurred in the model during the experiments. In addition to this vibration, the model was printed using a material with low mechanical strength which caused a continuous deformation in the model as the flow velocity increased. This deformation is shown in Figure 5.8 for all considered position.
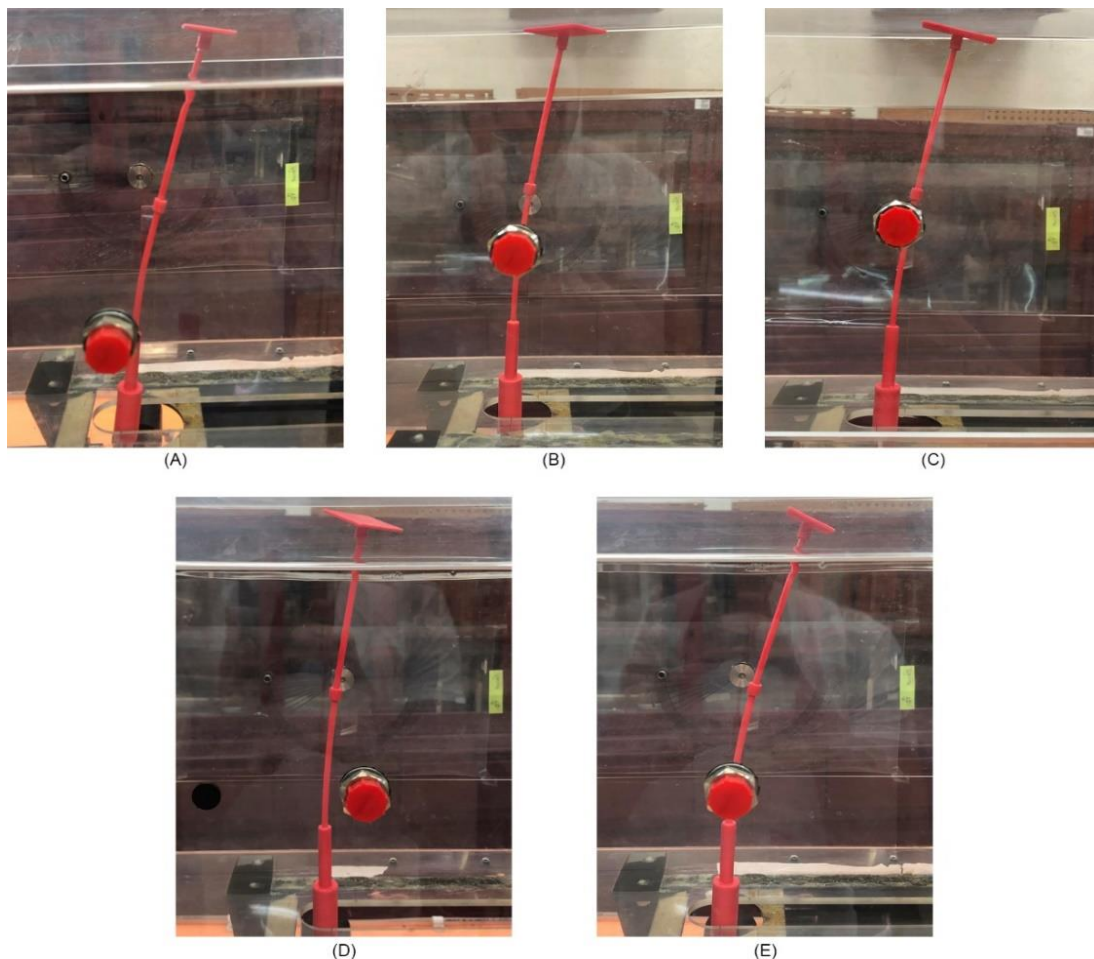
Figure 5.8 - Deformations on the models during the realization of the wind tunnel simulations to (A) position I, (B) position II, (C) position III, (D) position IV and (E) position V.

As stated, the drag forces are linked to the frontal area exposed to the flow and therefore, for equal areas expected equal or very close values for the drag force. Comparing the positions I and V shown in Figure 5.9 which have equal frontal areas, it is possible to notice that at the beginning of the experiment the force values are really close, but they start to distance as the flow velocity increases.

This distance can be explained by the deformation suffered by the model that was slightly higher for position I leading to smaller forces as shown in Figure 5.10. The difference in deformation suffered can be explained by changes in the set of forces that result in drag force due to the change in model position.
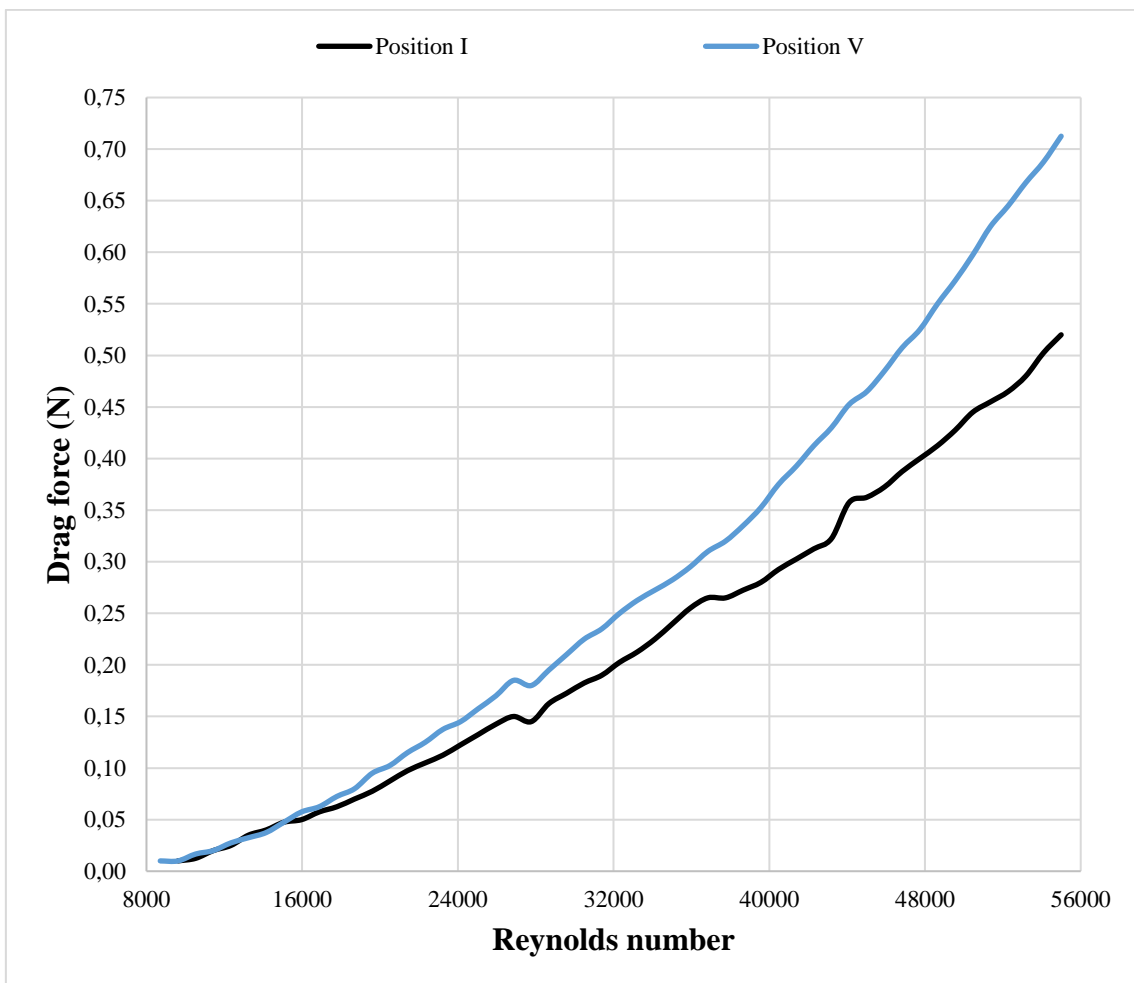
Figure 5.9 - Drag force behavior versus the number of Reynolds for position I and V.
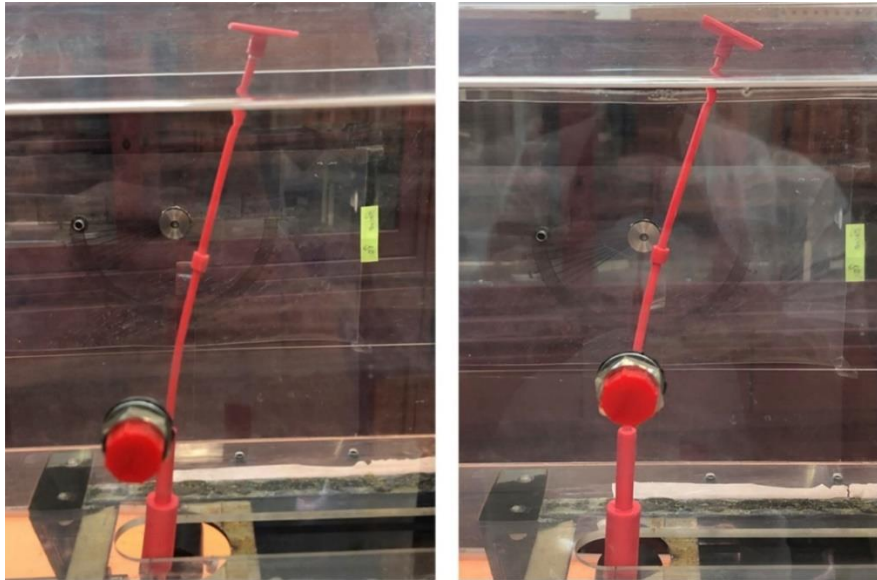
Figure 5.10 - Deformation on the model for position I and V.

The same comparation can be made using the position II and IV shown in Figure 5.11, where the initial frontal areas were the same, but the deformation shown in Figure 5.12 suffered by the model in position II were higher and therefore, the drag force values were lower. For this positions, at the end os the simulations the vibration effect starts to decrease which caused the values of forces measured for both positions to come closer
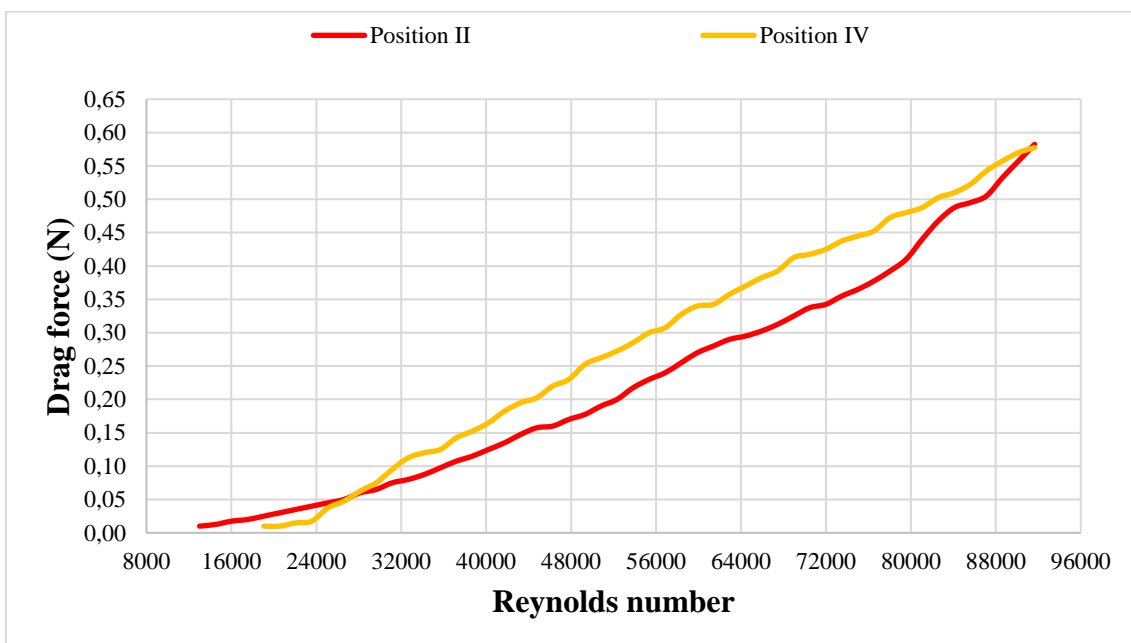
Figure 5.11 - Drag force curves for position II and IV.
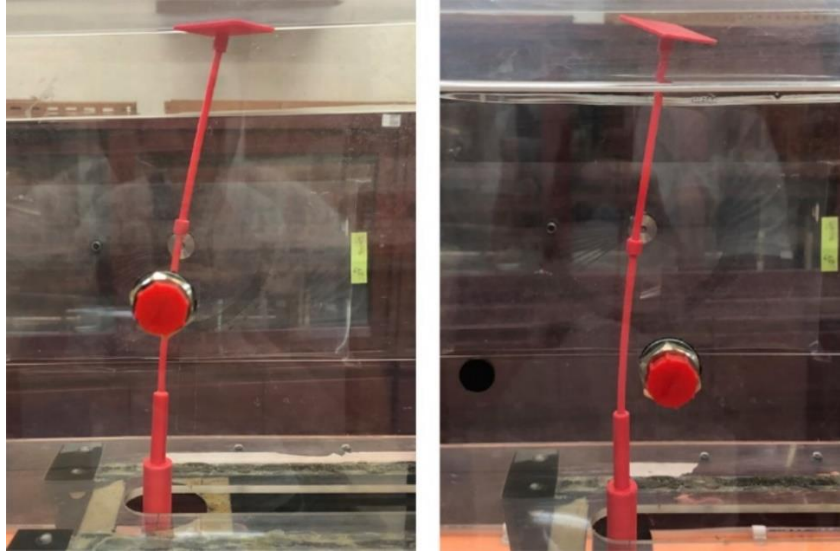
Figure 5.12 - Deformation on the model for position II and IV.

For the C_D values it is possible to notice a greater influence of the vibration levels and the deformation of the model for lower flow velocities.

As predicted, wind tunnel tests using the principle of incomplete similarity do not yield good results for low speeds and only results close to the maximum capacity of the equipment can be extrapolated as true for the full scale model are considered reliable.

This statement becomes evident when analyzing the C_D curves shown in Figure 5.7 where where there is an inconsistency in the behavior of this property for the lower speeds used in the equipment.

By analyzing separately the final velocities of the flow shown in Figure 5.13, it is possible to see an adequacy of the results to the theoretical postulates which also proves the application of the principle of incomplete similarity. At this point, the C_D value for positions with similar frontal area becomes equal, or very close.
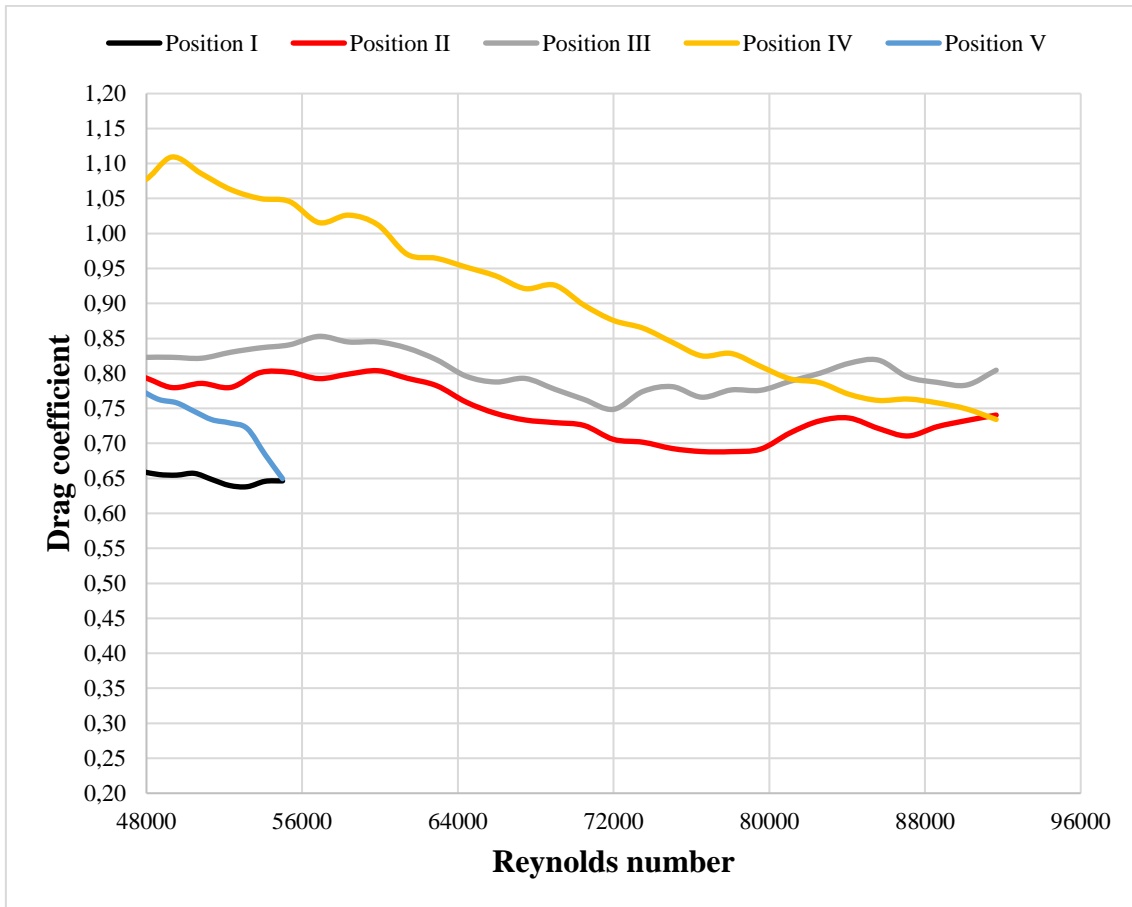
Figure 5.13 - C_D values for the final flow velocities of the wind tunnel experiments.

5.2.   Obteined results for CFD analyses

For CFD analyses, two different results were obtained, one for each software that was used.

5.2.1. Obtained results for ANSYS™ software

A CFD analysis using ANSYS™ softwares allows the visualization of the streamlines for the flow studied and the generation of pressure contours on the modelbody. For each considered position, the streamlines created and the pressure contour are shown in Figue 5.14.

With these lines, it is possible to see the formation of the wake turbulence on the region opposite the flow. This phenomena can explain the vibration suffered by the model during the wind tunnel simulations.

Using the methodology previously discussed, it is possible to determinate the behavior of the drag force acting on the body in all position considered. The results obtained are shown in Figure 5.15.

Figue 5.14 - Streamlines obtained with ANSYS™ software where (A) is the first position, (B) is the second position, (C) is the third position, (D) is the fourth position and (E) is the fifth position.

Figure 5.15 - Drag force values for each position considered using CFD analysis in ANSYS™.

Solving Eq. 1 using the data collected from ANSYS™ analysis, it is possible to determinate the behavior of C_D for each considered position. The obtained results are shown in Figure 5.16.

Figure 5.16 - C_D values for each position considered using CFD analysis in ANSYS™.

5.2.1.1.   Results discussion for ANSYS™ software

Using the streamlines and the pressure contour, is possible to compare the oposite behavior that pressure and flow velocity present. For the high pressure points the velocity presents the lowest values demonstrating the stagnation point previously discussed For the different position considered, it is possible to see the influnce that the model position have in the flow behavior specially in the wake turbulence region

In a CFD analysis, the deformation that occurred in the wind tunnel simulation is no longer a problem once the solver does not consider this phenomenon, which means that a good CFD software can deliver reliable results without interference.

As is possible to see in Figure 5.15, the behavior of the drag force values is according to what is expected once its values decrease when the frontal area decrease with the position change and therefore, position III has the lowest values for the drag force once its frontal area is the smallest between all position considered.

Analysing the position I and V, once their frontal areas are equal the values for the drag force should also be equal, or very close to. This behavior can be seen in Figure 5.15 and, once they have the biggest frontal area of the considered positions, they also have the higher drag force values.

For position II and IV the same behaviour occurs, and their drag force values are higher than the values for position III but loer than the values for position I and V.

For the drag coefficient, the behavior shown in Figure 5.16 can be explained through an analysis of the values applied in Eq. 1. For position I to II, the drag force values presented a large decrease than the frontal area, wich causes a decrease on the C_D value. For position III, once the frontal area for this position is the smallest between the considered positions it presentes the highest values for C_D.

In Figure 5.16 is also possible to see that for position I and V the values for C_D are close to each other as expected once their frontal area is equal and the force values have a small diference. The same behavior is noticed to the postioning II and IV.

5.2.2. Obtained results for SOLIDWORKS™ software

Equally as done for the other methods, Using the methodology previously discussed, it is possible to determinate the behavior of the drag force acting on the body in all position considered. The results obtained are shown in Figure 5.17.
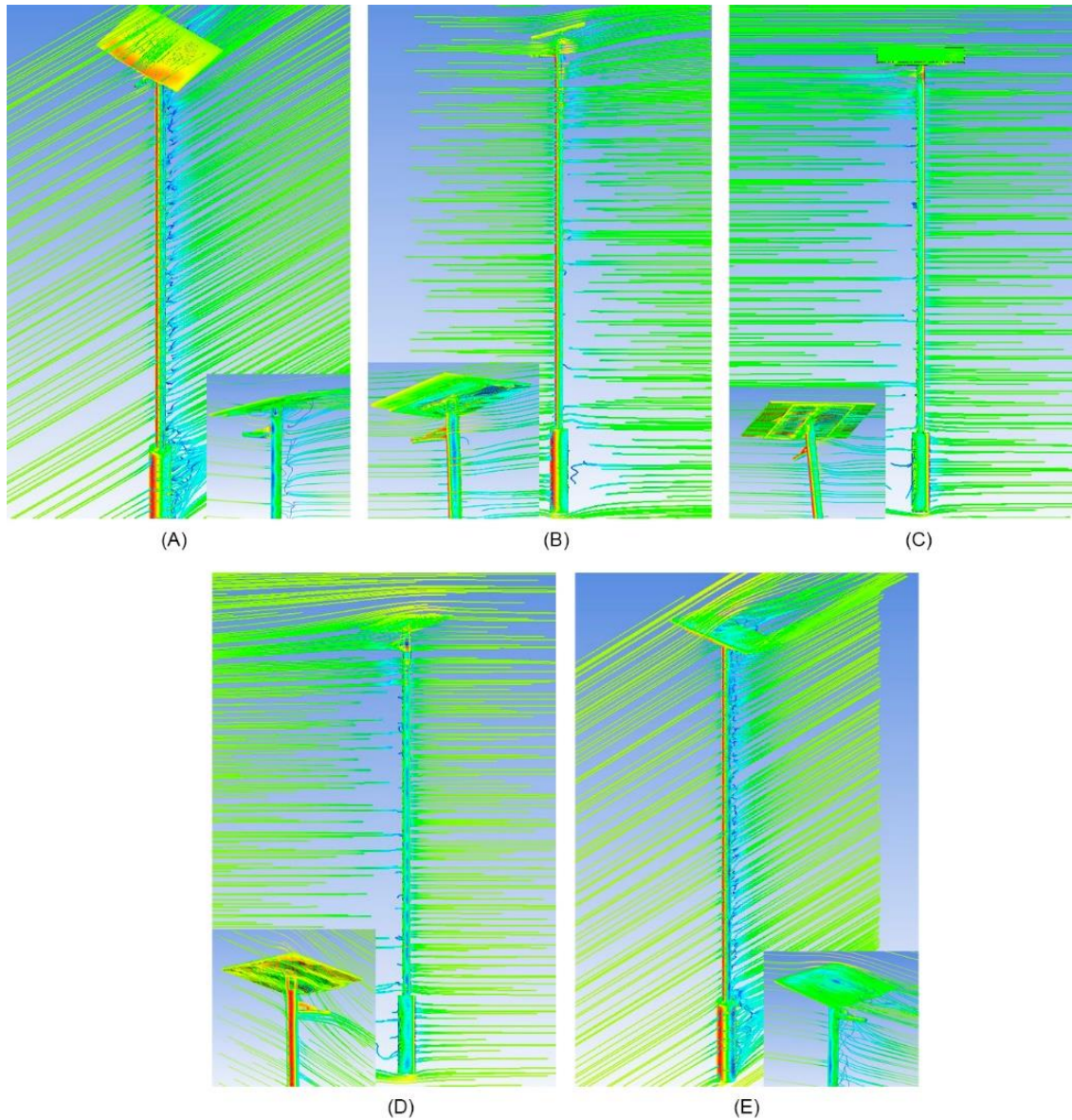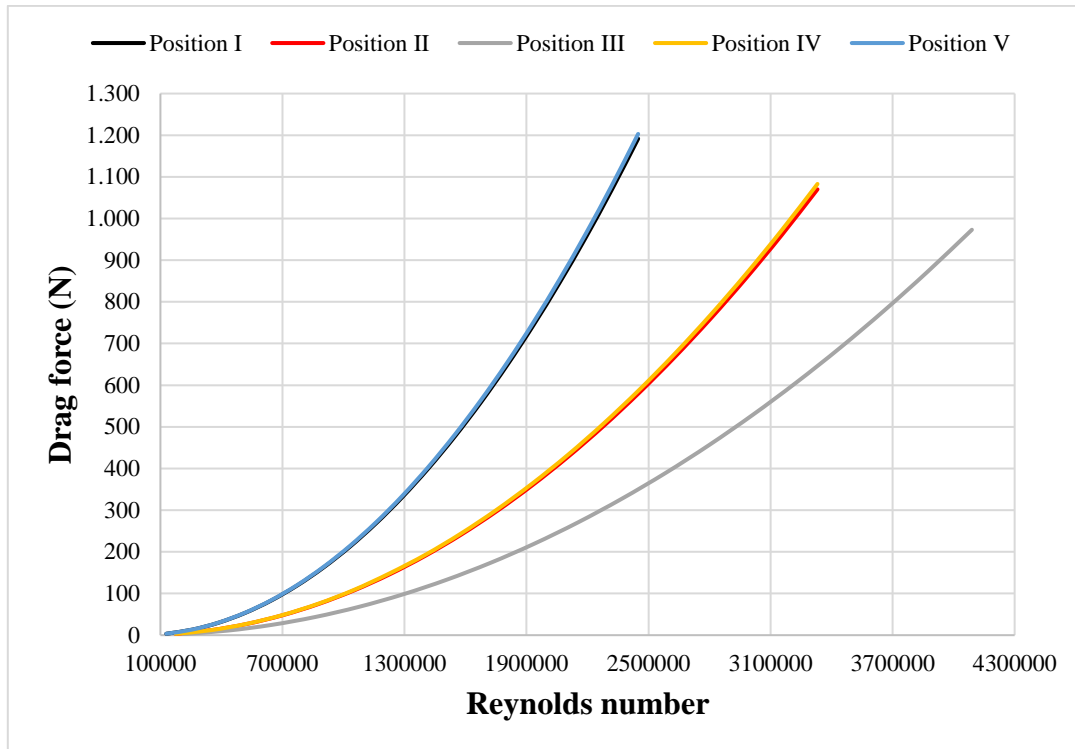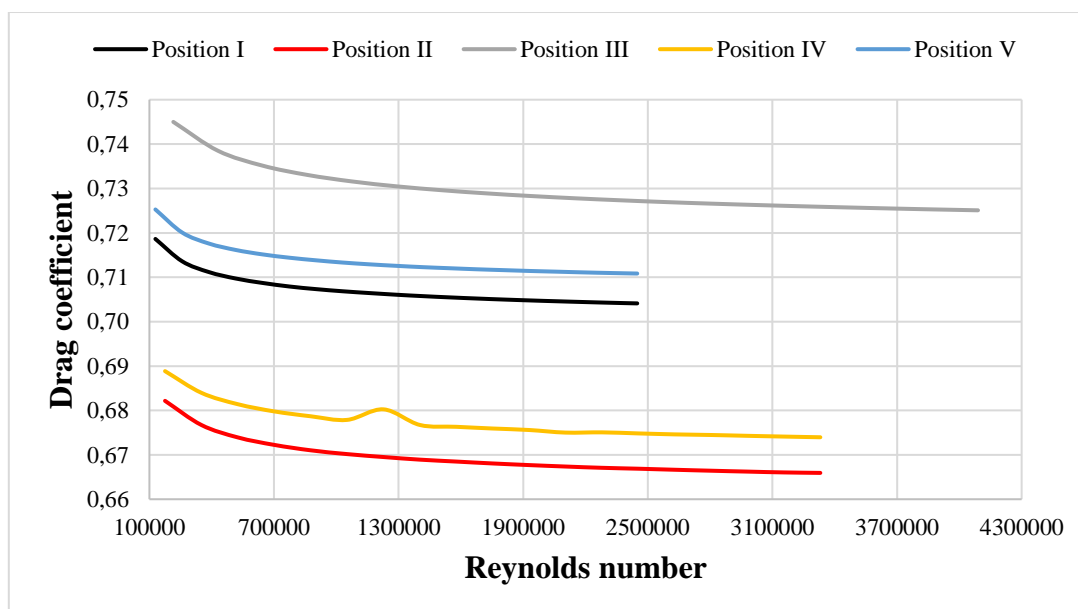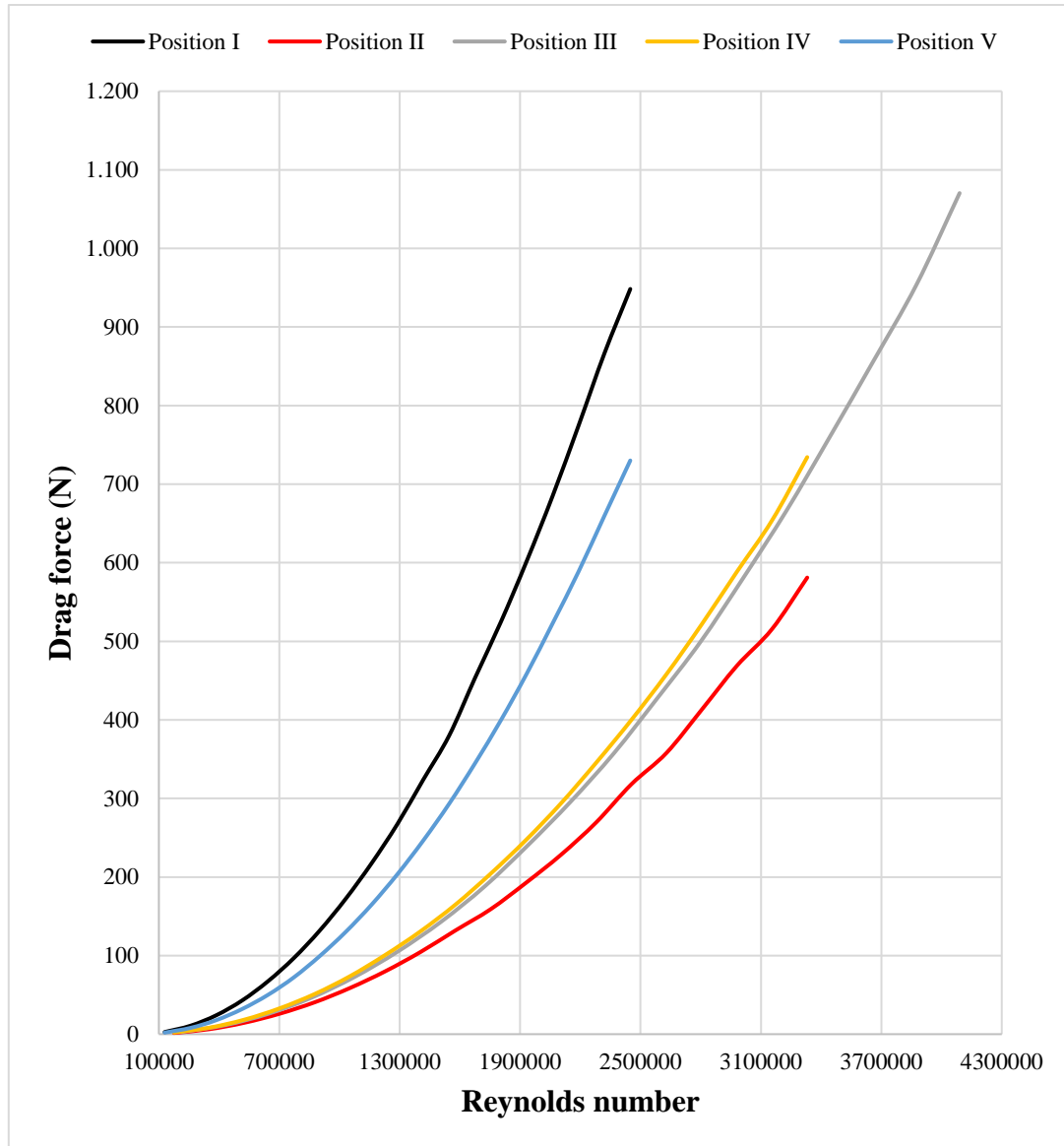

Figure 5.17 - Drag force values for each position considered using CFD analysis in SOLIDWORKS™.

Solving Eq. 1 using the data collected from SOLIDWORKS™ analysis, it is possible to determinate the behavior of C_D for each considered position. The obtained results are shown in Figure 5.18.
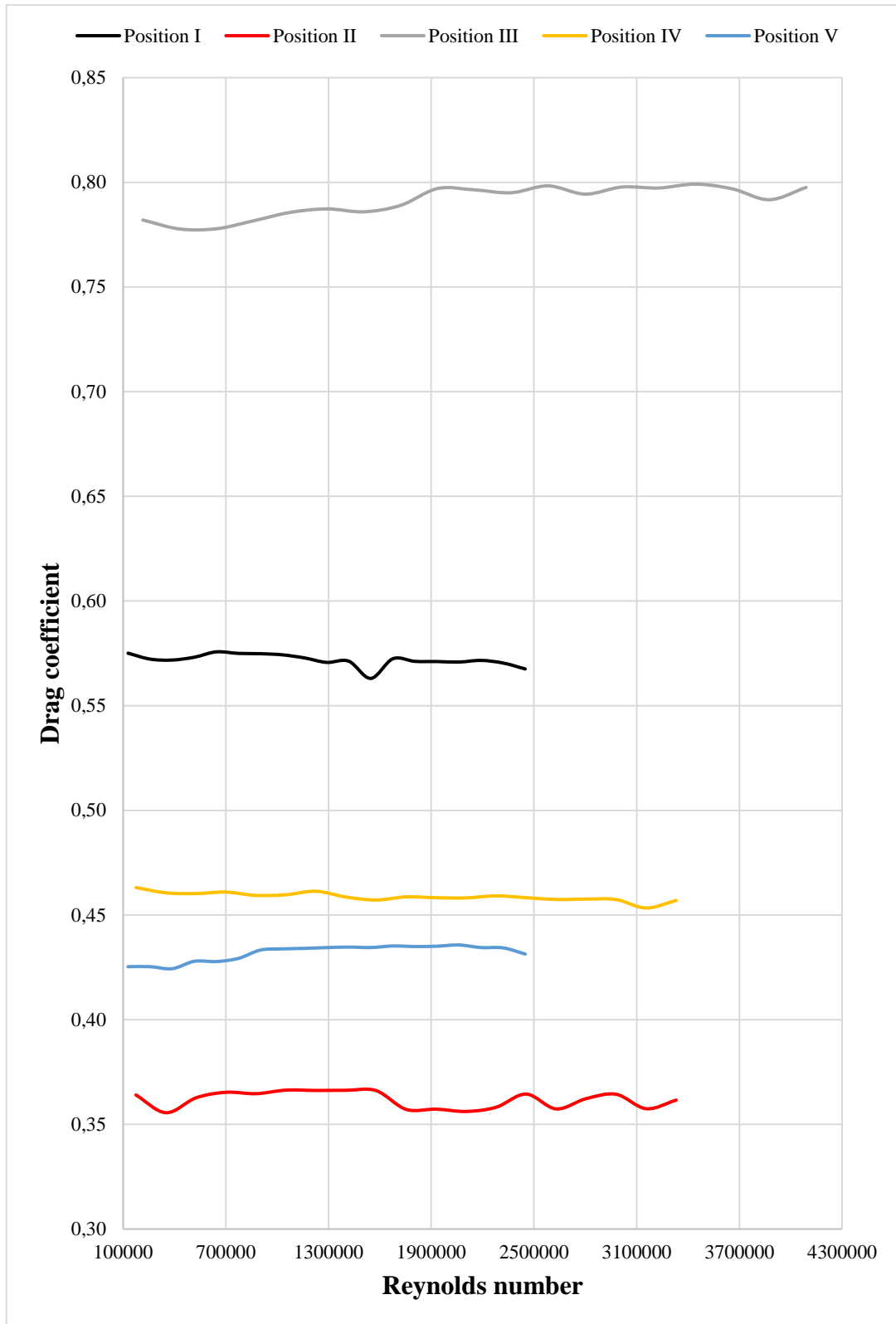
Figure 5.18 - C_D values for each position considered using CFD analysis in SOLIDWORKS™.

5.2.2.1.   Results discussion for SOLIDWORKS™ software

For SOLIDWORKS™ software, even the deformation is not considered the results obtained showed in Figure 5.17 are different for every method previouslly used. The drag force values shown a radon behavior instead of a ordenated one.

For position I to II, occurs a decrease in the frontal area and the drag force also decreases. For position II to III the frontal area also decrease but the drag force value increase. For position III to IV, the frontal area increase but the drag force value decrease. For the position IV to V the frontal area also increase but the drag force value remain constant.

Analysing the C_D behavior shown in Figure 5.18, it is possible to see that for position I to II, the frontal area value decrease and the drag coefficient decrease instead of increase. For position II to III the frontal area value decrease and the drag coefficient value increase as expected. For position III to IV the frontal area increase and the drag coefficient decrease as expected but the value is not closer to the values for position II that have an equal frontal area. For position IV to V, the frontal area increase and and the drag coefficient decrease as expected but the value is not close to the values for position I that have an equal frontal area.

5.2.3. General discussions

With all the data collected, a comparation between each method can be made, and once the wind tunnel simulations are considered as the ideal method to evalute fluid dynamics properties, the results obtained for this method will be considered as the standard values to the comparisons.

Once the sind tunnel simulations model used a scale factor of 1/34, the Reynolds number for this equipment are much lower than the ones for CFD analyses. To be able to make comparisons between methods shown below, the Reynolds number values for CFD analyses were divided by the same scaling factor, i.e. divided by 34, to obtain values that fall within the same range to allow direct analysis between the curves.

Since the velocity values for wind tunnel simulations are lower than those used in CFD analysis due to equipment limitations, the curves of this method present their maximum

values first. C_D value at the end of the experiments for each considered method are shown in Table 5.1.

First for the ANSYS™ results, it is possible to see that the drag force behavior is better determined for the CFD software, showing soft curves compared to the curves obtained for wind tunnel simulations. This diference is explained by the problems experienced during the execution of the wind tunnel simulations that possibly causes erros in the measurement process. A comparison between the curves can be seen in Figure 5.19, Figure 5.21, Figure 5.23, Figure 5.25 and Figure 5.27 for all considered position. The values for C_D obtained with ANSYS™ software are closer to the ones obtained for the wind tunnel simulations, generally presenting a small error when comparing these two values as shown in Table 5.2. A comparison between the curves can be seen in Figure 5.20, Figure 5.22, Figure 5.24, Figure 5.26 and Figure 5.28 for all considered position.

For SOLIDWORKS™ results, the curves for the drag force also present a soft behavior, but its values are more distant to the wind tunnel values as is possible to see in Figure 5.19, Figure 5.21, Figure 5.23, Figure 5.25 and Figure 5.27 for all considered position. The values for C_D obtained with SOLIDWORKS™ software present a higher error shown in Table 5.2 when comparing its values to the ones obtained with wind tunnel simulations because once the results for the drag force are distant to the wind tunnel values, the drag coefficient were also affected. A comparison between the curves can be seen in Figure 5.20, Figure 5.22, Figure 5.24, Figure 5.26 and Figure 5.28 for all considered position.

Table 5.1 - C_D value at the end of experiments

	C_D value				
	Pos. I	Pos. II	Pos. III	Pos. IV	Pos. V
Wind tunnel	0,65	0,74	0,80	0,73	0,65
ANSYS™	0,7	0,67	0,73	0,67	0,71
SOLIDWORKS™	0,57	0,36	0,80	0,46	0,43

Figure 5.19 - Drag force comparison for position I.

Figure 5.20 - Drag coefficient comparison for position I.

Figure 5.21 - Drag force comparison for position II.

Figure 5.22 - Drag coefficient comparison for position II.
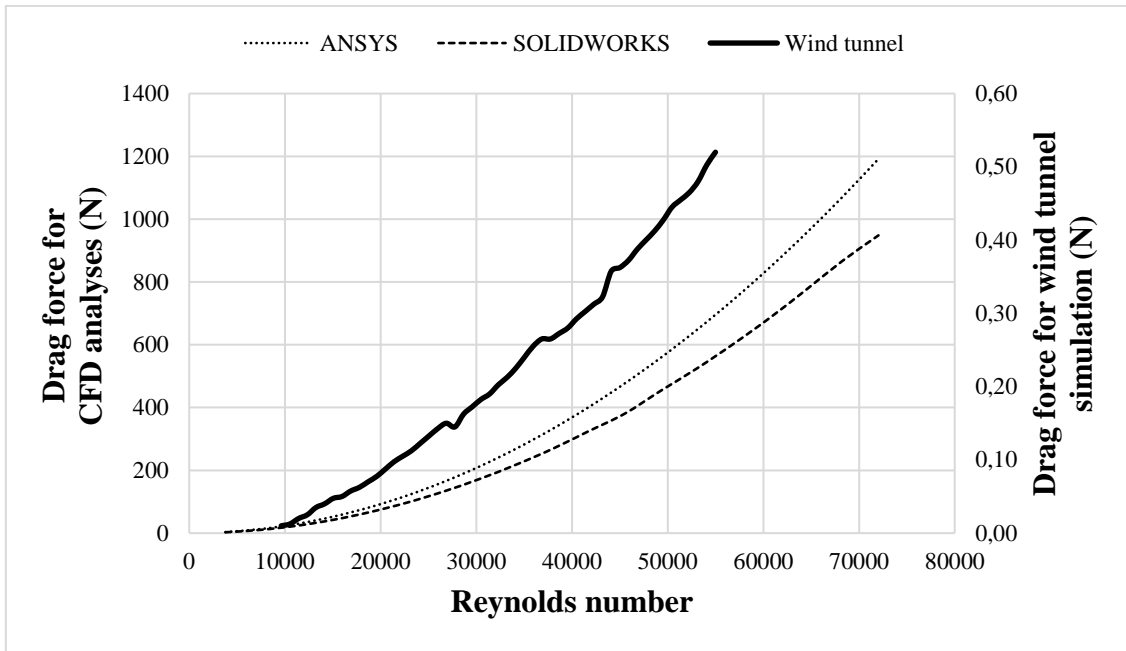
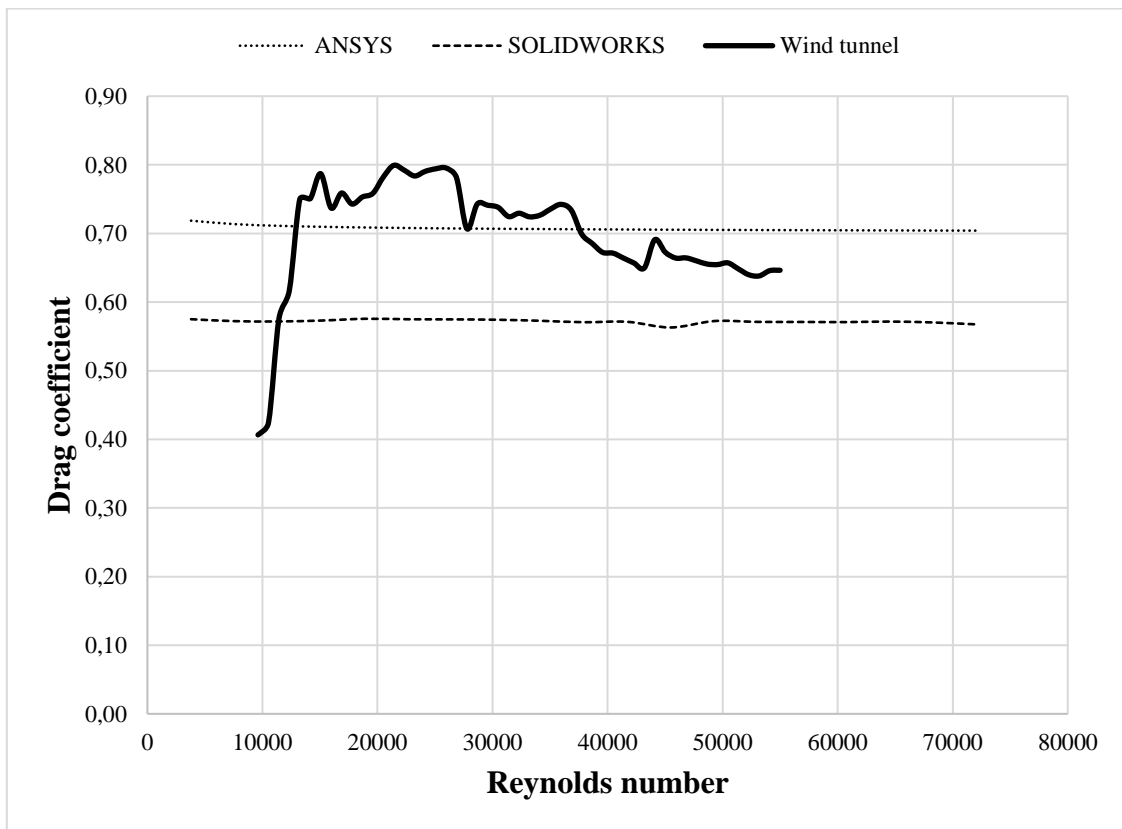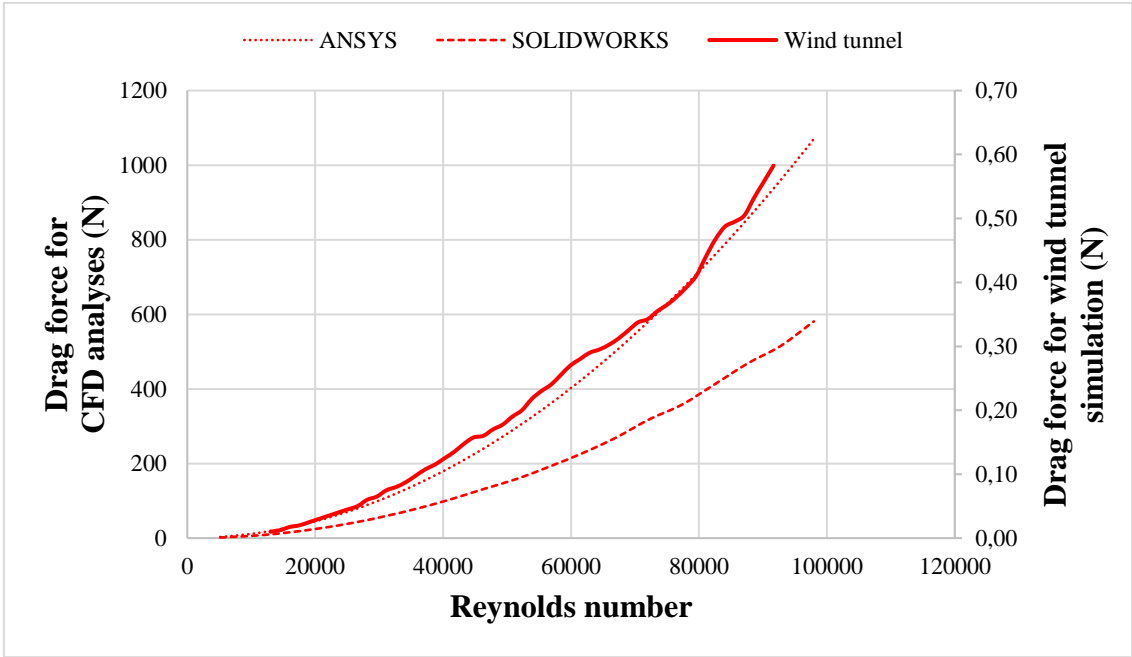**Figure 5.23** - Drag force comparison for position III.
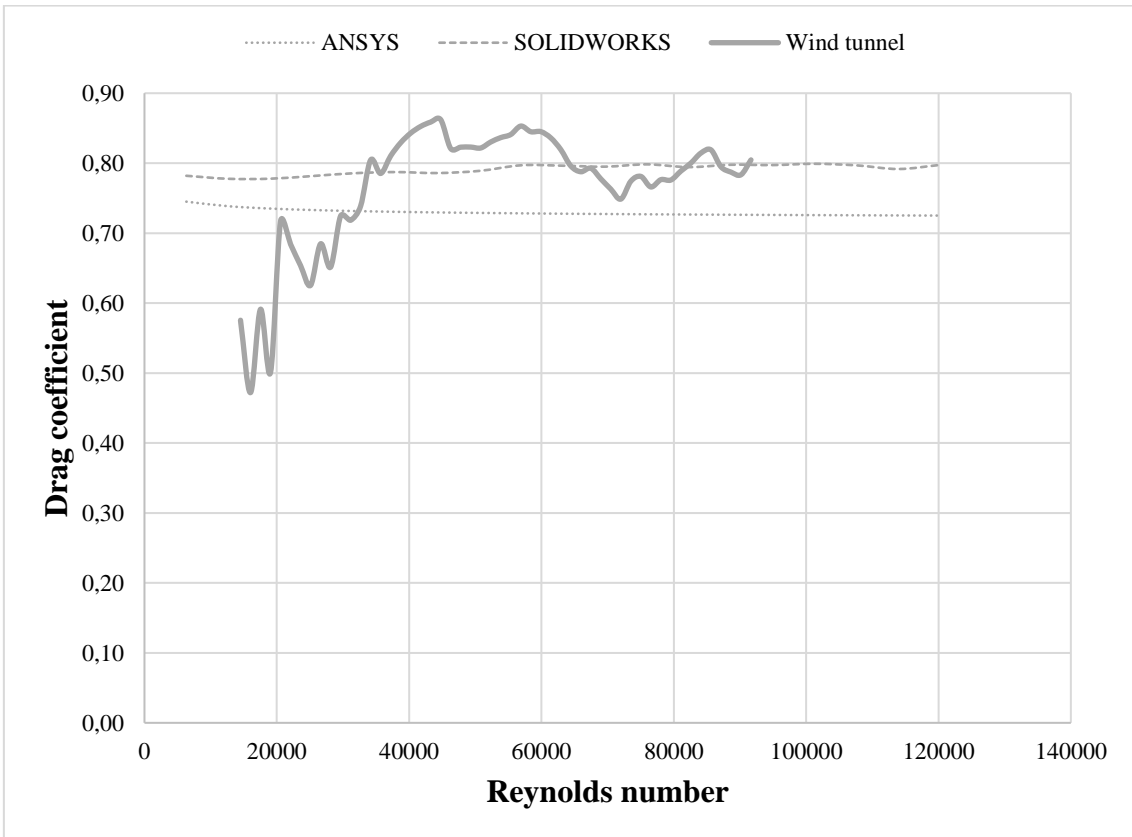
Figure 5.24 - Drag coefficient comparison for position III.
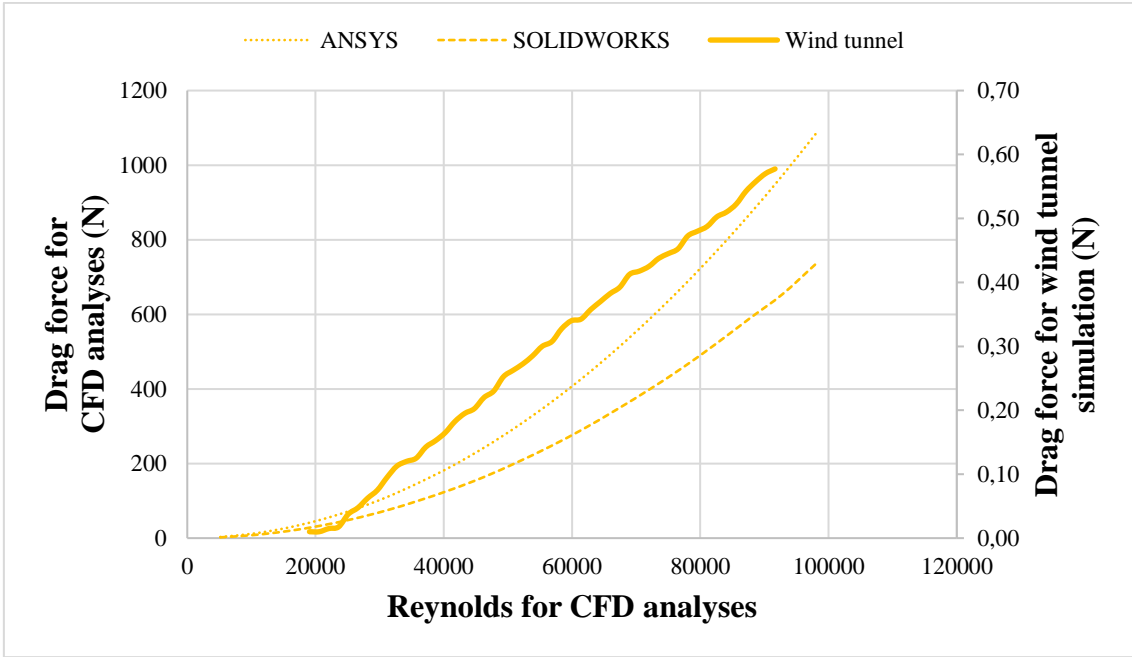
Figure 5.25 - Drag force comparison for position IV.
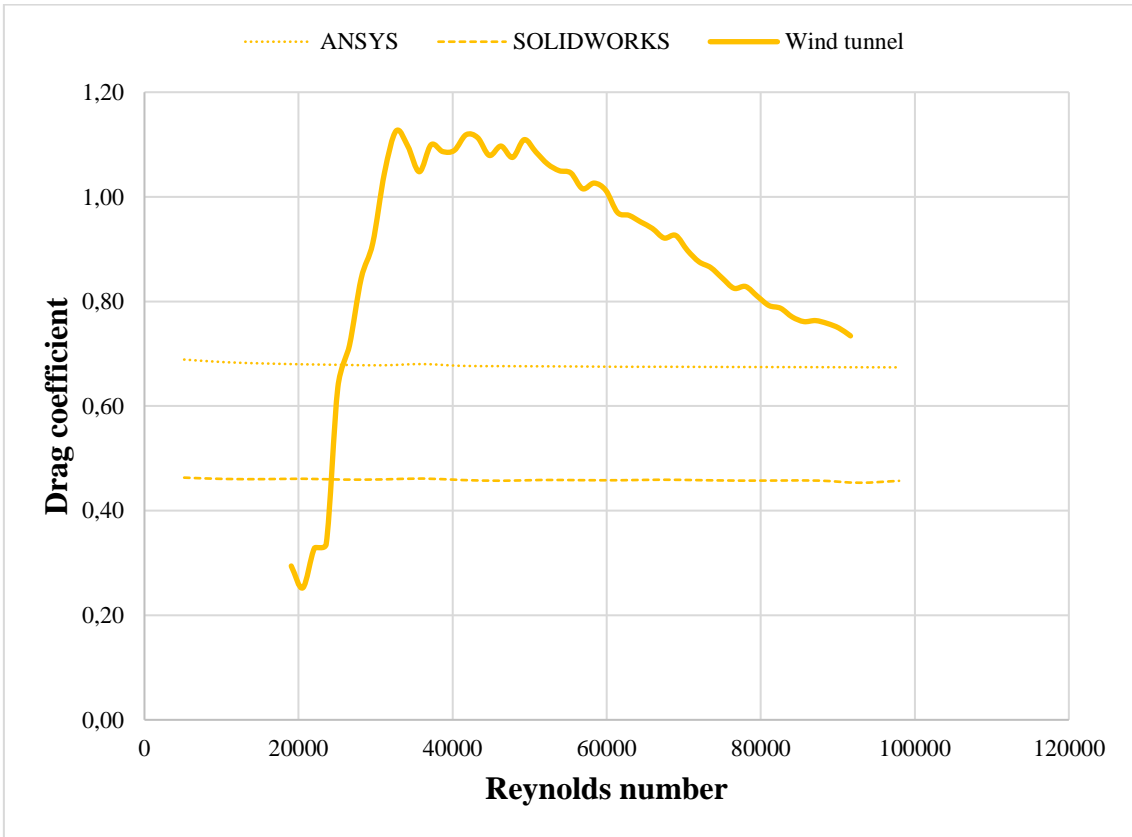
Figure 5.26 - Drag coefficient comparison for position IV.
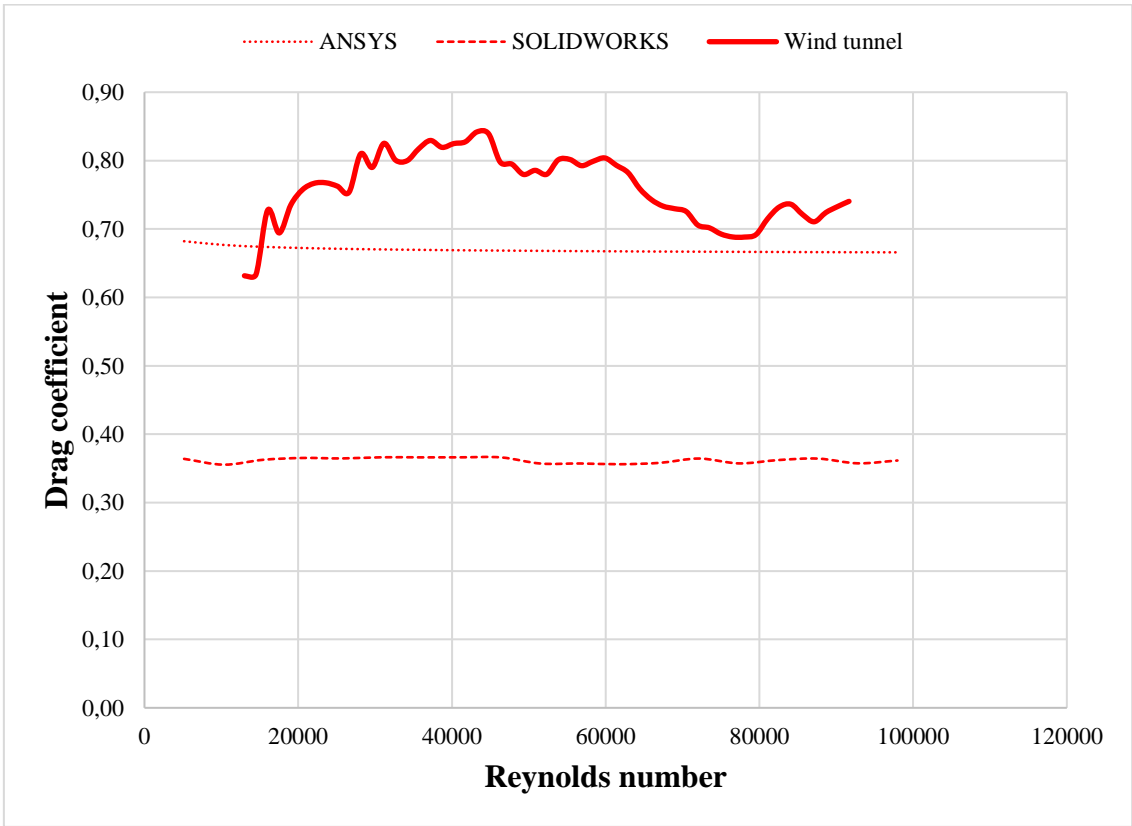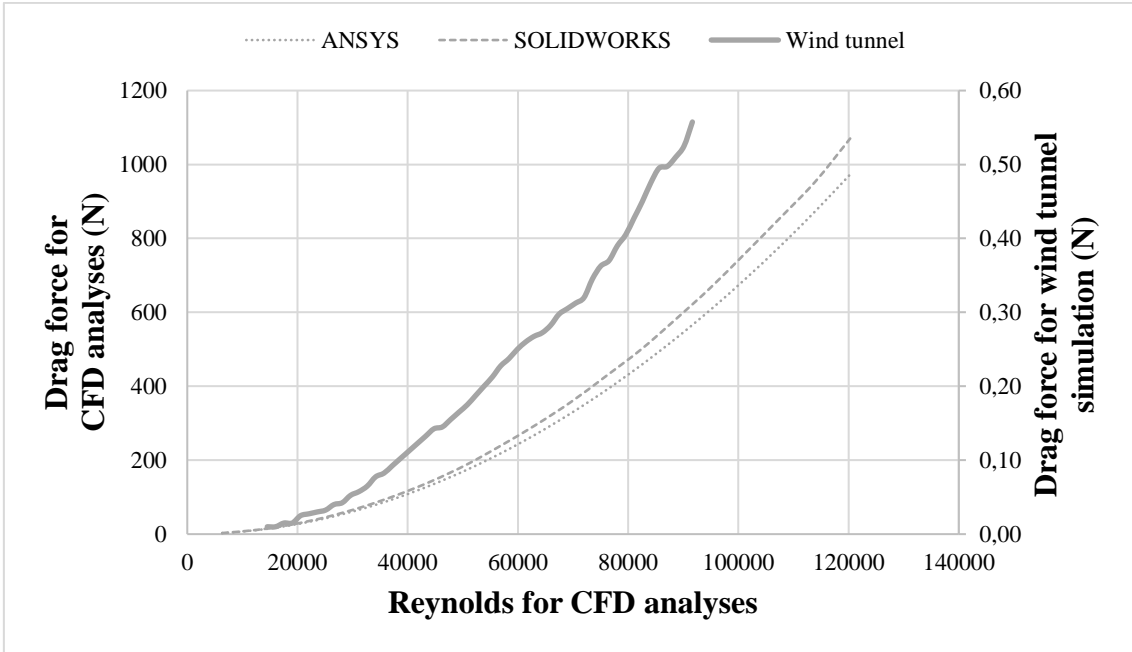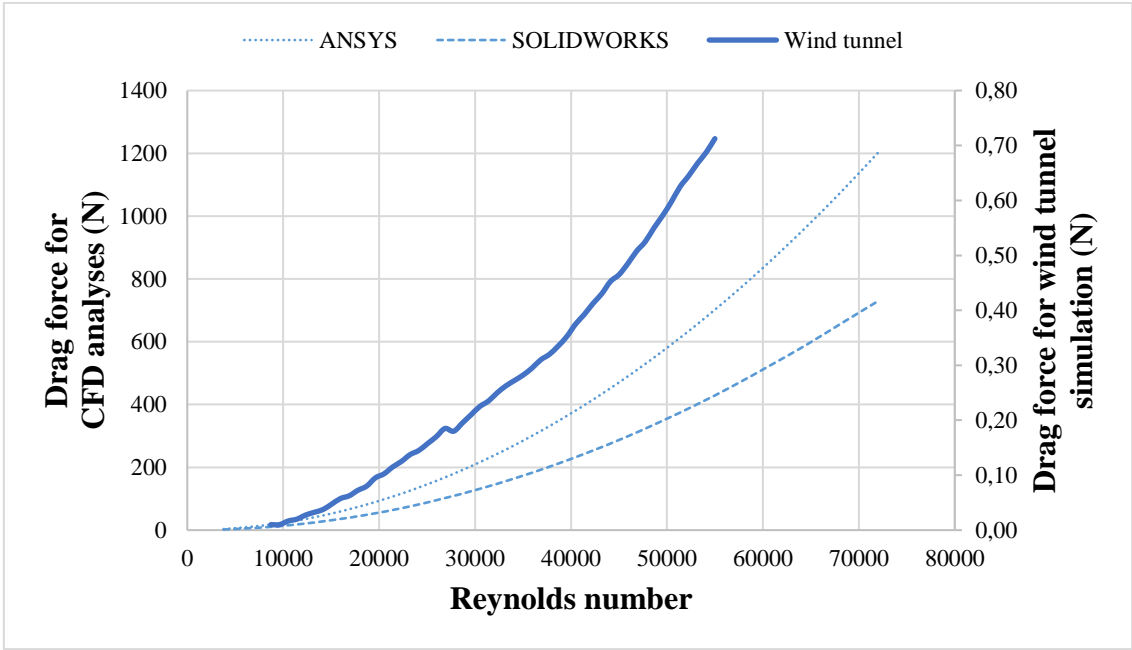
Figure 5.27 - Drag force comparison for position V.
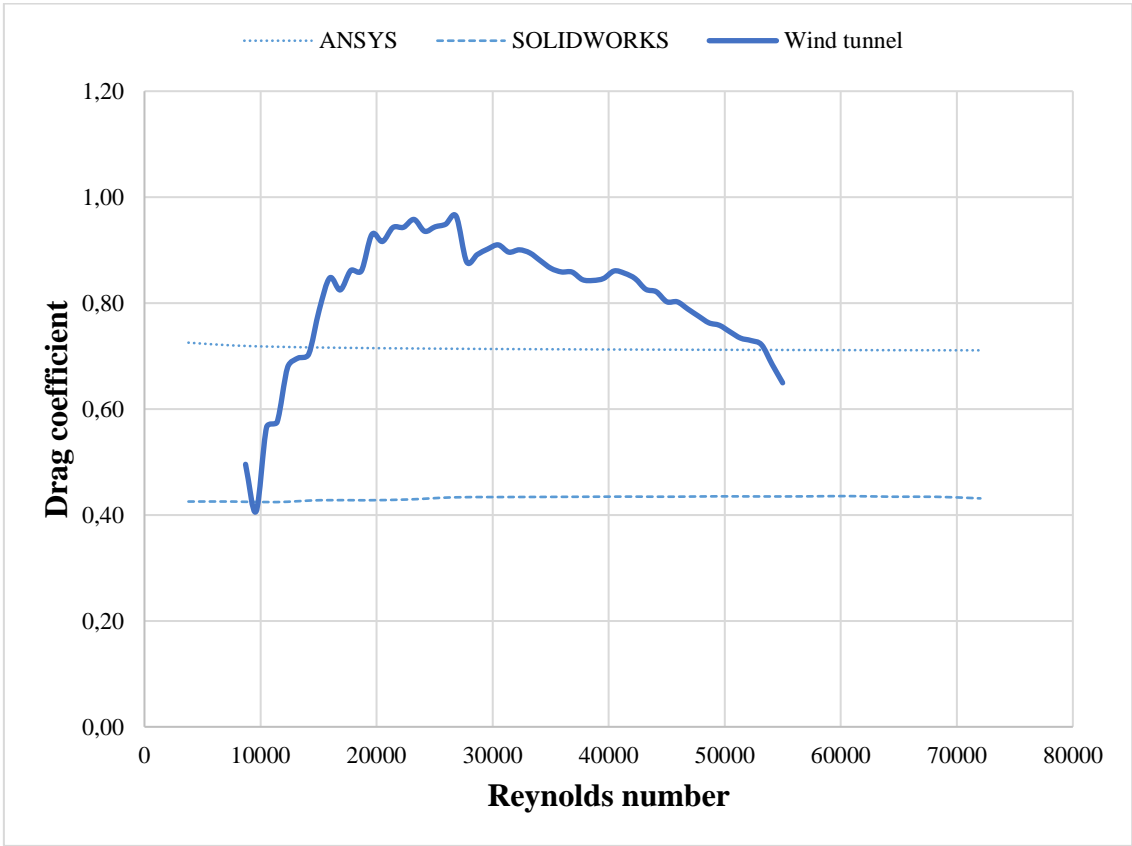
Figure 5.28 - Drag coefficient comparison for position V.

Table 5.2 - Percentual errors of the versus obtained for C_D comparing the used methods.

	Percentual error				
	Pos. I	Pos. II	Pos. III	Pos. IV	Pos. V
ANSYS™	9%	10%	10%	8%	9%
SOLIDWORKS™	12%	51%	1%	38%	34%

Using the computational analysis, it is possible to determinate the total force acting on the column body when air is flowing at the critical velocity of 38 m/s. To do it, the equivalent force were caculated using the components X, Y and Z of the force that can be directly obtained form the softwares. In Table 5.3 the results obtained for each position is showed for the used softwares.

Table 5.3 - Equivalent force acting on column body at 38 m/s .

	Equivalent force (N)				
	Pos. I	Pos. II	Pos. III	Pos. IV	Pos. V
ANSYS™	1541,97	1211,74	974,54	1270,54	1624,43
SOLIDWORKS™	1148,97	669,50	1134,74	895,17	994,35

6. Conclusion

Fluid mechanins is a study area that seek to determinate the bahavior of a fluid in flow condition when it encounter a solid body, detemintaing a series os properties for both the fluid and the body including the drag coefficient of the body and the drag force imposed by the fluind on it.

In the preseted work, the determination of the drag force and the drag coefficient of an autonomous lighting column fabricated by the VALLED company, was made using three diferent tools, beeing then experimental tests in a subsonic suction-type wind tunnel provided by IPB and two CFD analyses using ANSYS™ and SOLIDWORKS™ software.

To produce the results, the model as submited to analyses in four diferent positions and under a series of flow velocities, respecting the tecnincal limitations impose by the used tools.

After the conclusion of the tests, it is possible to see how difficult it is to produce perfect results with a wind tunnel simulation where, in this case, the usage of a wrong material with low mechancical resistance affected negatvilly the results obtained, especially for the drag force.

The CFD simulations presented an easier execution without any interference. The objective of this work was the creation of a CFD analyses model that can be used during the design process of a component and to do it in the easier method, transition effects were not considered.

The results obtained using ANSYS™ software were more reliable once the behaviors shown respected what was expected in theory. Considering the results obtained in the wind tunnel simulation as the standard values, the results for ANSYS™ shown a average error of 9,2% which is an acceptable error for a software and makes ANSYS™ a riliable tool to replace the wind tunnel simulations with.

For SOLIDWORKS™, the results were not so riliable presenting an average error of 27,2% wich is not acceptable for project purposes. The tool can be used as a support tool to use during the desing to assist in not critical parts of the project, but is not a riliable tool to replace the wind tunnel simulations with.

For both CFD methods, the determinated values for C_D are generally lower than the ones obtained with the wind tunnel simulation in the same position, which requires a correction during the project taking into account the error associated with the method. By these results, disregarding the transiction effects did not have a big impact on average error, at least for ANSYS™ software.

To the equivalent force acting on the column body, a difference is noticed between the softwares used once ANSYS™ indicates that the maximum force is 1624,43 N in position V and for SOLIDWORKS™ it is 1148,97 N in position I. Both positions represents the same area exposed to the flow so, both softwares indicate that the critical force occurs when the flow is orthogonal to the biggest dimension of the solar pannel and there is an error of 29,26% between them.

Analysing the wind tunnel simulations, despite the errors caused by the low mechanical resistance of the material used in the model and the high vibrations experienced that made the drag force measurements go wrong, the final results for the drag coefficient are not so affected once its value is close to the ones obtained in the CFD analysis. This proximity is an example that demonstrates C_D independence at high flow velocity values, wich makes possible to consider the results obtained in the wind tunel simulations as valid results.

A better determination can be made if the same simulations were made using another material in the model that presents better mechanical properties wich will produce a better aproximation of the results obtained in the CFD analysis, problably to the one performed in ANSYS™ software. To improve the results obtained with CFD analyses, trasitions effects can be considered.

6.1. Future work

To continue with this work, it is possible to perform the wind tunnel simulations using a model made from other material that presents better mechanical properties. This study can be helpfull in terms of validation for reliability of the CFD softwares, specially for ANSYS™.

Another possible work is the imprrovment of the force measument system, once the current system is very influenced by human errors. The damping system present in the equipment can be improoved as well, to decrease the vibration levels that occur during the experimental process.

Bibliografy

[1] VILLALVA, M. G. Energia Solar Fotovoltaica: Conceitos e Aplicações. 2 ed. São Paulo: Editora Saraiva, 2015

[2] WORLD ENERGY RESOURCES: 2016. World Energy Council. Avaliable at: < https://www.worldenergy.org/assets/images/imported/2016/10/ World-Energy-Resources-Full-report-2016.10.03.pdf >. Access in: 20 out. 2019.

[3] Gaiato, J. M. C. Projeto de Colunas de Iluminação Autonomas Solares. 2017. 155p. Project Course Report. Instituto Politécnico de Bragança, Bragança, 2017.

[4] GAZELA: POSTE DE ILUMINAÇÃO AUTÓNOMO FOTOVOLTAICO VALLED. Avaliable at: <https://www.chlengenharia.pt/compra/gazela-poste-de-iluminacao-autonomo-fotovoltaico-valled-589010>. Access in: 20 out. 2019.

[5] Núñez, G. J. Z. Determinação Experimental e Teórica da Resposta Transversal à Ação do Vento de uma Torre de Telecomunicações de Concreto Armado. 2001. 141p. Masters Dissetation. Universidade Federal do Rio Grande do Sul, Porto Alegre, 2001.

[6] Limas, L. F. Determinação das Características Aerodinâmicas de Seções Transversais de Pontes em Túnel de Vento. 2003. 175p. Masters Dissetation. Universidade Federal do Rio Grande do Sul, Porto Alegre, 2003.

[7] Machado, A. C. Caracterização das Propriedades Aerodinâmicas de Torres Metálicas para Determinação da Resposta Devida ao Vento. 2003. 154p. Masters Dissetation. Universidade Federal do Rio Grande do Sul, Porto Alegre, 2003.

[8] Rippel, L. I. Estudo em Túnel de Vento do Arrasto Aerodinâmico Sobre Torres Treliçadas de Linhas de Transmissão. 2005. 152p. Masters Dissetation. Universidade Federal do Rio Grande do Sul, Porto Alegre, 2005.

[9] Santos, N. F. P. L. Medição Experimental do Coeficiente de Resistência ao Rolamento e do Coeficiente de Arrasto Aerodinâmico de um Veículo Automóvel de Elevada Eficiência Energética. 2012. 66p. Masters Dissetation. Faculdade de Ciências e Tecnologia Universidade de Coimbra, Coimbra, 2012.

[10] Arnoldi, P. H. C., Estudo de Parâmetros Aerodinâmicos de Perfis em Túnel de Vento. 2011. 49p. Final Report. Universidade Regional do Noroeste do Estado do Rio Grande do Sul, Panambi, 2011.

[11] Sarmento, C. V. da S.; Souza Junior, M. A.; Ribeiro, P. M. V. Estimativa do Coeficiente de Arrasto com a Aplicação da Dinâmica dos Fluidos Computacionais: Estudo de Caso de um Aqueduto da Transposição do Rio São Francisco. 2014. 21p. Proceedings of the XXXV Iberian Latin-American Congress on Computational Methods in Engineering. CILAMCE, 2014.

[12] Fox, R. W.; Mcdonald, A. T.; Pritchard, P. J. Introdução à Mecânica dos Fluidos: 8 ed. Gen/LTC, 2014.

[13] Çengel, Y. A.; Cimbala, J. M. Mecânica dos Fluidos: Fundamentos e Aplicações. Porto Alegre: AMGH, 2007

[14] AIR - DENSITY, SPECIFIC WEIGHT AND THERMAL EXPANSION COEFFICIENT AT VARYING TEMPERATURE AND CONSTANT PRESSURES. Avaliable at: < https://www.engineeringtoolbox.com/air-density-specific-weight-d_600.html >. Access in: 20 out. 2019.

[15] NP EN 1991-1-4:2009. Eurocódigo 1 – Ações em estruturas. Parte 1-4: Ações gerais. Ações do vento. Insituto Português de Qualidade, 2009.

[16] Maia, V. M. J. M.. Análise e Dimensionamento de Torre Eólica Offshore: Estudo paramétrico. 2009. 135p. Masters Dissertation. Faculdade de Engenharia da Universidade do Porto, Porto, 2009.

[17] Escusa, G. G. Análise do Comportamento Dinâmico da Estrutura de Suporte de um Túnel de Vento. 2014. 137p. Masters Dissertation. Faculdade de Engenharia da Universidade do Porto, Porto, 2014.

[18] HISTORY OF WIND TUNNELS. Avaliable at: < https://www.grc.nasa.gov/WWW/K-12/WindTunnel/history.html>. Access in: 20 out. 2019.

[19] THREAD: WINGS. Avaliable at: < http://www.fsae.com/forums/showthread.php?1948-WINGS/page18>. Access in: 20 out. 2019.

[20] Barbosa, T. P. Túnel de Vento para Ensaios de Componentes. 2008. 88p. Masters Dissertation. Faculdade de Engenharia do Porto, Porto, 2008.

[21] AIR – DYNAMIC AND KINEMATIC VISCOSITY. Avaliable at: < https://www.engineeringtoolbox.com/air-absolute-kinematic-viscosity-d_601.html>. Acces in: 20 out. 2019.

[22] Rech, G. M. Análise Numérica e Experimental do Comportamento Aerodinâmico da Carroceria de um Ônibus Rodoviário. 2016. 99p. Masters Dissertation. Universidade de Caxias do Sul, Caxias do Sul, 2016.

[23] Barlow, J. B.; Rae, W. H.; Pope, A. Low-speed Wind Tunnel Testing: 3 ed. Wiley, 1999

[24] Antón, P. S. Wind Tunnel and Propulsion Test Facilities: An Assessment of NASA's Capatibilities to Serve National Needs. Rand, 2004.

[25] WIND TUNNEL DESIGN. Avaliable at: < https://www.grc.nasa.gov/WWW/K-12/airplane/tunnozd.html>. Access in: 20 out. 2019.

[26] OPEN RETURN WIND TUNNEL. Avaliable at: < https://www.grc.nasa.gov/WWW/k-12/airplane/tunoret.html>. Access in: 20 out. 2019

[27] CLOSED RETURN WIND TUNNEL. Avaliable at: < https://www.grc.nasa.gov/WWW/K-12/airplane/tuncret.html>. Access in: 20 out. 2019.

[28] Mehta, R.D.; Bradshaw, P. Design Rules for Small Low Spees Wind Tunnels. Aeronautical Journal. 1979. p. 443-449.

[29] Mehta, R.D.; Bradshaw, P. Wind Tunnel Design. Avaliable at: <http://navier.stanford.edu/bradshaw/tunnel/index.html>. Access in: 20 out. 2019.

CURVES FOR THE ROUGHNESS COEFFICIENT BY HEIGHT IN RELATION TO SOIL FOR EACH LAND TYPE ACCORDING TO EUROCODE EN 1991-1-4

Coeficiente de rugosidade

Altura z(m)
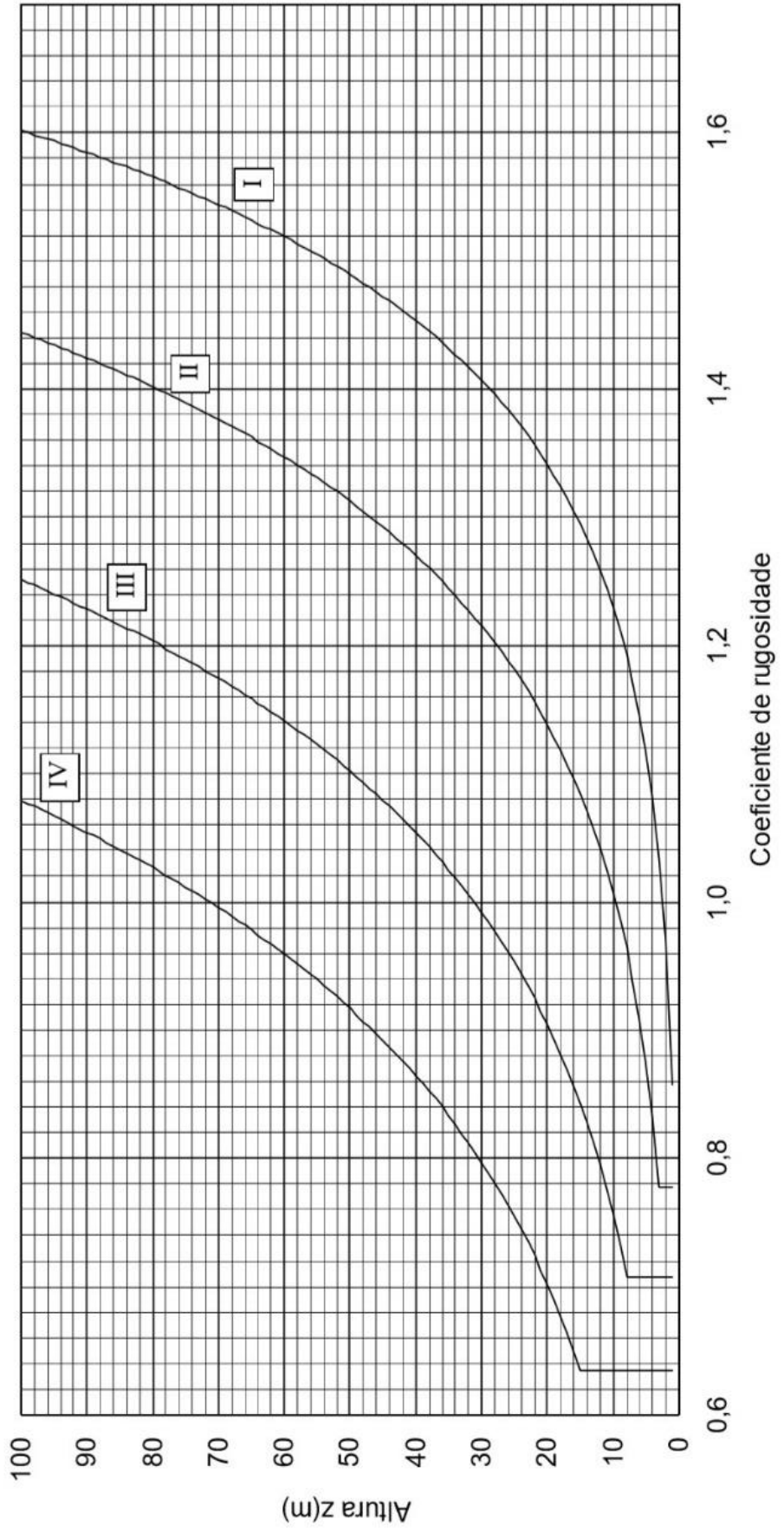
TECHNICAL SHEETS

WIND TUNNEL SIMULATION

Position: I

Flow type: Subsonic

Local temperature: 20 - 25ºC

Re	F (N)	C_D	Re	F (N)	C_D	Re	F (N)	C_D
9617	0,01	0,41	25045	0,1325	0,79	40474	0,2925	0,67
10524	0,0125	0,42	25953	0,1425	0,80	41381	0,3025	0,66
11432	0,02	0,58	26860	0,15	0,78	42289	0,3125	0,66
12339	0,025	0,62	27768	0,145	0,71	43196	0,3225	0,65
13247	0,035	0,75	28675	0,1625	0,74	44104	0,3575	0,69
14155	0,04	0,75	29583	0,1725	0,74	45011	0,3625	0,67
15062	0,0475	0,79	30490	0,1825	0,74	45919	0,3725	0,66
15970	0,05	0,74	31398	0,19	0,72	46826	0,3875	0,66
16877	0,0575	0,76	32306	0,2025	0,73	47734	0,4	0,66
17785	0,0625	0,74	33213	0,2125	0,72	48641	0,4125	0,66
18692	0,07	0,75	34121	0,225	0,73	49549	0,4275	0,65
19600	0,0775	0,76	35028	0,24	0,74	50457	0,445	0,66
20507	0,0875	0,78	35936	0,255	0,74	51364	0,455	0,65
21415	0,0975	0,80	36843	0,265	0,73	52272	0,465	0,64
22323	0,105	0,79	37751	0,265	0,70	53179	0,48	0,64
23230	0,1125	0,78	38658	0,2725	0,69	54087	0,5025	0,65
24138	0,1225	0,79	39566	0,28	0,67	54994	0,52	0,65
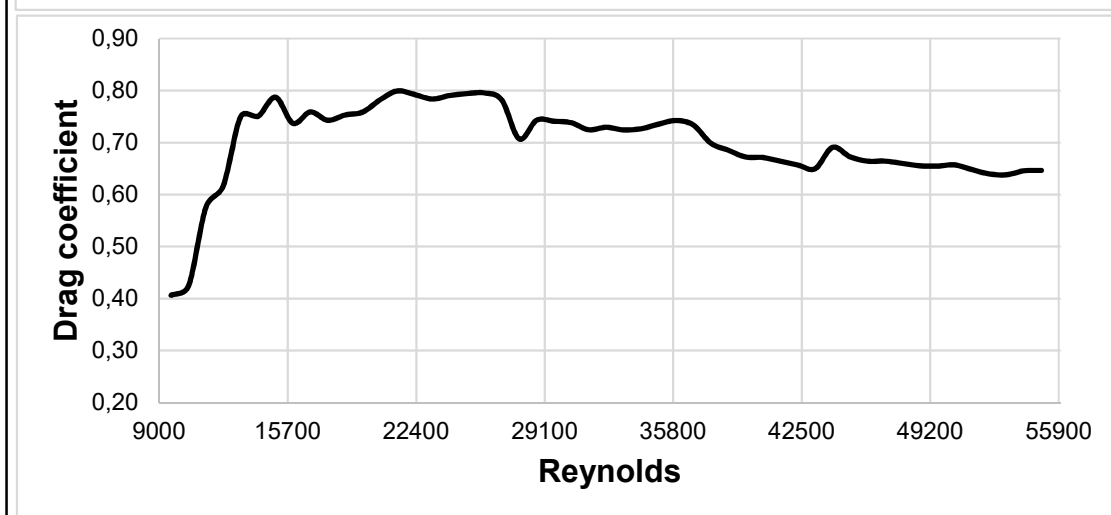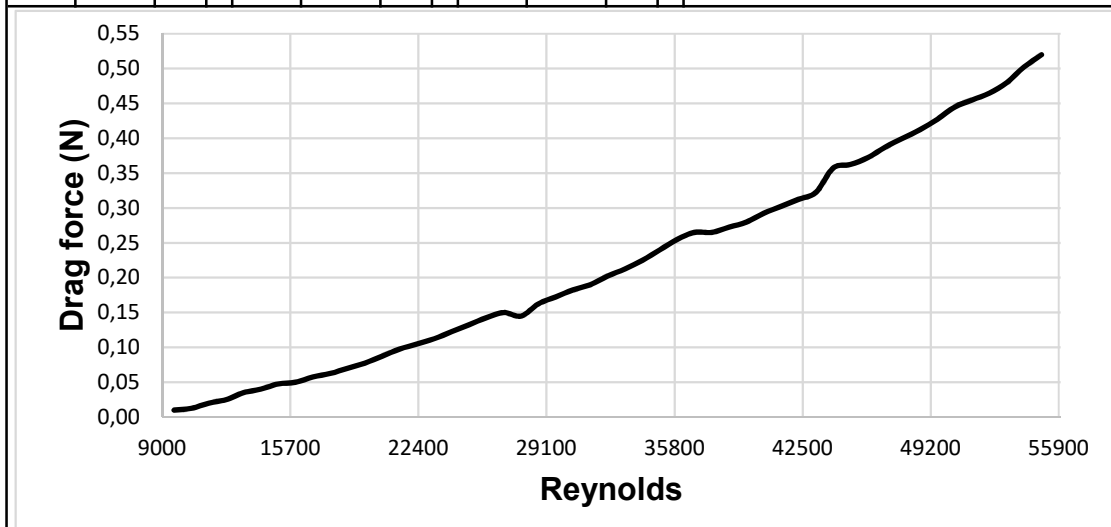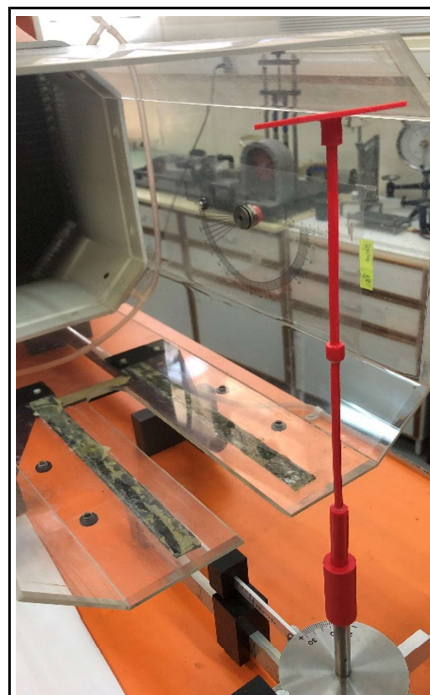
Re	F (N)	C_D	Re	F (N)	C_D	Re	F (N)	C_D
13003	0,010	0,63	40229	0,125	0,82	67456	0,313	0,73
14516	0,013	0,63	41742	0,135	0,83	68968	0,325	0,73
16028	0,018	0,73	43255	0,148	0,84	70481	0,338	0,73
17541	0,020	0,69	44767	0,158	0,84	71994	0,343	0,71
19053	0,025	0,74	46280	0,160	0,80	73506	0,355	0,70
20566	0,030	0,76	47792	0,170	0,79	75019	0,365	0,69
22078	0,035	0,77	49305	0,178	0,78	76531	0,378	0,69
23591	0,040	0,77	50817	0,190	0,79	78044	0,393	0,69
25104	0,045	0,76	52330	0,200	0,78	79557	0,410	0,69
26616	0,050	0,75	53843	0,218	0,80	81069	0,440	0,72
28129	0,060	0,81	55355	0,230	0,80	82582	0,468	0,73
29641	0,065	0,79	56868	0,240	0,79	84094	0,488	0,74
31154	0,075	0,83	58380	0,255	0,80	85607	0,495	0,72
32666	0,080	0,80	59893	0,270	0,80	87119	0,505	0,71
34179	0,088	0,80	61406	0,280	0,79	88632	0,533	0,72
35692	0,098	0,82	62918	0,290	0,78	90145	0,558	0,73
37204	0,108	0,83	64431	0,295	0,76	91657	0,583	0,74
38717	0,115	0,82	65943	0,303	0,74			
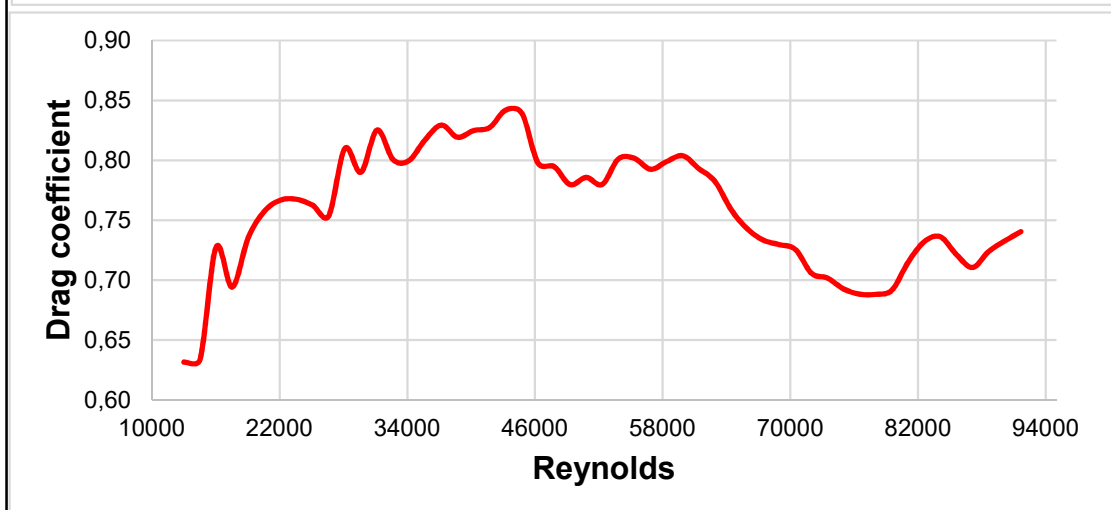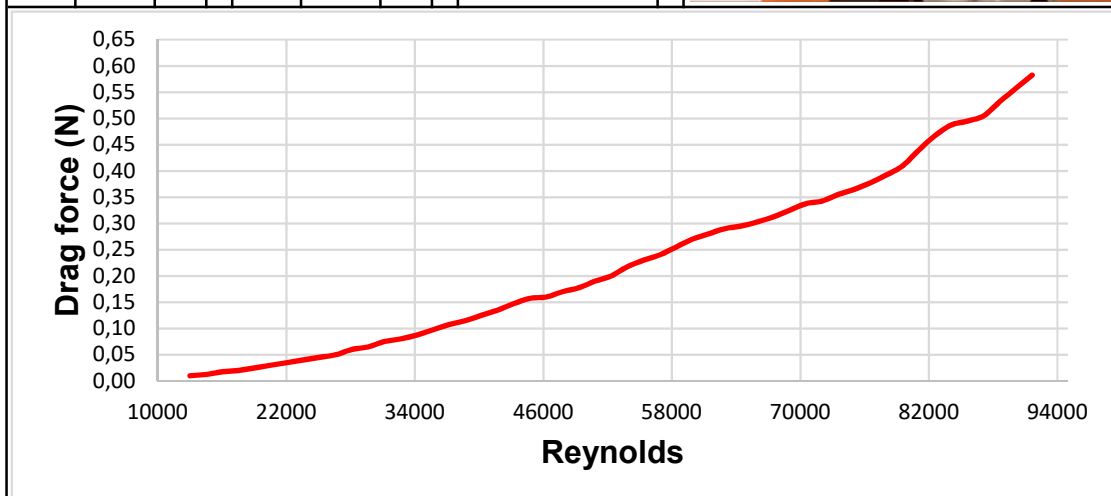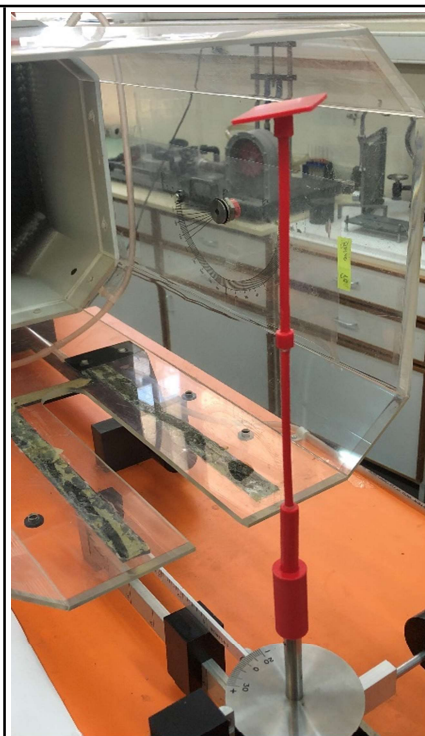
WIND TUNNEL SIMULATION

Position: III

Flow type: Subsonic

Local temperature: 20 - 25ºC

Re	F (N)	C_D	Re	F (N)	C_D	Re	F (N)	C_D
14516	0,010	0,58	41742	0,123	0,85	68968	0,305	0,78
16028	0,010	0,47	43255	0,133	0,86	70481	0,313	0,76
17541	0,015	0,59	44767	0,143	0,86	71994	0,320	0,75
19053	0,015	0,50	46280	0,145	0,82	73506	0,345	0,77
20566	0,025	0,72	47792	0,155	0,82	75019	0,363	0,78
22078	0,028	0,68	49305	0,165	0,82	76531	0,370	0,77
23591	0,030	0,65	50817	0,175	0,82	78044	0,390	0,78
25104	0,033	0,63	52330	0,188	0,83	79557	0,405	0,78
26616	0,040	0,68	53843	0,200	0,84	81069	0,428	0,79
28129	0,043	0,65	55355	0,213	0,84	82582	0,450	0,80
29641	0,053	0,72	56868	0,228	0,85	84094	0,475	0,81
31154	0,058	0,72	58380	0,238	0,84	85607	0,495	0,82
32666	0,065	0,74	59893	0,250	0,85	87119	0,498	0,79
34179	0,078	0,80	61406	0,260	0,84	88632	0,510	0,79
35692	0,083	0,79	62918	0,268	0,82	90145	0,525	0,78
37204	0,093	0,81	64431	0,273	0,80	91657	0,558	0,80
38717	0,103	0,83	65943	0,283	0,79			
40229	0,113	0,84	67456	0,298	0,79			
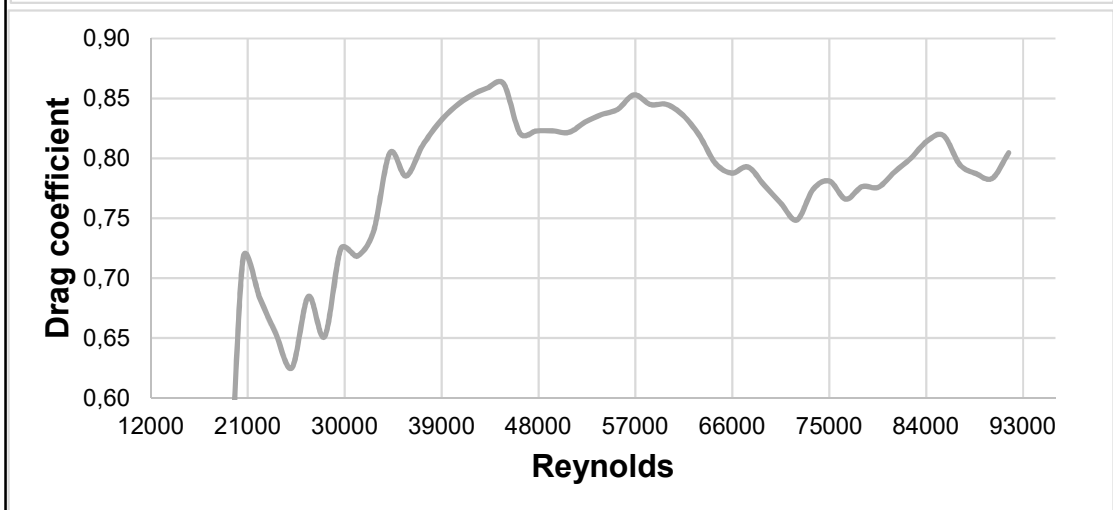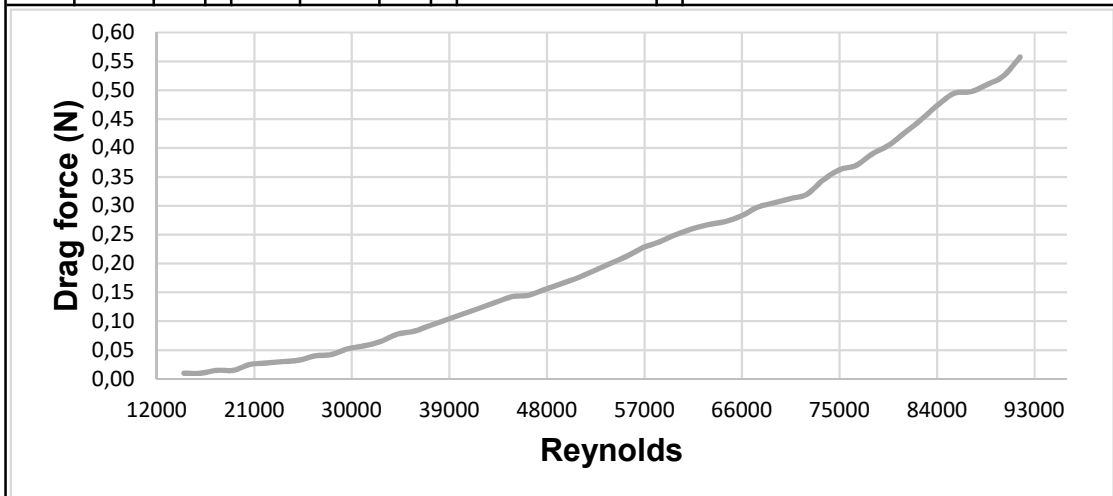
WIND TUNNEL SIMULATION
Position: IV
Flow type: Subsonic
Local temperature: 20 - 25ºC

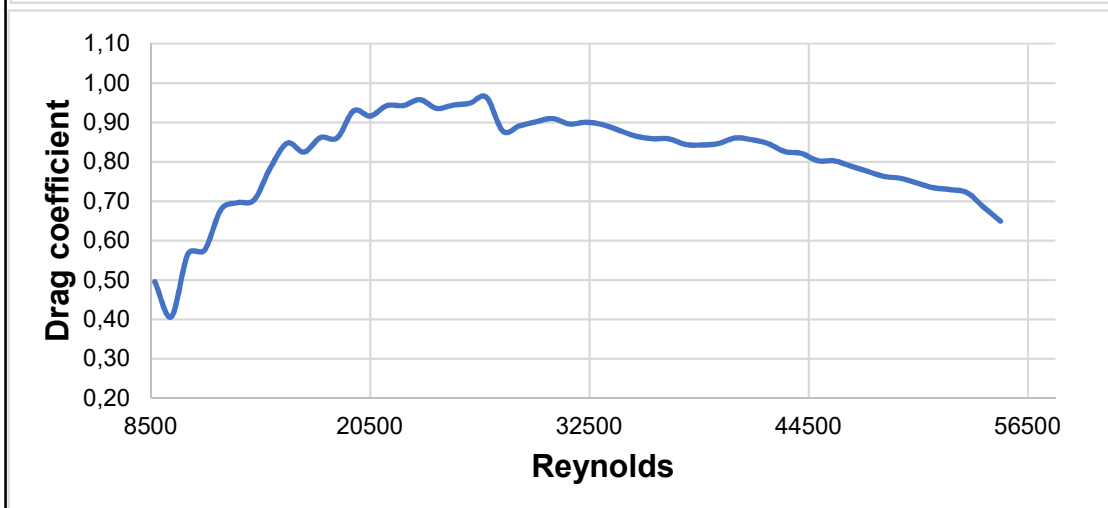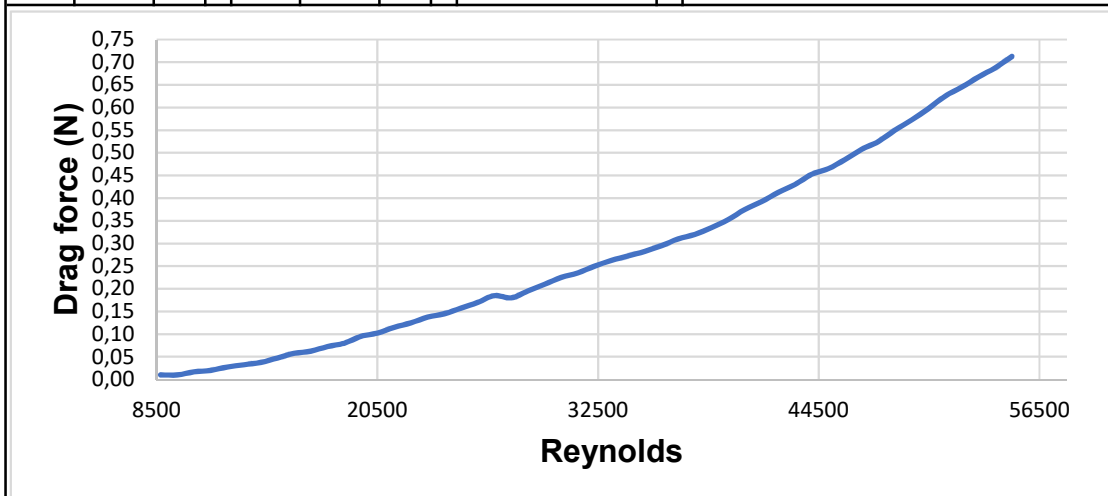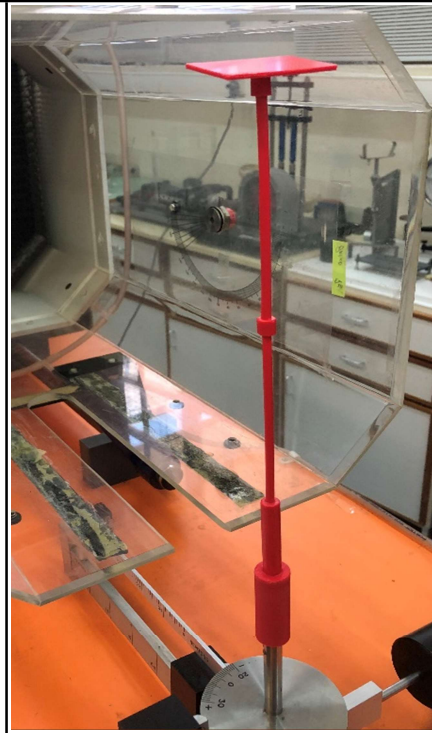| Re	F (N)	C_D	Re	F (N)	C_D	Re	F (N)	C_D
19053	0,010	0,29	46280	0,220	1,10	73506	0,438	0,86
20566	0,010	0,25	47792	0,230	1,08	75019	0,445	0,84
22078	0,015	0,33	49305	0,253	1,11	76531	0,453	0,83
23591	0,018	0,34	50817	0,263	1,09	78044	0,473	0,83
25104	0,038	0,64	52330	0,273	1,06	79557	0,480	0,81
26616	0,048	0,72	53843	0,285	1,05	81069	0,488	0,79
28129	0,063	0,84	55355	0,300	1,05	82582	0,503	0,79
29641	0,075	0,91	56868	0,308	1,02	84094	0,510	0,77
31154	0,095	1,05	58380	0,328	1,03	85607	0,523	0,76
32666	0,113	1,13	59893	0,340	1,01	87119	0,543	0,76
34179	0,120	1,10	61406	0,343	0,97	88632	0,558	0,76
35692	0,125	1,05	62918	0,358	0,96	90145	0,570	0,75
37204	0,143	1,10	64431	0,370	0,95	91657	0,578	0,73
38717	0,153	1,09	65943	0,383	0,94			
40229	0,165	1,09	67456	0,393	0,92			
41742	0,183	1,12	68968	0,413	0,93			
43255	0,195	1,11	70481	0,418	0,90			
44767	0,203	1,08	71994	0,425	0,88			
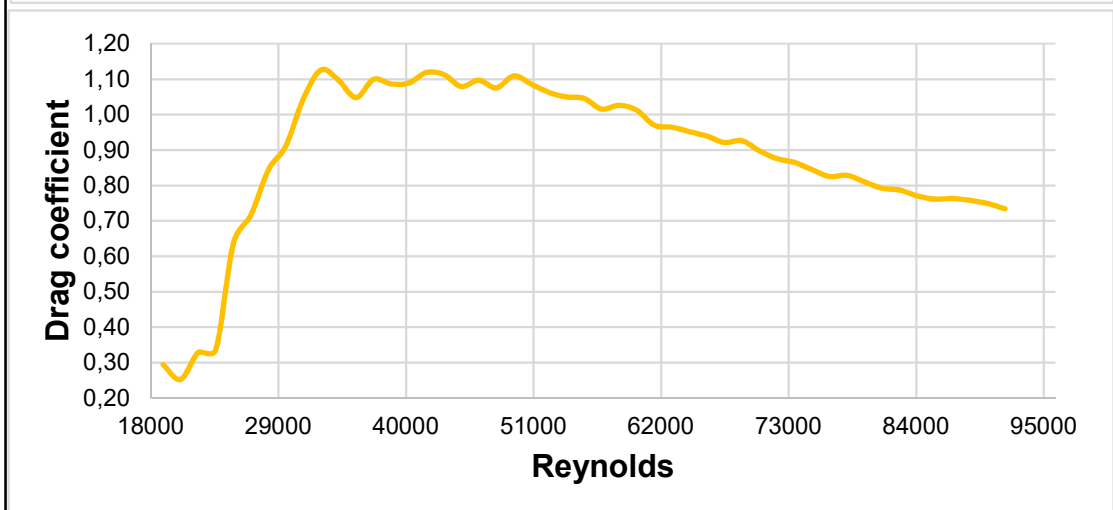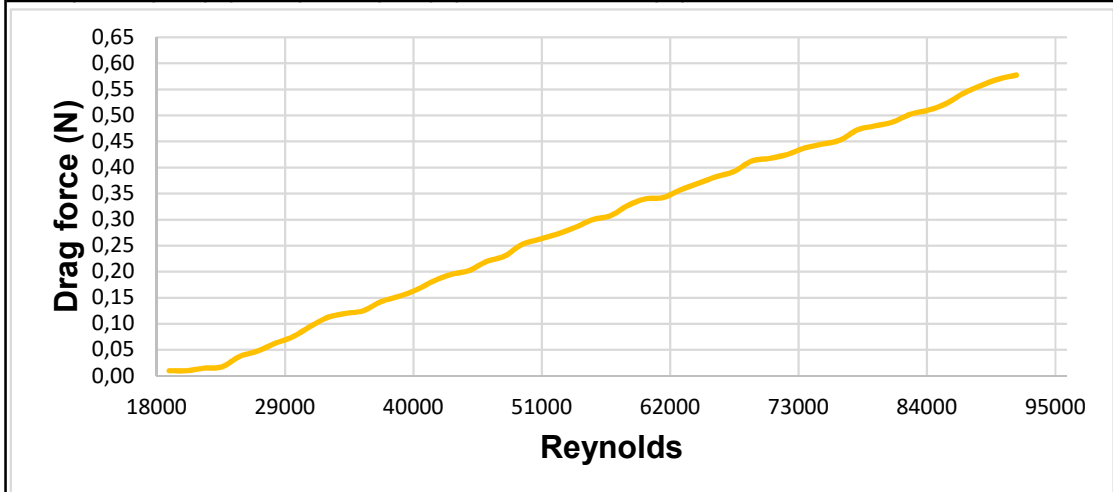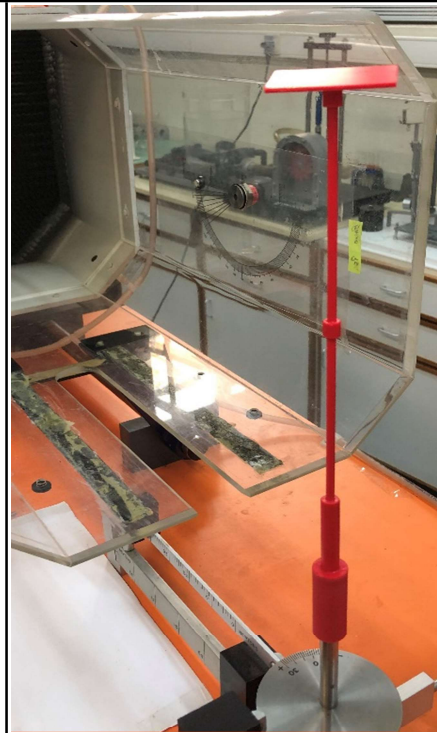
WIND TUNNEL SIMULATION
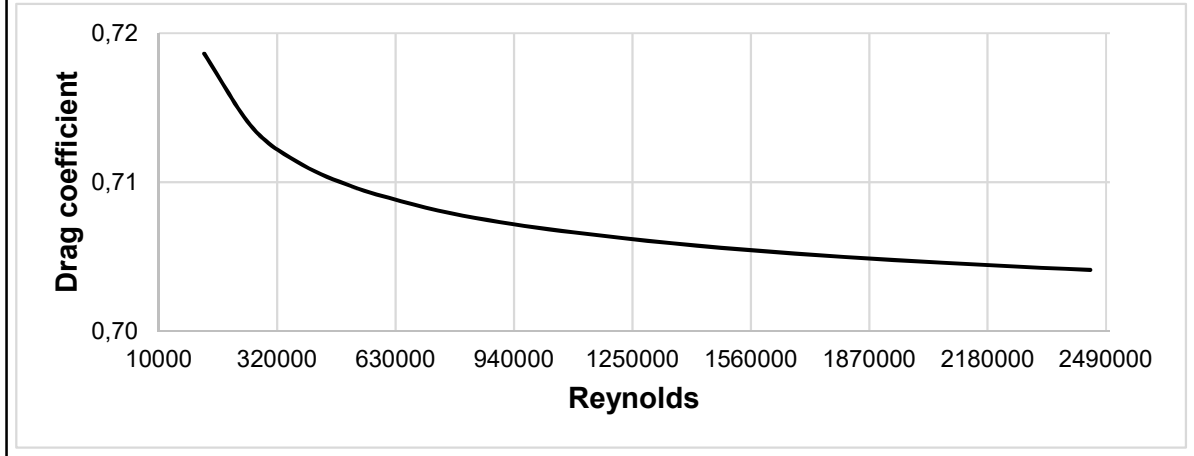Position: V
Flow type: Subsonic
Local temperature: 20 - 25ºC

Re	F (N)	C_D	Re	F (N)	C_D	Re	F (N)	C_D
8709	0,010	0,50	25045	0,158	0,94	41381	0,393	0,86
9617	0,010	0,41	25953	0,170	0,95	42289	0,413	0,85
10524	0,017	0,57	26860	0,185	0,96	43196	0,430	0,83
11432	0,020	0,58	27768	0,180	0,88	44104	0,453	0,82
12339	0,028	0,68	28675	0,195	0,89	45011	0,465	0,80
13247	0,033	0,70	29583	0,210	0,90	45919	0,485	0,80
14155	0,038	0,70	30490	0,225	0,91	46826	0,508	0,79
15062	0,048	0,79	31398	0,235	0,90	47734	0,525	0,78
15970	0,058	0,85	32306	0,250	0,90	48641	0,550	0,76
16877	0,063	0,82	33213	0,263	0,89	49549	0,573	0,76
17785	0,073	0,86	34121	0,273	0,88	50457	0,598	0,75
18692	0,080	0,86	35028	0,283	0,87	51364	0,625	0,73
19600	0,095	0,93	35936	0,295	0,86	52272	0,645	0,73
20507	0,103	0,92	36843	0,310	0,86	53179	0,668	0,72
21415	0,115	0,94	37751	0,320	0,84	54087	0,688	0,68
22323	0,125	0,94	38658	0,335	0,84	54994	0,713	0,65
23230	0,138	0,96	39566	0,353	0,85			
24138	0,145	0,94	40474	0,375	0,86			

	ANSYS CFD analysis			SOLVER PREFERENCE: CFX
	Position: I			ELEMENT ORDER: LINEAR
	Domain: Fluid			NODES: 93018
	Material: Air at 25ºC			ELEMENTS: 516615

Re	F (N)	C_D
128895	3,369	0,72
257790	13,382	0,71
386685	30,007	0,71
515580	53,237	0,71
644475	83,067	0,71
773370	119,481	0,71
902265	162,490	0,71
1031159	212,086	0,71
1160054	268,269	0,71
1288949	331,022	0,71
1417844	400,354	0,71
1546739	476,263	0,71
1675634	558,748	0,71
1804529	647,807	0,70
1933424	743,439	0,70
2062319	845,644	0,70
2191214	954,419	0,70
2320109	1069,760	0,70
2449004	1191,68	0,70
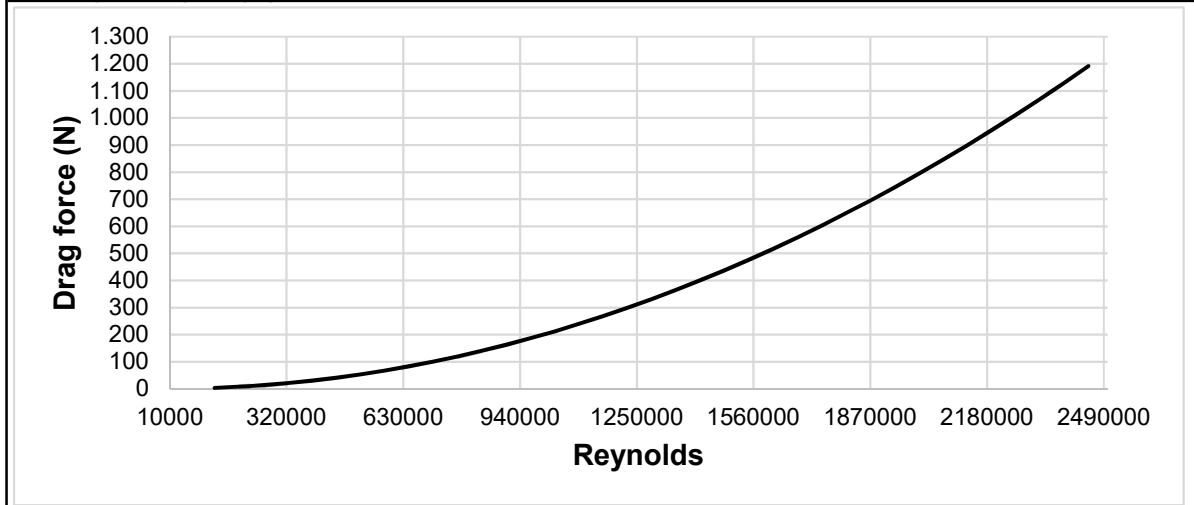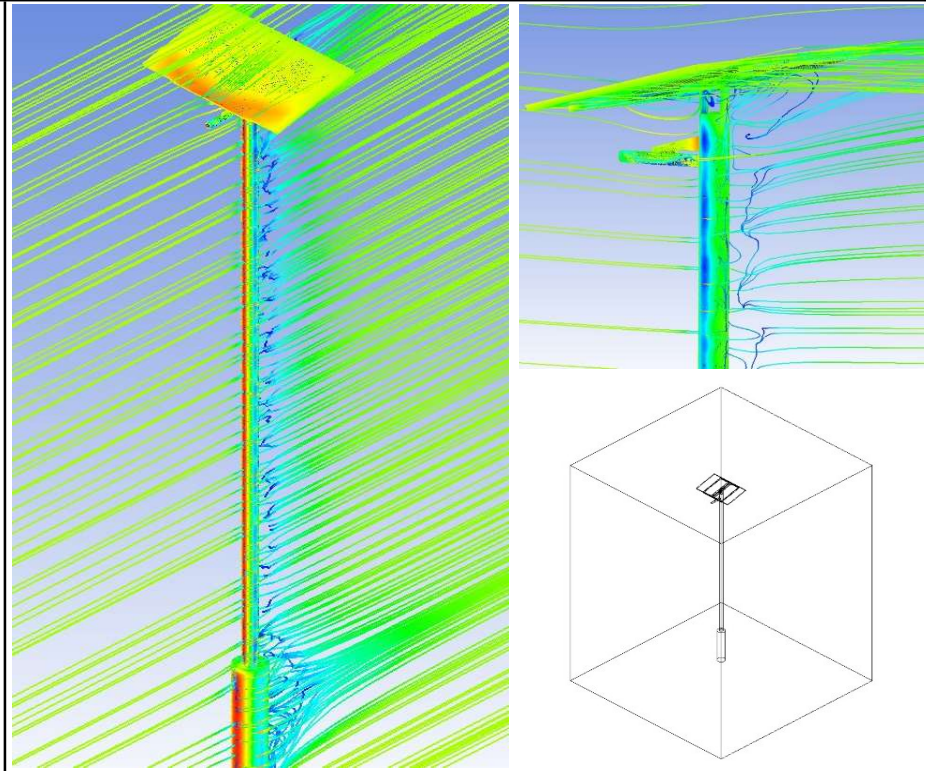
ANSYS CFD analysis	SOLVER PREFERENCE: CFX
Position: II	ELEMENT ORDER: LINEAR
Domain: Fluid	NODES: 93018
Material: Air at 25ºC	ELEMENTS: 516615

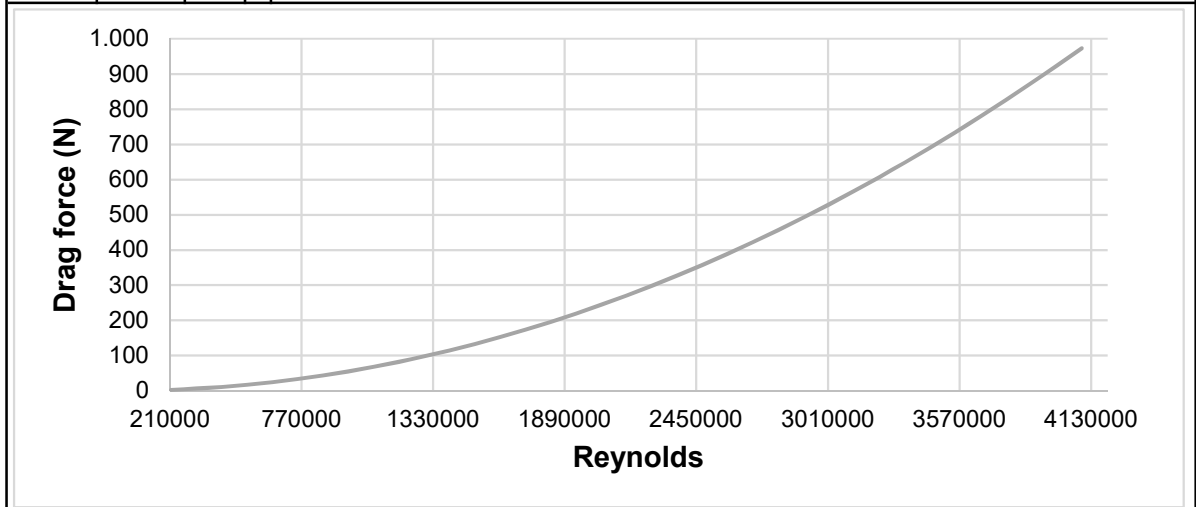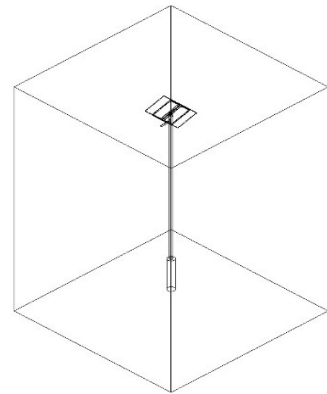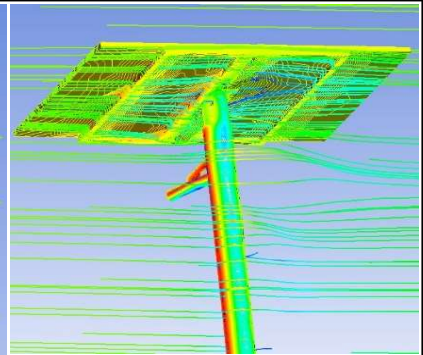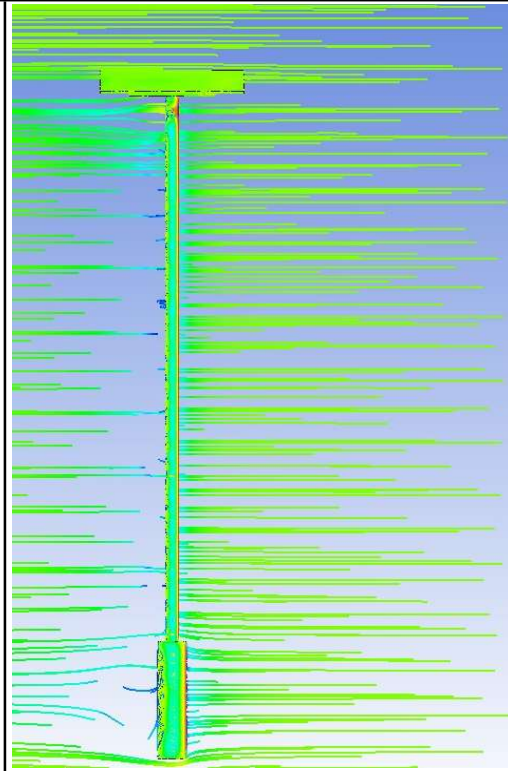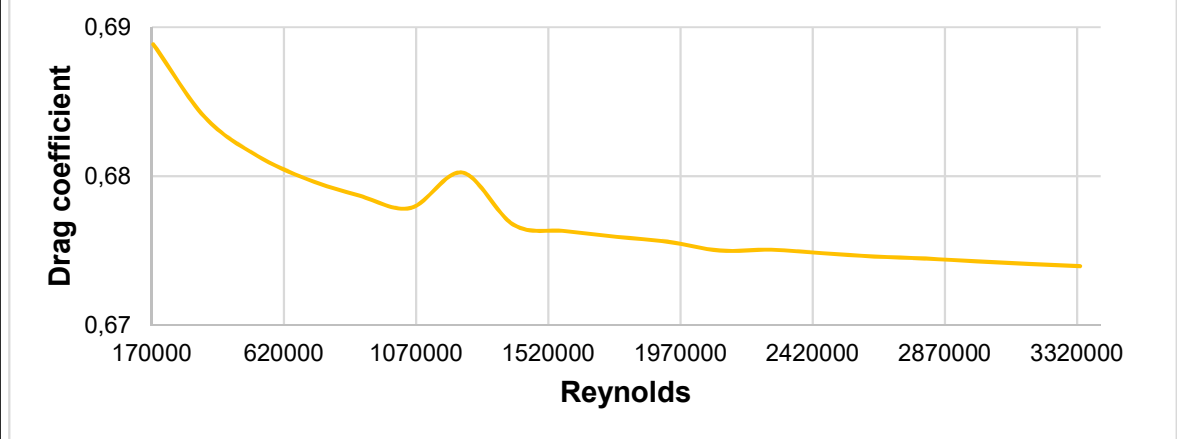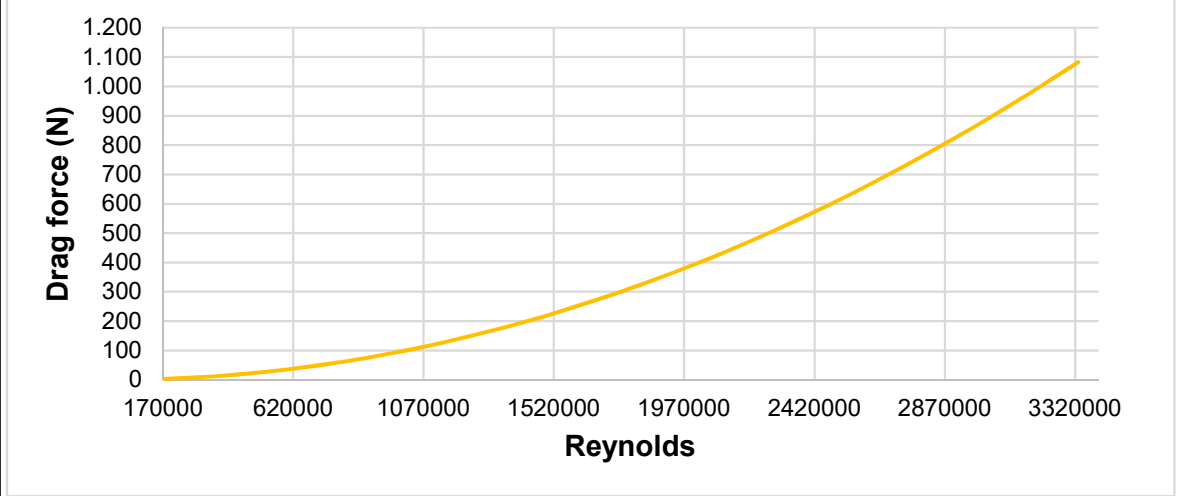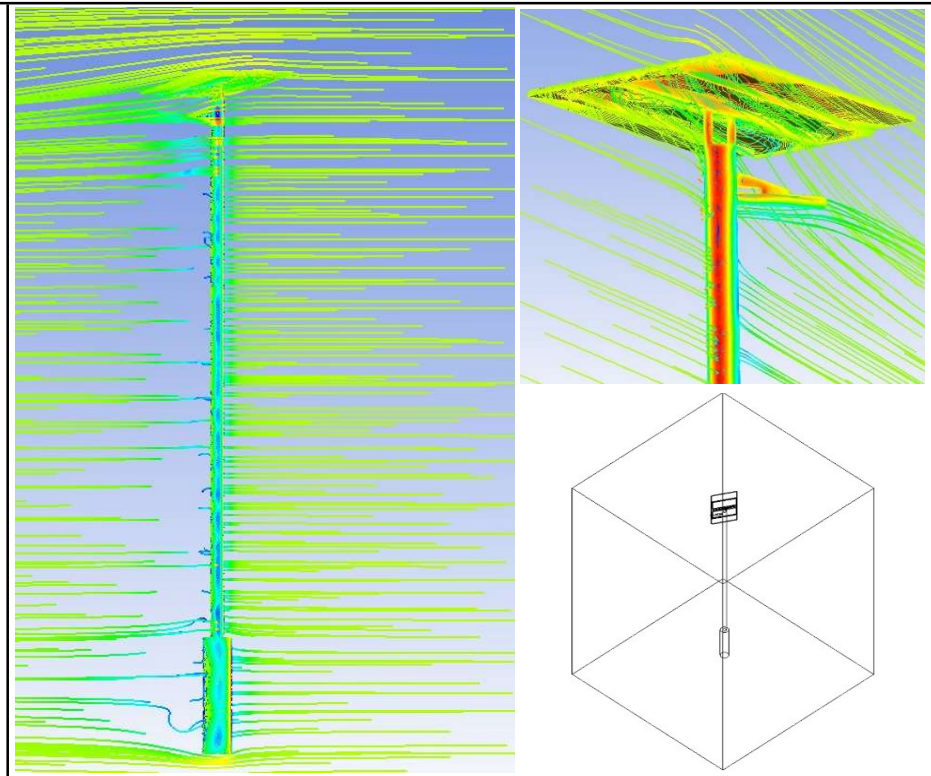| Re	F (N)	C_D
175297	3,037	0,68
350594	12,050	0,68
525891	27,000	0,67
701188	47,879	0,67
876486	74,675	0,67
1051783	107,396	0,67
1227080	146,035	0,67
1402377	190,571	0,67
1577674	241,035	0,67
1752971	297,385	0,67
1928268	359,638	0,67
2103565	427,789	0,67
2278862	501,841	0,67
2454160	581,841	0,67
2629457	667,693	0,67
2804754	759,439	0,67
2980051	857,080	0,67
3155348	960,614	0,67
3330645	1070,13407	0,67
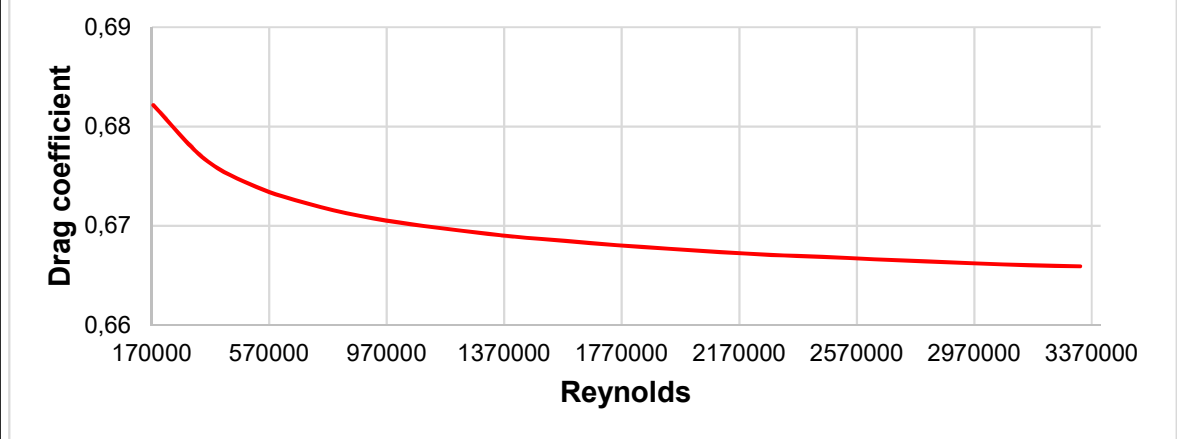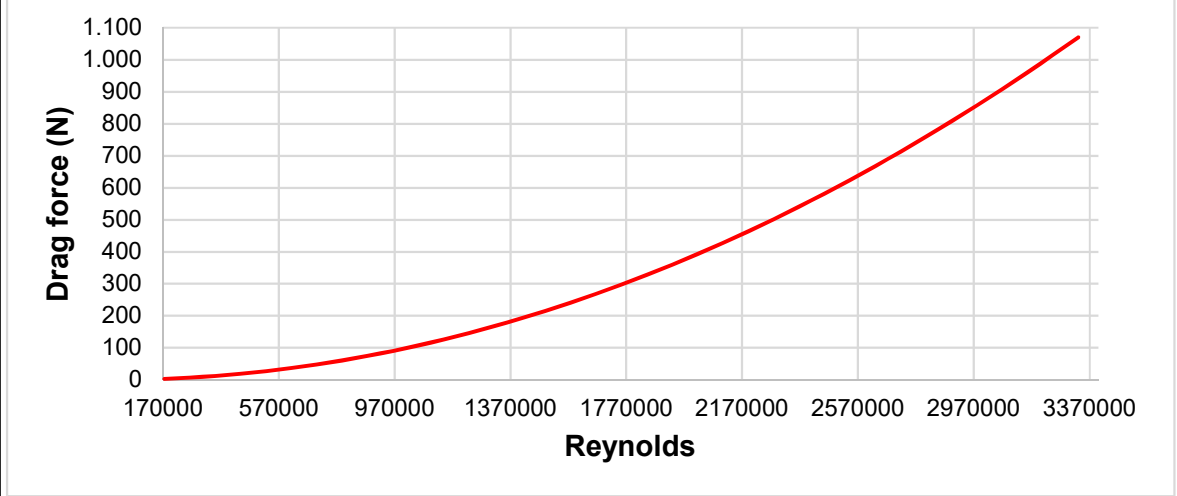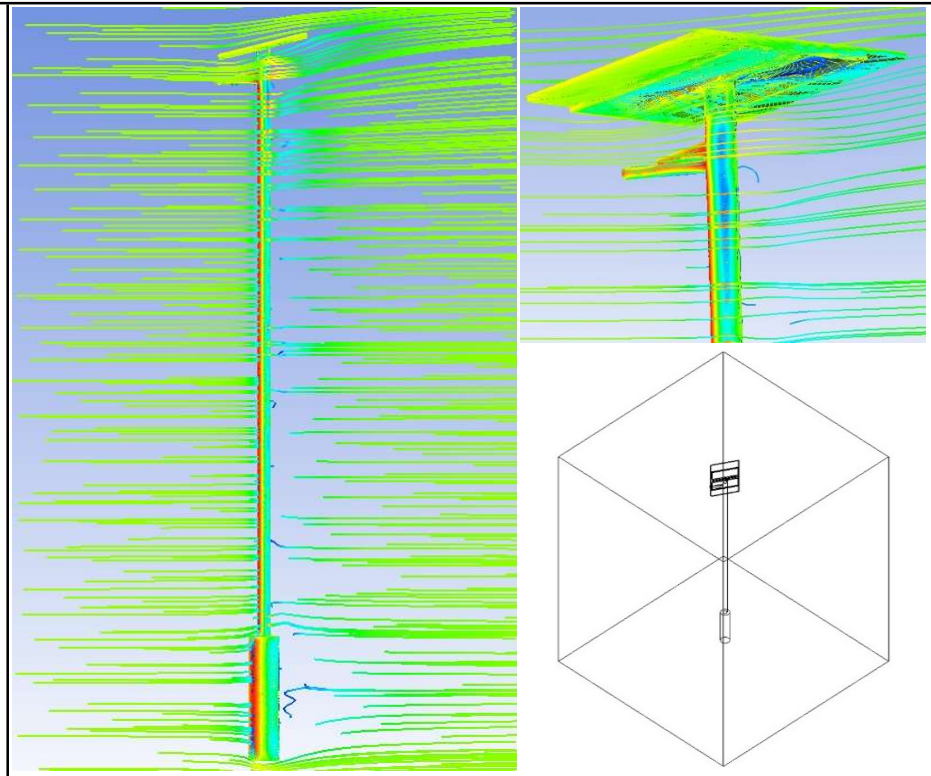
ANSYS CFD analysis	SOLVER PREFERENCE: CFX
Position: III	ELEMENT ORDER: LINEAR
Domain: Fluid	NODES: 93018
Material: Air at 25ºC	ELEMENTS: 516615

Re	F (N)	C_D
215255	2,769	0,74
430509	10,981	0,74
645764	24,595	0,74
861018	43,601	0,73
1076273	67,990	0,73
1291527	97,758	0,73
1506782	132,902	0,73
1722036	173,417	0,73
1937291	219,300	0,73
2152545	270,550	0,73
2367800	327,164	0,73
2583055	389,141	0,73
2798309	456,480	0,73
3013564	529,189	0,73
3228818	607,249	0,73
3444073	690,667	0,73
3659327	779,442	0,73
3874582	873,572	0,73
4089836	973,057	0,73
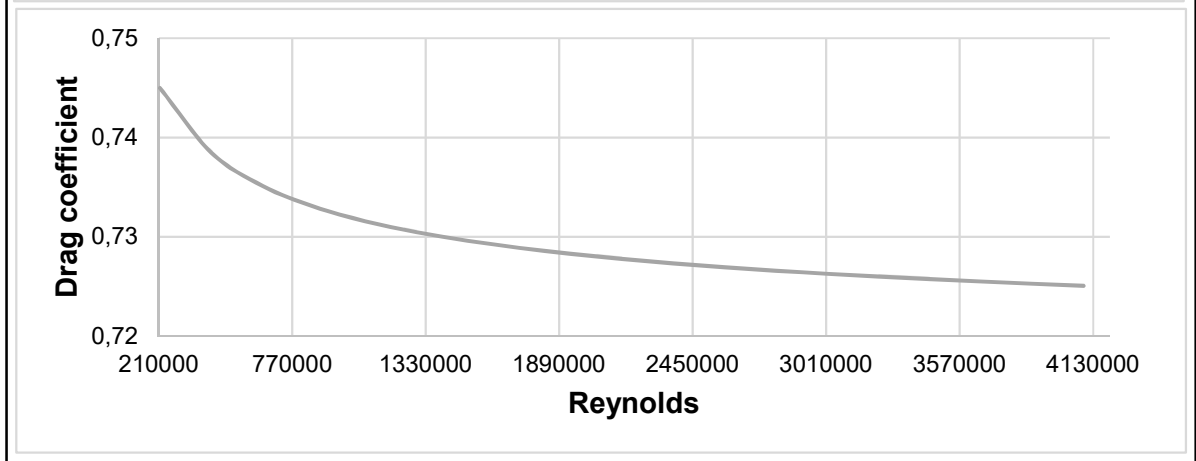
ANSYS CFD analysis	SOLVER PREFERENCE: CFX
Position: IV	ELEMENT ORDER: LINEAR
Domain: Fluid	NODES: 93018
Material: Air at 25ºC	ELEMENTS: 516615

Re	F (N)	C_D
175297	3,066	0,69
350594	12,179	0,68
525891	27,299	0,68
701188	48,417	0,68
876486	75,529	0,68
1051783	108,631	0,68
1227080	148,376	0,68
1402377	192,796	0,68
1577674	243,859	0,68
1752971	300,889	0,68
1928268	363,894	0,68
2103565	432,690	0,68
2278862	507,851	0,68
2454160	588,779	0,67
2629457	675,676	0,67
2804754	768,613	0,67
2980051	867,447	0,67
3155348	972,258	0,67
3330645	1083,0373	0,67

ANSYS CFD analysis	SOLVER PREFERENCE: CFX
Position: V	ELEMENT ORDER: LINEAR
Domain: Fluid	NODES: 93018
Material: Air at 25ºC	ELEMENTS: 516615

Re	F (N)	C_D
128895	3,400	0,73
257790	13,504	0,72
386685	30,278	0,72
515580	53,720	0,72
644475	83,820	0,72
773370	120,575	0,71
902265	163,981	0,71
1031159	214,028	0,71
1160054	270,727	0,71
1288949	334,071	0,71
1417844	404,058	0,71
1546739	480,700	0,71
1675634	563,969	0,71
1804529	653,894	0,71
1933424	750,440	0,71
2062319	853,643	0,71
2191214	963,463	0,71
2320109	1079,940	0,71
2449004	1203,06	0,71